CHARACTERIZATION OF THE EFFECT OF CRITICAL CATHODE DESIGN PARAMETERS ON THE LITHIUM SULFUR CELL RESISTANCE USING ELECTROCHEMICAL IMPEDANCE SPECTROSCOPY

by

Ayşegül Karakuş

B.S., Chemical Engineering, Boğaziçi University, 2016

Submitted to the Institute for Graduate Studies in
Science and Engineering in partial fulfillment of
the requirements for the degree of
Master of Science

Graduate Program in Chemical Engineering
Boğaziçi University

2019

CHARACTERIZATION OF THE EFFECT OF CRITICAL CATHODE DESIGN PARAMETERS ON THE LITHIUM SULFUR CELL RESISTANCE USING ELECTROCHEMICAL IMPEDANCE SPECTROSCOPY

APPROVED BY:

Asst. Prof. Damla Eroğlu Pala (Thesis Supervisor)	…..……
Prof. Ramazan Yıldırım	…..……
Assoc. Prof. Uğur Ünal	…..……

DATE OF APPROVAL: 02.08.2019

ACKNOWLEDGEMENTS

First of all, I would like express my gratitude to Asst. Prof. Damla Eroğlu Pala for his patience, encouragement, and for her timeless supports for both academic and non-academic life. I am very grateful to have the opportunity to work with her in one of the most important topic of electrochemical engineering.

I am very grateful to my thesis committee Prof. Ramazan Yıldırım and Assoc. Prof. Uğur Ünal for to read and comment on my thesis and to be my jury when I am closing my MSc. part of my academic life.

I would like to send my special thanks to my friends Gülşah Gül, Feyza Kevser Öner, Özlem Özbek, Zarife Begüm Yağcı, Selin Baç Bilgi, Elif Esvap, Özge Selçuk, Müge Kasım, Dilara Göreke, İlke Kaykanat, Merve Yüce, Burcu Oral and Merve Bilal.

Finally, I would like to present my sincere appreciation to my big family. I am very grateful to have my parents Nezahat and İdris Karakuş, my sisters Tuğba and Melike, my brothers Cemal and Cemil, my lovely niece Zeynep Erva and finally my fiancé Fikret Kılıç. My life is more meaningful and enjoyable with them.

Finally, financial support provided by TÜBİTAK 3501 – Project No: 116M574 is acknowledged.

This thesis is devoted to my big family…

ABSTRACT

CHARACTERIZATION OF THE EFFECT OF CRITICAL CATHODE DESIGN PARAMETERS ON THE LITHIUM SULFUR CELL RESISTANCE USING ELECTROCHEMICAL IMPEDANCE SPECTROSCOPY

Lithium-sulfur batteries have gained significant attention as an alternative for Li-ion batteries for electric vehicle applications in the recent years. This is due to their high theoretical specific energy (2600 Wh/kg) coming from one of the most abundant and non-toxic element, sulfur and the lightest metal lithium. On the other hand, Li-S batteries have some drawbacks, which are Li anode degradation, polysulfide shuttle mechanism and low electronic conductivity; these all cause low specific capacity and poor cyclability. Hence, Li-S cells suffer from some transport and kinetic resistances. In this study, the effect of the electrolyte to sulfur ratio (E/S) and the carbon to sulfur ratio (C/S), which are two critical cathode design parameters, on the transport and kinetic resistances in a Li-S cell are investigated as a function of degree of discharge in the first cycle by using electrochemical impedance spectroscopy. First, the main resistances in the cell are identified as the electrolyte, charge transfer, film and Warburg resistances. The effect of E/S ratio on the cell resistance is investigated for Li-S cells having E/S ratios of 34 µl/mg, 19 µl/mg, 12 µl/mg, 6 µl/mg and 3 µl/mg at a C/S ratio of 1. For these cells, the highest resistances are obtained with 3 µl/mg and 6 µl/mg E/S ratios for all of the resistances. Furthermore, the lowest resistances are obtained for the cell with E/S=19 µl/mg and further increase of the E/S ratio do not reduce the resistances. Secondly, the effect of C/S ratio on the cell resistance is investigated for Li-S cells with the C/S ratios of 3.5, 2.0, 1.0, 0.5 and 0.3 having 19 µl/mg E/S ratio. The cell with a C/S ratio of 3.5 has considerably higher resistances than the other C/S ratios for all the three resistances whereas the lowest resistances are obtained with C/S=1; lower C/S ratios result in higher resistances. These results showed that, there is an optimum point for both E/S and C/S ratios, where the cells deliver minimum transport and kinetic resistances.

ÖZET

Li-S BATARYALARINDA KRİTİK KATOT TASARIM PARAMETRELERİNİN HÜCRE RESİSTANSINA ETKİSİNİN ELEKTROKİMSAYAL EMPEDANS SPEKTROSKOPİSİ KULLANARAK KARAKTERİZASYONU

Lityum-sülfür bataryaları, elektrikli araç uygulamalarında kullanılan Li-iyon bataryalarına alternatif olarak son yıllarda oldukça dikkat çekmiştir. Bunun sebebi, aktif madde olarak dünyada bol miktarda olan ve zararsız olup yüksek kapasite veren sülfür ve en hafif metal Li içeren Li-S bataryalarının yüksek teorik spesifik enerjisidir (2600 Wh/kg). Öte yandan, Li-S bataryalarının elde edilen kapasiteyi azaltan ve çevrim ömrünü düşüren problemleri vardır. Li anot bozunması, polisülfit mekik mekanizması ve düşük elektronik iletkenlik bu problemlerin en önemlileridir ve bunlar hücre içerisinde kinetik ve taşınım rezistanslarına yol açarlar. Bu çalışmada, katottaki 2 kritik dizayn parametresi olan karbona sülfür (C/S) ve elektrolite sülfür (E/S) oranlarının hücre içerisindeki kinetik ve taşınım rezistanslarına etkisi deşarj derinliğine bağlı olarak, elektrokimyasal empedans spektroskopisiyle incelenmiştir. İlk olarak, hücre içerisindeki ana rezistanslar elektrolit, yük transfer, film ve Warburg rezistansları olarak belirlenmiştir. E/S oranının rezistans üzerine etkisi 34 µl/mg, 19 µl/mg, 12 µl/mg, 6 µl/mg ve 3 µl/mg E/S oranlarına sahip, C/S oranı 1 olan hücreler ile test edilmiştir. Bu hücrelerde en yüksek rezistanslar E/S oranının 3 µl/mg ve 6 µl/mg olduğu durumlarda elde edilmiştir. Öte yandan, en düşük rezistanslar E/S=19 µl/mg olduğu durumda gözlemlenmiştir ve E/S oranının daha fazla yükseltilmesi rezistansı düşürmemiştir. C/S oranının hücredeki rezistanslar üzerine etkisi ise C/S oranı 3.5, 2.0, 1.0, 0.5 ve 0.3, E/S oranı ise 19 µl/mg olan hücreler ile araştırılmıştır. C/S oranının 3.5 olduğu hücreler, diğer hücreler ile kıyaslandığında çok yüksek rezistans göstermiş, minimum rezistans ise C/S=1 ile elde edilmiştir. Bu sonuçlara göre, E/S ve C/S oranlarının hücrelerde azami kinetik ve taşınım rezistansları sağlayan optimum bir değeri bulunmaktadır.

TABLE OF CONTENTS

LIST OF FIGURES

LIST OF TABLES

LIST OF SYMBOLS

$\|Z\|$	Absolute Value of Impedance (ohm)
f	Frequency (Hz)
i	Faradaic Current (mA)
n	Order of Polysulfide
t	Impedance Time (s)
U_0	Standard Cell Potential (V)
ω	Angular Frequency (rad/s)
α_1	Integer Number
σ_1	Warburg Constant
φ	Phase Shift (rad)

LIST OF ACRONYMS/ABBREVIATIONS

C	Capacitance (F)
C/S	Carbon to Sulfur Ratio
CPE	Constant Phase Element
DME	Dimethyl Ether
DOD	Degree of Discharge (%)
DOL	1,3-Dioxolane
E/S	Electrolyte to Sulfur Ratio (µl/mg)
EDS	Energy Dispersive X-ray Spectroscopy
EIS	Electrochemical Impedance Spectroscopy
HPC	Hydroxypropyl Cellulose
Im(Z)	Imaginary Part of Impedance (ohm)
Li-S	Lithium-sulfur
LiTFSI	Lithium bis-trifluoromethanesulfonimide
MWCNT	Multiwalled Carbon Nanotubes
NMP	N-methyl-2-pyrolidone
NP	Not Provided
OCV	Open Circuit Potential (V)
PEO	Polyethylene Oxide
PS	Polysulfide
PSS	Polysulfide Shuttle
PVDF	Polyvinylidene Difluoride
Q	Constant Phase Element
R1	Electrolyte Resistance (ohm)
R2	Charge Transfer Resistance (ohm)
R3	Non-conductive Film Resistance (ohm)
Re(Z)	Real Part of Impedance (ohm)
SEM	Scanning Electron Microscopy
W	Warburg Diffusion Resistance
wt.	Weight Percentages

XRD	X-Ray Diffraction

1. INTRODUCTION

Today's major sources of energy are crude oil and natural gas and they are used in most of the high-tech human activities [1]. The use of fossil fuels in the energy sector as the basic energy source leads to environmental and air pollutions. Because of that, the average temperature of the world has increased 4 °C, risking the lives of millions of people [2]. Furthermore, fossil fuels will not last long and they will run out eventually. According to a previous study, oil, gas and coal reserves will last for another 35, 37 and 107 years, respectively [3]. Moreover, the exponential growth of the energy demand in the past decade shows that, by 2030 the energy need will be 50 % higher than 2012 [4]. The concerns of both reserve shortages and environmental pollution have led many researchers to focus on harvesting, storing and utilizing renewable energies, mostly wind and solar [1]. One disadvantage with the renewable energies is that the production of them change seasonally and even daily. Not only that the production of renewable energies differs during day and night but also demand for energy change. Thus, efficient ways of short and long term energy storage are essential for the future energy market [5].

According to the U.S. Energy Information Administration, transportation sector has one of the highest energy demands. In 2013, energy demand in the transportation sector was equivalent to the 28 % of the world energy consumption. However, most of this energy is supplied from the fossil fuels, mainly oil. So, it is important to use green energy in transportation sector to mitigate the dependence on fossil fuels. Efficient energy storage systems are essential to use renewable energy, in the form of electricity, which are able to provide continuous, stable and flexible power supply. There are various electric storage technologies in chemical, electrochemical, mechanical or thermal forms [6]. For transportation industry, electrochemical storage systems are widely accepted and show promise for the future [7].

Among electrochemical storage systems, lithium batteries have an important place in the transportation sector as being used in both hybrid and electric vehicles. Due to the high specific energy and energy density of the rechargeable lithium batteries, they are widely accepted and researched; great progress has been made towards reaching the theoretical

values of these batteries. Today, secondary lithium-ion batteries electrify most of the electric vehicles on the roads. However, with gravimetric energy densities of 150-300 Wh/kg, Li-ion batteries are not capable of fulfilling the increasing demand in the transportation industry even with working with 100 % efficiency [8]. The work done by Nazar *et al.* (2009) showed the capabilities of lithium-sulfur (Li-S) cells and drew attention to the development of Li-S batteries [9]. With this work, Li-S batteries have gained attention as a promising post lithium-ion chemistry due to its high theoretical energy density. Researches about the gravimetric and volumetric energy densities of the electrochemical systems show that the Li-S cells can exceed the performance of Li-ion batteries and can attain higher gravimetric energy densities in the future [10], [11].

The main components of Li-S cells are similar to the other rechargeable batteries, which are the anode, the cathode, the electrolyte and a porous separator. Pure Li metal film is used as the anode whereas the conventional positive electrode is made of elemental sulfur, conductive matrix and binder. The basic scheme of a Li-S battery can be seen in Figure 1.1.

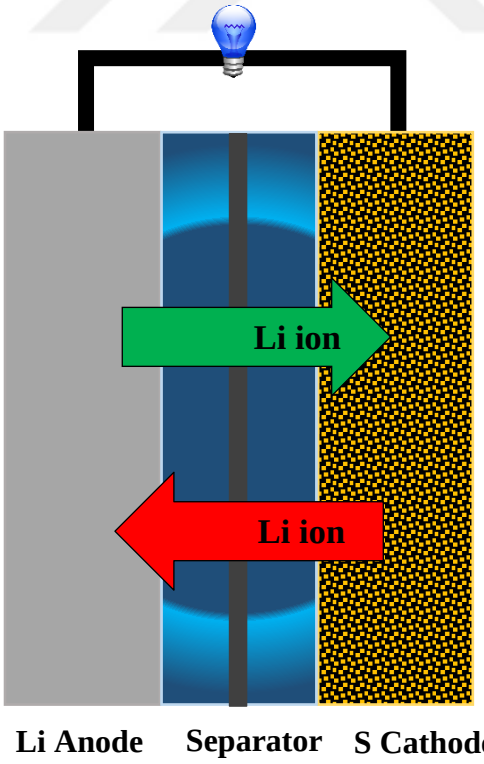

Figure 1.1. The basic schematic diagram of a Li-S cell.

Li metal is used as the anode material due to its very high theoretical specific capacity of 3860 mAh/g Li. It is one of the best candidates as an anode material due to 0.534 g/cm^3 density and -3.040 V standard reduction potential, which are the lowest values possible [12].

Electrolyte is the medium for the ion transfer, Li ion in this case, from the anode to the cathode during discharge and from the cathode to the anode during charge for all electrochemical systems. In addition, electrolyte should be chemically and electrochemically stable over the voltage and temperature ranges. Electrolytes in Li-S batteries should have additional properties; they should have high solubility for the short chain polysulfides and low solubility for the high chain polysulfides [13].

The cathode design of Li-S batteries is very important since it determines the system and cell level electrochemical performances. Sulfur has high specific capacity of 1675 mAh/g S and it is abundant in nature and non-toxic. Because of these factors, utilization of sulfur in the cathode can lead to relatively inexpensive batteries with high capacities [11], [14]. However, both sulfur and the discharge product, Li_2S, are insulating [15]. Therefore, additional conductive material is needed, which adds up to the dead weight of the cell. In the battery industry, carbonaceous materials are preferred as the conductive medium [9]. Binder is also needed to increase the contact between the carbonaceous materials and sulfur. In addition, structural stability can be maintained with an efficient binder [16].

Anode and cathode capacities with the complete conversion of the active materials are 3860 mAh/g Li and 1675 mAh/g S, respectively. Thus, the theoretical gravimetric energy density of a Li-S battery is 2600 Wh/kg with a thermodynamic voltage of 2.2 V, whereas it is 387 Wh/kg for $LiCoO_2$ based Li-ion batteries [17]. A typical discharge voltage profile of a Li-S cell can be seen in Figure 1.2 [17]. Beforehand, the overall reaction in a Li-S battery is shown in Equation 1.1.

$$16Li^+ + 8S + 16e^- \rightarrow 8Li_2S \qquad U_0 = 2.2\ V \qquad (1.1)$$

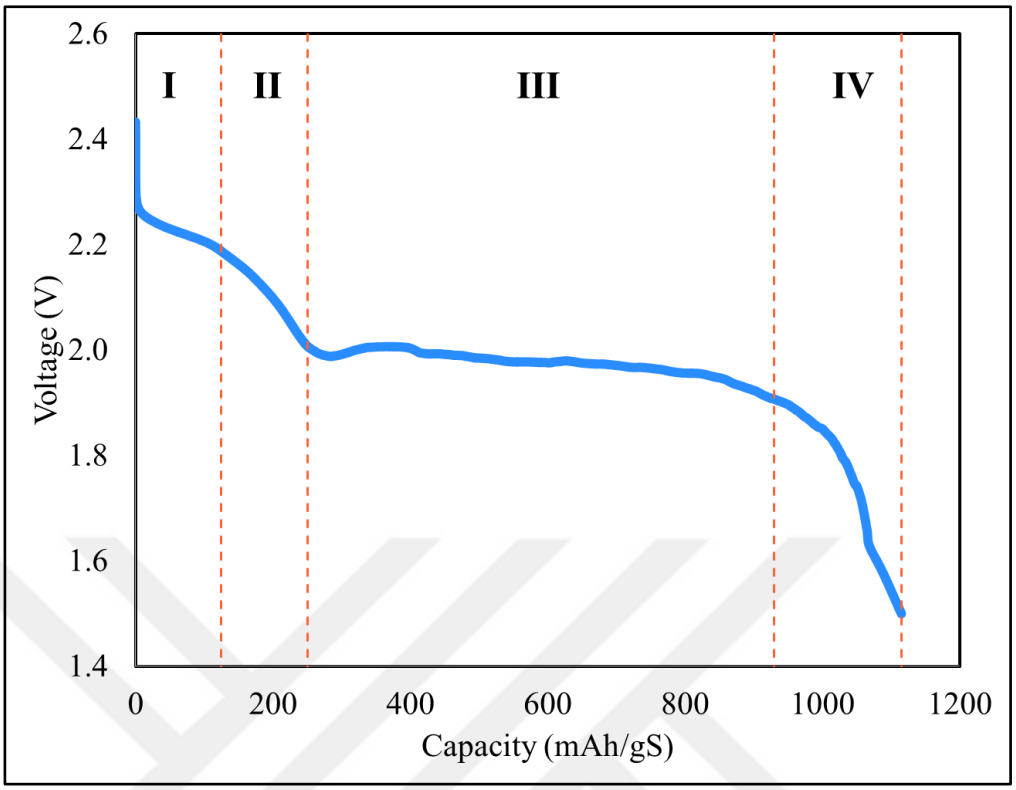

Figure 1.2. Cell voltage versus capacity graph of a typical Li-S cell.

During discharge of a Li-S cell, Li metal at the anode is oxidized and Li ions are formed (Equation 1.2). The Li-ions pass through the porous separator and electrolyte to reach the sulfur cathode. Meanwhile, sulfur is reduced with the electrons coming from the external circuit that leads to the formation Li polysulfides. As can be seen from the discharge profile in Figure 1.2, there are two apparent plateaus, which are called as the 2.4 V high plateau and the 2.1 V low plateau, and 4 discharge regions [18].

In the region I, solid S_8 is reduced to form Li_2S_8 with Li ions coming from the anode as in Equation 1.3. Then, Li_2S_8 is dissolved in the electrolyte (Equation 1.4). In this step, voids occur in the cathode due to sulfur dissolution.

$$Li \rightarrow Li^+ + e^- \tag{1.2}$$

$$\frac{1}{2}S_8 + e^- \rightarrow \frac{1}{2}S_8^{2-} \tag{1.3}$$

$$2Li^+ + S_8^{2-} \rightarrow Li_2S_8 \quad (1.4)$$

In the region II, the cell voltage significantly decreases with the liquid-liquid reduction of Li_2S_8 (Equation 1.5). As the shorter polysulfides are formed, the viscosity of the electrolyte-polysulfide mixture increases due to an increase in the concentration of the polysulfides [18].

$$Li_2S_8 + 2Li \rightarrow Li_2S_{8-n} + Li_2S_n \quad (1.5)$$

In the region III, the solid discharge products of Li_2S and Li_2S_2 are produced from the dissolved short chain polysulfides (Equation 1.6 and 1.7). In this region, the cell voltage is constant between 1.9-2.1 V where the major cell capacity is obtained [18].

$$2Li_2S_n + (2n-4)Li \rightarrow nLi_2S_2 \quad (1.6)$$

$$Li_2S_n + (2n-2)Li \rightarrow nLi_2S \quad (1.7)$$

In the final region, the solid Li_2S_2 further reduces to Li_2S (Equation 1.8). Since both the product and reactant are nonconductive these reactions are very slow and the cell voltage suddenly and sharply decreases [18].

$$Li_2S_2 + 2Li \rightarrow Li_2S \quad (1.8)$$

Although representative reactions are listed above, the exact reaction mechanism is still unclear. However, it is known that the reactions taking place in the cell are highly complex involving multi-step reactions [19]–[22] . According to Kumaresan *et al.* (2008), there may be 10 reactions taking place during discharge of the cell [23].

There are many challenges in Li-S batteries that result in low capacity and short cycle life, which prevent Li-S mass commercialization. These challenges are mainly stemming from the complex working mechanism of Li-S cells during charge and discharge [24]. The insulating nature of sulfur and final product of discharge, Li_2S causes additional problems

such as low sulfur utilization. Therefore, specially designed conductive medium is needed to fully utilize sulfur in the cathode [25]. Moreover, densities of sulfur and Li_2S are 2.07 g/cm^3 and 1.66 g/cm^3, respectively. This density difference leads to volume expansion-contraction up to 76 % between charge and discharge steps that results in morphology change on the cathode surface [26]. The other main problem of Li-S batteries is the polysulfide shuttle mechanism due to the polysulfide migration from the cathode to the anode. Polysulfides are the intermediate products of the step reactions and they should be reduced to the final product of Li_2S in the cathode to give high capacity. However, due to the high solubility of the polysulfides in the electrolyte, these polysulfides migrate to the anode and they either precipitate on the anode surface or migrate back to the cathode and re-oxidize there during charging. This is called the polysulfide shuttle mechanism and it results in a decrease in the Coulombic efficiency of the cell, deterioration of Li anode and the active material loss from the cathode [27], [28]. In addition, Li is a very reactive metal and it can react with the electrolyte that cause both Li and electrolyte loss [29]. Each of these issues cause additional resistances in the cells. Consequently, the researchers are trying to address these problems of Li-S cells by finding and imparting optimum design parameters and conditions.

Electrolyte volume per sulfur amount, in other words electrolyte-to-sulfur (E/S) ratio, is a key factor since it affects the performance of Li-S batteries in a great manner. The desired characteristics of electrolytes in Li-S batteries are high Li ion conductivity, high polysulfide solubility, and high electrochemical and chemical stability towards the lithium anode. These characteristics of electrolytes are utilized only if the sufficient amount of electrolyte volume is present to completely wet the electrode surfaces and the separator [30]. In addition, the polysulfide concentration is determined by the electrolyte volume and this concentration affects the reaction kinetics and polysulfide shuttle mechanisms. For example, at low E/S ratios, since the polysulfide concentration increases in the electrolyte, shuttle mechanism becomes more favorable. Hence, low amount of electrolyte in the cell results in capacity loss and less sulfur utilization. On the other hand, even though better cycle life and higher capacities are obtained by having enhanced cathode kinetics with high amount of electrolyte, it also increases the dead mass of the cells leading to a decrease in the system level energy density [31], [32]. Therefore, the E/S ratio is a very important design parameter for Li-S batteries.

Optimum carbon amount is another critical design parameter to mitigate the adverse effects of low electronic conductivity. Sulfur cathode is mainly composed of a conductive medium, which is mostly carbon, and sulfur. The carbon type and amount are critical factors that affect the Li-S battery performance significantly. Both S and Li_2S are insulating against electrons and ions in nature. However, for the reduction reactions to take place, sulfur should accept the electrons coming from the external circuit. Therefore, the addition of conductive carbon into the sulfur cathode is crucial. When all the carbon surface is covered with S and Li_2S precipitates at the end of discharge, further reduction of the polysulfides is inhibited. Therefore, cell voltage suddenly drops and it causes battery failure. To reach high specific energy and capacity in Li-S batteries, sulfur should be fully utilized and this is only possible with increased cathode electronic conductivity. On the other hand, since carbon does not contribute to the specific capacity, increasing carbon amount in the cell decreases both cell and system level energy density [33]. So, the carbon amount should be optimized to obtain not only high sulfur utilization and thus high discharge capacity but also high energy density. Hence, the carbon-to-sulfur (C/S) ratio is very important for the cathode design.

Complicated mechanisms taking place in a Li-S cell can be identified individually as a function of discharge depth by using a widely accepted electro-analytical method, electrochemical impedance spectroscopy (EIS). EIS is a powerful tool to measure the contributions of all the kinetic and transport resistances in the cell to the total cell resistance. There are several studies in the literature applying EIS method to study novel positive electrode materials, the effect of electrolyte compositions and reaction mechanisms in Li-S cells [34]–[36]. However, to our knowledge there is no study investigating the dependence of the cell impedance on the E/S and C/S ratios in the cathode as functions of degree of discharge of Li-S batteries. To address the aforementioned issues with Li-S cells, the individual contributions of the design parameters to the cell resistance should be identified. In this work, the effect of carbon-to-sulfur (C/S) ratio and electrolyte-to-sulfur (E/S) ratio on the resistance of the cell is investigated in order to connect the cell design with the characteristic processes taking place in a Li-S cell during discharge.

1.1. Scope of Current Work

There are great efforts to utilize Li-S batteries in the transportation applications. This is only possible if Li-S batteries can deliver high energy density, high cyclability and high rate capability. However, there are several issues that must be overcome to reach these goals; polysulfide shuttle mechanism, Li anode deterioration and insulating nature of sulfur and discharge products are the main problems. These issues can be linked to various resistances in the cell, which vary throughout the cycle life and discharge state of the batteries. E/S ratio is one of the critical design factors that can affect the cell resistance since it influences the polysulfide shuttle mechanism and sulfur utilization in the cell and hence determines the reversible specific capacity and cyclability. C/S ratio is another key cathode design parameter which contributes to the electronic conductivity and electrochemically active area of the sulfur cathode. However, excess amounts of both carbon and electrolyte cause dead mass and volume in the cell and result in low system level energy density. Since E/S ratio and C/S ratio have a critical impact on the battery performance, it is important to know their effect on the cell resistances to reveal the mechanisms inside Li-S cells and the link between these mechanisms and the cell design. The individual resistances can be identified with the EIS, which is a conventional powerful tool for electrochemical systems. The Li-S literature contains several studies on the effect of E/S and C/S ratios on the electrochemical performances of the cells. The most relevant ones are summarized in the "Chapter 2: Literature Survey" part of this thesis. From our literature survey, we concluded that although, there are limited number of previous studies aiming to identify the cell resistances, none of them investigate the effect of C/S and E/S ratios on these internal resistances as a function of depth of discharge.

In this respect, the aim of this thesis is to determine the effect of the two most important design parameters, C/S and E/S ratios, on the reaction and degradation mechanisms in the Li-S batteries by using an important electrochemical characterization technique, electrochemical impedance spectroscopy (EIS). We believe that, our research will give a new perspective to the Li-S battery literature by identifying the effect of E/S and C/S ratios on the individual kinetic and transport resistances in the cell throughout the discharge process. This analysis will help to have a better understanding of the mechanisms inside Li-S cells during discharge.

In this study, the effect of E/S and C/S ratios are investigated with the conventional Li-S cells having Li metal anode and a cathode containing elemental sulfur, carbon and binder with a standard electrolyte commonly used in the literature. The method of the construction of the cells together with the procedure to carry out the electrochemical characterization and EIS fitting analysis are given in the “Chapter 3: Experimental Work” chapter.

After construction of the experimental set-up, the kinetic and transport resistances in the cell are measured with the EIS technique as a function of depth of discharge and an equivalent circuit is proposed for the EIS spectrums obtained. These spectrums are then analyzed by equivalent circuit fittings. After that, the effect of C/S and E/S ratios on these kinetic and transport impedance results as a function of depth of discharge are discussed. All of these results and discussions are given in the “Chapter 4: Results and Discussion” chapter.

Finally, I present my conclusions and recommendations in “Chapter 5: Conclusion”. Appendix includes the data for the replicate cells.

2. LITERATURE SURVEY

This thesis is on the determination of the effect of E/S and C/S ratios on the kinetic and transport resistances in a Li-S cell as a function of depth of discharge by using EIS method. Therefore, the literature survey about the E/S ratio, C/S ratio and EIS applications are conducted and the relevant experimental outputs and discussions are provided in this section of the thesis.

2.1. Previous Studies on the Effect of C/S Ratio on the Li-S Battery Performance

Eroglu *et al.* (2015) investigated the impact of electrode design parameters on the battery performance and cost by a techno-economic model for Li-S batteries used in electric vehicles [37]. A materials-to-system analysis was done to interpret the effect of these parameters on the system-level energy density, specific energy and battery price. It was found that electrolyte and carbon to sulfur weight percentages and reaction kinetics are critical to determine the energy density and cost of the batteries. It was concluded that, in order to develop inexpensive and high energy density batteries for the electric vehicles, electrode areal capacity should be higher than 8 mAh/cm^2.

Chen *et al.* (2011) investigated the effect of C/S ratio on the electrochemical performance by changing the sulfur weight percentages in the sulfur and ordered mesoporous carbon composite between 50-75 %. The ordered mesoporous carbon was specially synthesized with 2101 m^2/g surface area, 2.0 cm^3/g and 5.6/2.3 nm pore size. They have found that the composite with 60 wt.% sulfur has the highest sulfur utilization. The cells obtained are stable for 400 cycles even at 6C current rate and they have high rate capability. High surface area and pore volume are the main reasons of these superior results. Since large pores can ease the ion transport inside carbon particles rather than sulfur, 70 wt.% sulfur loading has a lower capacity even though it has a higher S/C ratio, or higher sulfur loading in other words [38].

Ding *et al.* (2014) studied the effect of key parameters in designing Li-S batteries on the cell performance. In this work, the effect of C/S ratio, electrolyte amount and sulfur

loading density in the cathode on the specific capacity and cyclability of the cells have been investigated. It was found that the cell with a 1:2 weight ratio of C/S has three times higher capacity than that of $LiCoO_2$, which is 538 mAh/g. The capacity of a cell is greatly influenced by the sulfur utilization and thus it is highly sensitive to the C/S ratio. It was proposed that this is due to the increasing amount of insulating Li_2S_2 and Li_2S precipitates on the carbon surface at the end of discharge. Since the electrochemical reactions are heterogeneous and take place at the surface, reactions are inhibited due to decreasing available surface area at low amounts of carbon, which lead to a capacity loss [39].

Gao and Abruna (2014) studied the gravimetric and volumetric energy densities of the cell based on the total weight and volume of the electrodes. It was stated that the volumetric energy density should be taken into consideration for electric vehicle applications. It was found that, volumetric energy density of the cell is more sensitive to the sulfur loadings and it increases more than the gravimetric energy density of the cell as the sulfur loading increases. At high sulfur loadings (70 %), the volumetric energy density of a Li-S battery can exceed that of a Li-ion battery. The important point is that, the capacities should be presented based on the total mass of sulfur and carbon when system performance is considered, in contrast to the most of the papers in the literature, which have reported the capacities based on sulfur amount only [40].

Duo *et al.* (2013) utilized peapod-like mesoporous carbon with 4.69 cm^3/g pore volume as the conductive matrix. The high pore size of the matrix enabled high sulfur loadings such as 84 %, and to have flexible sulfur-carbon composite which allowed volume expansion during discharge. In addition, there was enhanced electron transfer due to 3-4 nm thickness of the carbon walls. Three C/S ratios were tested with 84, 77 and 60 wt.% sulfur containing cathodes. The highest capacity was obtained with the 60 wt. % S cathodes when the capacity is based on the amount of sulfur whereas 84 wt. % sulfur loading had the highest capacity when the capacity was normalized based on the composite. However, for all of the C/S ratios, cells suffered from capacity fading due to the polysulfide shuttle mechanism [41].

Park *et al.* (2015) prepared active carbon/sulfur composite cathodes by a solution based method, which had sulfur contents between 32.37 wt.% and 55.33 wt.%. According to the specific capacity and rate capability results, the composite with the lowest sulfur

loading, i.e. 32.37 %, showed the best performance with a specific capacity of 1360 mAh/g at 1C in the first discharge and 702 mAh/g reversible capacity at 10C. This was due to the dissolved high order polysulfide presence in the anode and the separator for the medium and high sulfur contents; hence conversion of these polysulfides to low order polysulfides is limited in the cathode. In addition, sulfur infiltration in amorphous state was limited to the cathode with 41.21 wt.% S, and after that point crystalline sulfur was obtained in the surface [42].

Brückner *et al.* (2014) investigated the impact of sulfur loading on the cycle stability and sulfur utilization. Experiments conducted with 20-40-60-80 % of sulfur loadings in the cathode showed that increasing the sulfur amount in the cathode decreases the discharge capacity of the cell. For instance, no efficient capacity was obtained for the cell with 80 % of sulfur in the cathode, showing that when the carbon amount is too low, sulfur utilization is also very low in the cathode.

To sum up, there are a number of studies in the literature focusing on the impact of C/S ratio on the discharge capacity and cycle life of a Li-S battery. However, the literature is lack of explaining the effect of C/S ratio on the cell resistance and thus the reaction and degradation mechanisms in a Li-S cell during discharge.

2.2. Previous Studies on the Effect of E/S Ratio on the Li-S Battery Performance

Brückner *et al.* (2014) also investigated the effect of amount of electrolyte on the cycle stability and sulfur utilization. It was also discussed that the cells with a high electrolyte ratio have higher discharge capacities and lower deformability. Moreover, lower capacity degradation is obtained for cells with high electrolyte amounts and low sulfur loadings. However, the electrolyte amount should not exceed 4 $\mu L\ mg^{-1}$ because the dead weight of the cell then prevents to reach the energy densities provided by Li-ion cells [43].

Li-S cells typically use excess electrolyte in order to fully utilize the sulfur, decrease the polysulfide shuttle mechanism and prevent the electrolyte depletion in the cell. However, according to Eroglu *et al.* (2015), using an excess amount of electrolyte, or in other words having high electrolyte to sulfur ratios, results in a significant decrease in the system level

specific energy and energy density. As example, cells with electrolyte to sulfur (E/S) ratios of 10 mL/g and 1 mL/g provide pack-level energy densities of 100 Wh/kg and 400 Wh/kg, respectively [37].

The electrolyte amount has a great influence on the reaction kinetics since it determines the polysulfide concentrations on the cathode surface. Study performed by Fan and Chiang (2017) inspected the relationship between the polysulfide concentration and Li_2S electrodeposition kinetics [44]. It was proposed that the capacity of a battery is highly dependent on Li_2S electrodeposition. The experiments were conducted with E/S ratios of 7.9 (3.9 M S), 4.2 (7.4 M S) and 2.4 (13 M S) mL/gS at C/4 rate. 947 mAh/g of initial discharge capacity was obtained with the highest E/S ratio showing the standard discharge profile of Li-S cells. The same capacity was obtained with an E/S ratio of 4.2 mL/gS. However, here polarization was higher and cell voltage dropped to 1.81 V due to a high over-potential of 380 mV. Lastly, with 2.4 E/S ratio, much less capacity was obtained, less than 60 mAh/g. This is due to sulfur not being completely dissolved in the electrolyte because of the sulfur solubility limit of 8 M. It was concluded that, low E/S ratios result in sluggish electrodeposition of Li_2S and thus low specific capacities.

Another study was performed by Hagen *et al.* (2014) to investigate the dependence of cell energy density on the E/S ratio in Li-S cells [45]. Pouch cells with various E/S ratios and sulfur and carbon loadings were prepared to measure the energy densities. Sulfur loadings used between 0.5-20.0 mg/cm^2 with a constant 100 µl electrolyte volume results in E/S ratios of 5-20 mL/g. Energy densities of 150-300 Wh/kg were obtained with an E/S ratio of 5, which is comparable to the state-of-the-art Li-ion batteries in terms of the energy density but not in terms of safety and cyclability. To excel the Li-ion battery, 2/1 electrolyte to sulfur ratio was needed, which provides an energy density of 500 Wh/kg with 1300 mAh/g sulfur utilization at moderate current densities. However, cells having low E/S ratios tend to have significant capacity loss, which is possibly because of the Li-S reaction mechanism. With increasing polysulfide amounts in the electrolyte, the electrolyte viscosity thus, the electrolyte resistance increases. This can result in low discharge capacities.

Zhang (2012) claimed that there is an optimum electrolyte to sulfur ratio because the electrolyte amount is directly related to the polysulfide concentration. With the optimum E/S

ratio of 6.5 mL/g of the conventional DOL:DME liquid electrolyte, 72 % sulfur ratio and 2 mg/cm^2 sulfur loading, 780 mAh/g capacity can be obtained even after 100 cycles at 0.5 mA/cm^2. The effect of E/S ratios of 13.3 mL/g, 10 mL/g and 6.5 mL/g on the cycling were also investigated. The cell with excess electrolyte (13.3 mL/g) has 1000 mAh/g capacity in the first discharge and almost 800 mAh/g in the second cycle. This rapid decrease was because of the migration of the polysulfides to the dead zones inside the cathode. High polysulfide concentration in the cell with a low E/S ratio, 6.5 mL/g, resulted in short cycle life and reproducibility problems. On the other hand, the high viscosity of the electrolyte at low E/S ratios, which is due to higher polysulfide concentration in the electrolyte, prevents the polysulfides to escape from the cathode. Therefore, the capacity of the first cycles increase up to a point in the cells with low E/S ratios. However, capacity starts to decrease again as $LiNO_3$ is depleted in the cell. It was also stated that the type of the electrolyte, cathode thickness, active surface area and porosity of the conductive matrix and Li-S cell configurations affect the optimum E/S ratio in the cell [46].

Zheng *et al.* (2013) also examined the Li-S battery performance as a function of the E/S ratio with a sulfur-ketjen black composite cathode. S/E ratios of 15, 20, 30, 50, 75 and 100 g/L are tested galvanostatically at 0.2 C rate. In all cases, 2 discharge plateau were obtained. In the lowest S/E ratio (15 g/L), the cells suffered from the PS shuttle, low Coulombic efficiency and high capacity fading. However, increasing S/E ratio to 50 g/L improved the capacity retention to 66 % in the 100th cycle by oppressing the shuttle mechanism with increasing viscosity. After that point, the lower electrolyte amounts in the cell caused polarization due to wetting problems. However, it was stated that this optimum S/E ratio is only specific for the sulfur-ketjen black composite and optimizations are needed for the other configurations [47].

Urbonaite and Novak (2014), investigated the influence of electrolyte volume, the salt concentration, additive type, sulfur type and conductive type on the Li-S cell performance. 13, 22 and 43 µl/mg E/S ratios were tested. The best cyclability results are obtained with the E/S=22 µl/mg for both PEO and Kynar binders where E/S=43 µl/mg shows the poorest cell performance [25].

Sun *et al.* (2018) conducted a systematic performance analysis to investigate the impact of both electrolyte-to-sulfur ratio and sulfur loading. A novel carbon cathode was developed with sulfur, porous carbon, TiS_2, carbon black, PVDF and HPC and 12 different combination of cells were prepared with 60, 90, 120 µl electrolyte volume and 3, 6, 8 and 10 mg/cm^2 sulfur loading. According to their results, when the sulfur loading is kept constant and electrolyte volume decreases, the capacity and Coulombic efficiency also decrease due to infinite shuttling. It was concluded that high sulfur loadings and low E/S ratios cause fast lithium corrosion, which affects the performance intensely.

In these respect, there are various studies on optimization of the electrolyte amount in Li-S batteries [30], [43]–[45]. However, the effect of E/S ratio on the transport and kinetic resistances in the cell depending on the depth of discharge is not identified yet.

2.3. Previous Studies on the Characterization of Li-S Batteries Using EIS

Yuan *et al.* (2009) studied the electrochemical processes of formation, growth and dissolution of Li_2S in sulfur cathode during charge and discharge by using EIS [48]. When frequency range of 100 mHz-100 kHz with 5 mV signal amplitude is applied to the sulfur cathode, two different impedance spectra is obtained. It was concluded that these differences are due to the variation in the resistances in the high and the low voltage plateaus. The authors suggested that the semicircle obtained in the middle frequency range by EIS corresponds to the Li_2S formation on the cathode matrix, whereas the one in the high frequency range represents the charge transfer resistance at the carbon interface. The apparent drop of charge transfer resistances between the upper plateau and the beginning of the lower plateau shows that the reaction of $S \rightarrow Li_2S_x (8 \geq x \geq 4)$ has higher charge transfer resistance then the reaction of $Li_2S_x \rightarrow Li_2S_y (8 \geq x \geq y \geq 4)$. In addition, it was found that the interfacial charge transfer and the mass transport resistances are the rate determining factors in the upper and lower plateau regions, respectively. These were supported by conducting SEM, XRD and EDS characterizations techniques and it was concluded that EIS is a powerful technique to characterize the complex electrochemical reactions independently [48].

EIS method was also used by Barchasz *et al.* (2012) to investigate the impedance of sulfur cathode containing sulfur, carbon and binder at various degree of discharges [49]. The obtained spectrums contain two semi-circles. The increase in the size of the high frequency semi-circle between 2.065 V and 1.85 V was attributed to the change in the sulfur electrode morphology. In addition, the middle frequency semi-circle which appears in the very early discharge stages was attributed to the charge transfer resistance. The decrease in the charge transfer resistance implies that the reaction with the charge transfer occurs faster. In parallel to that, due to the high amount of insulating materials dissolution, the lowest resistance is obtained in the half of the discharge. However, after that point the non-conductive solid products produce and that increase the charge transfer resistance again. Finally, surface of the electrode is blocked with these insulating layers at the end of the discharge which appeared as a line in the low frequency region of the EIS spectrum.

Another work by Canas *et al.* (2013) investigated the behavior of a Li-S cell with the sulfur cathode having 50 wt. % sulfur, 40 wt. % carbon black and 10 wt. % PVDF, at equal depth of discharge intervals using EIS. They have proposed an equivalent circuit with an ohmic resistance and four R//CPE elements to simulate semicircles. Charge transfer resistance, Li_2S nonconductive layer resistance and diffusion were selected as the main impedance elements and their change as a function of the depth of discharge and cycling were investigated. They proved that individual impedances are highly dependent on the depth of discharge of the cell. It is observed that, the highest polysulfide concentration results in the highest electrolyte resistance, which is obtained in 43 % depth of discharge. EIS results for 50 cycles show that, the electrolyte and anode impedances stay almost constant whereas 71 % decrease occurs in the charge transfer resistance with cycling [50].

Yan *et al.* (2016) used a binder free MWCNT-sulfur composite as the positive electrode to test the effect of electrolyte-to-sulfur ratio. First, the effect of E/S ratio of 5, 8 and 12 µl/mg on the cycling performances were tested. The highest initial capacity was obtained with the E/S ratio of 12 µl/mg but this cell suffered from severe capacity loss, 61 % of the initial discharge capacity, whereas the cell with 5 µl/mg E/S ratio showed a lower initial discharge capacity but have lost only 30.5% of its capacity after 100 cycles. The sulfur utilizations at the 100^{th} cycle were 48.5, 46.7 and 38.0 % for E/S ratios of 5, 8, 12 µl/mg, respectively. With considering both the Coulombic efficiency, peak discharge capacity and

capacity retention, 8 µl/mg has the optimum amount of the electrolyte. The capacity of the cells has decreased after 40 cycles even though the electrolyte contains $LiNO_3$ and this indicates that there are other factors that causes capacity decay. The impedances of these cells were measured by EIS after the 100^{th} cycle for fully charge and discharge states. There were 2 semicircles in the fully discharged whereas only one semi-circle in the fully charged state. Therefore, the semi-circle in the low frequency was defined as the resistance due to Li_2S/Li_2S_2 nonconductive films. It was seen that high electrolyte amount improves the charge transfer but it also causes a thicker nonconductive film. The impedances of the first discharge and charge of the cell with an E/S ratio of 12 µl/mg at various DOD's were also investigated to study the Li_2S/Li_2S_2 layer formation and sulfur agglomeration kinetics. The second semicircle was obtained in the second plateau supporting that the medium frequency depressed semi-circle represents the film resistance. It was concluded that the loss of sulfur, non-conductive Li_2S_2 and Li_2S precipitation and incomplete conversions are the main causes of the capacity fade [51].

Sun *et al.* (2016), investigated the sulfur loading effect on the performance of the Li-S cells by testing 0.5-7.5 mAh/cm^2 cells. For loadings smaller than 1.40 mg/cm^2, 50 % sulfur utilization (i.e. 800 mAh/g S) was obtained. These cells also showed 350 mAh/g S capacity in the 100^{th} cycle after a continuous capacity decay. For 1.85-2.38 mg/cm^2 sulfur loading, after 30 cycles of activation period, the cells also experienced capacity decay. Finally, for loadings higher than 4.18 mg/cm^2, only 150 mAh/g capacity was obtained due to the limitations in a very thick cathode. In this study, EIS was also used to study these trends stemming from sulfur loadings by comparing the cells having 0.77 mg/cm^2 and 2.62 mg/cm^2 loadings. The interface resistance decrease in the first cycle until 39 cycles is due to an increase in the sulfur utilization with redistribution of the sulfur into the active sites. According to their results, the interface resistance for the completely discharged and charged states have similar values after cycling for 40 cycles. It was explained by the eliminating the structural difference of the complete charge and discharges states for both high and low sulfur loadings. On the other hand, charge transfer resistance for the completely discharged state is high whereas no distinct difference was obtained due to other charged states and sulfur loadings. It was concluded that the charge transfer resistance was stemming from the Li_2S/Li_2S_2 film. Lastly, the highest electrolyte resistance was obtained at 2.1 V where polysulfide concentrations were at the highest amount for both loadings. Therefore, when

there are no polysulfides present, the electrolyte resistance should be at its lowest value, namely at the both the charge and discharge states. However, for 2.62 mg/cm^2 sulfur loading, the electrolyte resistance in the fully discharged state is higher than fully charged state for the first 12 cycles. This was attributed to non-efficient transformation of Li_2S/Li_2S_2 film in the first cycles and it increases the electrolyte resistance in the complete discharge [52].

To conclude, even though the effect of E/S ratio and C/S ratio on the capacity and cycling performances have been investigated before, there is no study to identify the effect of these parameters on the reaction and degradation mechanism of the Li-S cells as functions of DOD using EIS as the characterization technique. Some of the literature works which use EIS in various depth of discharges are given in the Table 2.1.

Table 2.1. The Literature Summary for EIS Experiments. (a:C/S ratio, b:S loading(mg/cm^2) c:Cathode thickness(μm), d:Electrolyte volume(μl), e:Frequency range(Hz), f:Signal amplitude(mV), g:DOD, h:Voltage range(V) and C rate)

Ref.	**a**	**b**	**c**	**d**	**e**	**f**	**g**	**h**
[53]	1/7	1.2	20	NP	1-65,000	<4	0.01-5-90-110-285-290-470-840-870 mAh/g	1.5-2.8 0.2 mA/cm2
[21]	4/5	NP	NP	14	0.06-100,000	5	0,10,20,30,40,50,60,70,80,90,100	1.5-2.8 0.18C
[50]	4/5	NP	NP	14	0.06-100,000	5	0-8-16-27-34-44-52-62-71-81-90-99-100	1.5-2.8 300 mA/g
[49]	1/8	NP	20	150	0,001-200,000	5	2.065-2.06-2.05-1.85V	1.5-3.0 0.1C
[54]	52/38	NP	NP	NP	0.01-100,000	5	NP	1.0-3.0

Table 2.1. The Literature Summary for EIS Experiments. (a:C/S ratio, b:S loading(mg/cm^2) c:Cathode thickness(μm), d:Electrolyte volume(μl), e:Frequency range(Hz), f:Signal amplitude(mV), g:DOD, h:Voltage range(V) and C rate) (cont.)

Ref.	**a**	**b**	**c**	**d**	**e**	**f**	**g**	**h**
[52]	3/6	0.77 1.29 2.62	15 25 52	80	0.05- 500,000	5	1.8-2.1-2.6 V	1.8-2.6 0.2C
[55]	3/6	2	85	25	0.01- 100,000	10	NP	NP
[56]	1/1	3.5	NP	NP	0.01- 100,000	5	1.792-2.009-2.169-2.412- 2.800 V	NP-1.7
[57]	27/ 53	NP	30	NP	0.01- 100,000	5	0-11-22-33-45-56-67-78- 98	1.6-2.8 100 mA/g
[48]	3/6	1.5	NP	NP	0.1- 100,000	5	0-8-14-30-46-52	1.5-2.5 100 mA/g

3. EXPERIMENTAL WORK

This section includes the description of the construction and the testing of the Li-S cells in details. The effect of C/S and E/S ratios on the cell resistance is investigated using the conventional materials of lithium-sulfur batteries: lithium foil as the anode, an organic electrolyte and the composite cathode consisting of sulfur, carbon black and binder. EIS spectrums are analyzed with Z-fitting procedure.

3.1. Chemicals

In this section, the chemicals used for the experiments are provided. The chemicals needed for the cathode preparation are as follows: conductive carbon black (Super C65, MTI), sulfur (Sigma Aldrich), polyvinylidene difluoride (PVDF, MTI) as the binder, N-methyl-2-pyrolidone (NMP, MTI) as the solvent and 15 μm thick aluminum foil (MTI) as the current collector. Lithium metal foil (MTI) with 170 μm thickness is used as the anode together with 25 μm copper foil (MTI) current collector. 1,3-Dioxolane (DOL, Sigma Aldrich), 1,2-dimethoxyethane (DME, Sigma Aldrich), lithium nitrate ($LiNO_3$, Sigma Aldrich) and lithium bis-trifluoromethanesulfonimide (LiTFSI, Sigma Aldrich) are used for the electrolyte preparation. A 25 μm thick polymer-based separator (Celgard) is used in between the anode and the cathode.

3.2. Cell Preparation

Cells are prepared with lithium foil anode, polymer separator, sulfur cathode and organic electrolyte. Li foil and polymer separator are directly used. However, cathodes and electrolytes are prepared according to the following procedure.

3.2.1. Cathode Preparation

Cathodes with different C/S ratios are prepared according to the following procedure. The preparation of a cathode with C/S=1 is described below as an example. For a cathode

with C/S=1, Sulfur/Carbon/Binder weight ratios are adjusted as 45/45/10. In order to do that, 500 mg of cathode mixture is prepared by the following procedure;

(i) First, 225 mg sulfur and 225 mg carbon black are mixed.

(ii) Sulfur-carbon mixture is put in the mortar and pestle for 5 min (To avoid binder loss, it is not added in this step).

(iii) 50 mg binder is added to the mixture and mixed.

(iv) Perfect mixing of the carbon, sulfur and binder and the dissolution of the final mixture in the solvent is very important for obtaining good coatings. Therefore, this mixture is mixed slowly with NMP, in which the total solvent added is 7:1 wt/wt ratio of the NMP and solid mixture eventually.

(v) For a better dispersion, the mixture is first mixed at 50 °C for 2 hours and then at room temperature for overnight in a magnetic stirrer. Finally, 2 hours of ultrasonic treatment is performed to obtain perfect mixing and to remove bubbles.

(vi) The doctor blade is set to 320 μm thickness and the slurry is casted on the less shiny side of the Al foil by gliding the doctor blade over the slurry.

(vii) The Al foil with the cathode layer is dried at 50 °C for almost 7 h in air atmosphere to remove NMP.

(viii) Cathodes with 2.01 cm^2 area is cut with a puncher and they are weighed before the experiments to calculate the sulfur loadings in the cathode.

The final thicknesses of the cathodes after drying are 70 μm for all of the C/S ratios. To obtain that thickness, the NMP amount added and the doctor blade thickness set are adapted accordingly. The picture of the prepared cathode with C/S=1 is given in Figure 3.1.

Figure 3.1. Prepared cathode film with C/S = 1.

The effect of E/S ratio is investigated by keeping C/S ratio and S loading constant at 1 and 0.9-1.1 mg/cm^2, respectively. Therefore, the same cathode is used for all of the E/S ratio experiments. On the other hand, to investigate the effect of the C/S ratio, different cathodes with desired C/S ratios are prepared with the same procedure described above. The only difference is the amount of carbon and sulfur used when preparing the cathode mixture. In these experiments, since the cathode thickness is kept constant, S loading varies with changing C/S ratio.

3.2.2. Electrolyte Preparation

The electrolyte used for all of the experiments is a conventional DOL:DME (1:1 vol.%) electrolyte with 1 M LiTFSI electrolyte salt and 0.1 M $LiNO_3$ electrolyte additive. First, equal volumes of DOL and DME are mixed in an erlanmayer to get 1:1 volume ratio solution. Then, this mixture is mixed with the required amounts of LiTFSI and $LiNO_3$ to get 1 M and 0.1 M concentrations in 10 ml of liquid electrolyte, respectively. Electrolyte preparation is carried out in MBraun Labstar Glovebox where both oxygen and water contents are below 0.5 ppm.

3.2.3. Coin Cell Assembly

2 electrode CR2032 coin cells are used for both capacity and impedance measurements. The cells are prepared in the same glove box where oxygen and water levels are below 0.5 ppm. First, lithium foil is punched to get 2.01 cm^2 pure metallic Li anode. Similarly, polymer separator film is prepared and it has 3.1 cm^2 area. Bigger separator is used to effectively separate the Li anode and S cathode to prevent short circuit inside the cell.

First one spring and one spacer are placed in the lower case with the O-ring. Copper and lithium foils are put above them. Then, the half of the previously determined electrolyte volume is placed in the anode part. Polymeric Celgard separator is placed subsequently ensuring the separator is placed in the middle so that the contact of anode and cathode is prevented. The rest of the electrolyte is then added for the cathode part. Finally, the sulfur cathode with Al foil is placed on the top and one more spacer is added to fill the extra space.

With the addition of the upper case, cell preparation is completed. Finally, the cell is crimpled in the cell crimper and taken out of the glove box for the EIS tests. The schematic of the coin cell preparation can be seen in Figure 3.2.

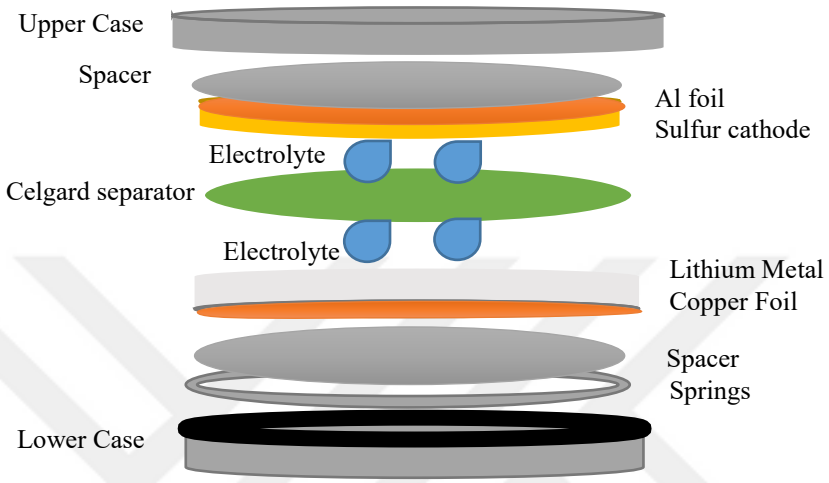

Figure 3.2. Coin cell components.

All of the experiments are performed 3 times and the average of these replicate experiment results are considered. The investigated E/S ratios with C/S=1 are 33, 19, 12, 6 and 3 µl/mg.

Cathode mass measured is the total mass of the positive electrode together with Al foil current collector. To find the electrode mass, the mass of the current collector is subtracted from the total cathode mass, as given in Equation (3.1) for an example 11.3 mg cathode. The Al foil mass for 2.01 cm^2 disc is found by averaging the mass of 5 samples and this average is found as 8.14 mg. Since the C/S ratio is 1 for this case (45 wt. % S in the cathode), the S amount is found by multiplying the cathode mass with 0.45, Equation (3.2). Sulfur loading of the cathode is found by dividing the sulfur amount to the cathode area, Equation (3.3). Since C/S ratio is constant the sulfur loading is around 0.8 mg/cm^2 for all of the E/S experiments. Then, E/S ratio is found by dividing the electrolyte volume to the sulfur amount, Equation (3.4). Finally, the discharge current is calculated to get C/10 rate for each cell, which is the current required to discharge the cell for 10 h, Equation (3.5).

$$\text{Cathode Mass} = 11.3 - 8.14 = 3.16 \text{ mg} \tag{3.1}$$

$$\text{Sulfur Mass} = \text{Cathode Mass x S wt.\%} = 3.16 \text{ x } 0.45 = 1.4 \text{ mg} \tag{3.2}$$

$$\text{S Loading} = \frac{\text{Sulfur Mass}}{\text{Cathode Area}} = \frac{1.4}{2.01} = 0.9 \text{ mg/cm}^2 \tag{3.3}$$

$$\frac{\text{E}}{\text{S}}\text{Ratio} = \frac{\text{Electrolyte Volume}}{\text{Sulfur Mass}} = \frac{50 \text{ µl}}{1.4 \text{ mg}} = 35.2 \text{ µl/mg} \tag{3.4}$$

$$\text{Current Rate} = \frac{1675 \frac{\text{mAh}}{\text{g S}}}{10 \text{ h}} \text{x Sulfur Mass} = 167.5 \frac{\text{mA}}{\text{g S}} \text{ x } 1.4 \text{ mg S} = 238.2 \text{ µA} \tag{3.5}$$

The cell parameters calculated as described above are given for all replicate cells in Table 3.1.

Table 3.1. Cell Parameters for E/S Experiments.

Cathode Total (mg)	Cathode Mass (mg)	Sulfur Mass (mg)	Sulfur Loading (mg/cm^2)	Electrolyte Volume (µl)	E/S Ratio (µl/mg)	Discharge Current (µA)
11.3	3.16	1.4	0.7	50	35.2	238.2
11.4	3.26	1.5	0.7	50	34.1	245.7
11.6	3.46	1.6	0.8	50	32.1	260.8
11.6	3.46	1.6	0.8	30	19.3	260.8
11.6	3.46	1.6	0.8	30	19.3	260.8
11.6	3.46	1.6	0.8	30	19.3	260.8
11.7	3.56	1.6	0.8	20	12.5	268.3
11.7	3.56	1.6	0.8	20	12.5	268.3
11.7	3.56	1.6	0.8	20	12.5	268.3

Table 3.1. Cell Parameters for E/S Experiments. (cont.)

Cathode Total (mg)	Cathode Mass (mg)	Sulfur Mass (mg)	Sulfur Loading (mg/cm^2)	Electrolyte Volume (µl)	E/S Ratio (µl/mg)	Discharge Current (µA)
11.8	3.66	1.6	0.8	10	6.1	275.9
11.9	3.76	1.7	0.8	10	5.9	283.4
11.9	3.76	1.7	0.8	10	5.9	283.4
12.1	3.96	1.8	0.9	5	2.8	298.5
12.1	3.96	1.8	0.9	5	2.8	298.5
12.1	3.96	1.8	0.9	5	2.8	298.5

For the investigation of the effect of C/S ratio, the C/S ratios are adjusted as 3.5, 2, 1, 0.5 and 0.3 with E/S=19 µl/mg. A similar calculation procedure is carried out to obtain the cell parameters given in Table 3.2.

However, in this case the electrolyte volume is recalculated in each cell to obtain 19 µl/mg E/S ratio. For example, for a C/S ratio of 3.5 the following calculations are done different from the previous calculations;

$$\text{S Amount} = \text{Cathode mass x S wt.\%} = 0.00266 \text{ x } 0.7 \text{ x } 1000 = 0.5 \text{ mg} \tag{3.6}$$

$$\text{Electrolyte Volume} = \frac{\text{E}}{\text{S}} \text{ Ratio x Sulfur Mass} = 19 \ \frac{\mu\text{l}}{\text{mg S}} \text{x } 0.5 \text{ mg} = 10.1 \ \mu\text{l} \tag{3.7}$$

Similarly, all the cell parameters for 3 replicate cells are given in the Table 3.2.

Table 3.2. Cell Parameters for C/S Experiments.

C/S Ratio	Cathode Total (mg)	Cathode Mass (mg)	Sulfur Mass (mg)	Sulfur Loading (mg/cm^2)	Electrolyte Volume (µl)	Current Rate(µA)
3.5	10.8	2.66	0.5	0.3	10.1	89.1
3.5	10.8	2.66	0.5	0.3	10.1	89.1
3.5	10.8	2.66	0.6	0.3	10.5	92.5
2	12.7	4.56	1.4	0.7	26.0	229.1
2	12.0	3.86	1.2	0.6	22.0	194.0
2	13.2	5.06	1.5	0.8	28.8	254.3
1	11.6	3.46	1.6	0.8	19.3	260.8
1	11.6	3.46	1.6	0.8	19.3	260.8
1	11.6	3.46	1.6	0.8	19.3	260.8
0.5	14.6	6.46	3.9	1.9	73.6	649.2
0.5	14.4	6.26	3.8	1.9	71.4	629.1
0.5	15.2	7.06	4.2	2.1	80.5	709.5
0.3	13.7	5.56	3.9	1.9	73.9	651.9
0.3	13.8	5.66	4.0	2.0	75.3	663.6
0.3	13.9	5.76	4.0	2.0	76.6	675.4

3.3. Electrochemical Characterization Experiments and Analysis Method

3.3.1. Electrochemical Characterization Experiments

The impedance measurements are performed with Biologic SP300 potentiostat/galvanostat at room temperature. The cells are rested for 16 hours at the open cell voltage (OCV) for the stabilization after cell construction. The impedance measurements are taken at different depth of discharges with C/10 discharge current rate at 1.5 V-3.0 V voltage interval. The EIS measurements are performed within 10 mHz and 100 MHz

frequency range and with 10 mV signal amplitude at constant voltage. In addition, at each discharge depth after discharge, the cells are equilibrated for 30 minutes to allow the cell to reach thermal and electrochemical equilibrium before the EIS measurements.

3.3.2. EIS Fitting Analysis

EIS is applied with 10 mV signal amplitude in the 100 MHz-10 mHz frequency range. The frequency response of the system to the sinusoidal signal with 10 mV applied potential is analyzed by Nyquist plots and this response depend on cell impedance which is represented with Figure 3.3.

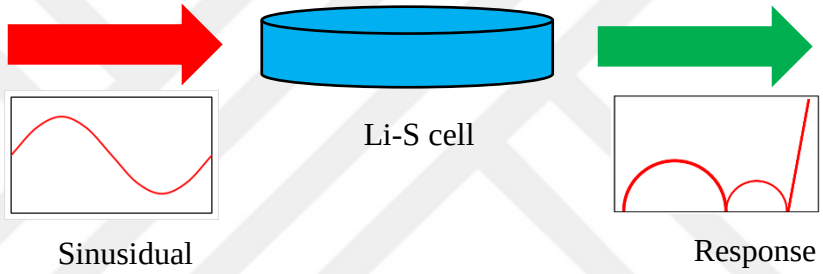

Figure 3.3. EIS analysis.

During the EIS, the response of the signal is recorded by the voltage (v(t)) and the phase shift ϕ [58]. The general formula for a cell impedance is shown in the Equation (3.8).

$$\bar{Z} = |\bar{Z}| \frac{\sin(\omega t)}{\cos(\omega t - \phi)} \tag{3.8}$$

where $|\bar{Z}|$ is the absolute value of impedance and ω is the angular frequency. Frequency response can be divided to real and imaginary impedances and can be expressed with Equations (3.9), (3.10) and (3.11).

$$\mathrm{Re}(Z) = |\bar{Z}| \cos(\phi) \tag{3.9}$$

$$\mathrm{Im(Z)} = |\bar{\mathrm{Z}}| \sin(\phi) \tag{3.10}$$

$$|\bar{\mathrm{Z}}| = \sqrt{\mathrm{Re(Z)}^2 + \mathrm{Im(Z)}^2} \tag{3.11}$$

With the equations of Re(Z) and Im(Z), cell impedances can be shown in the Nyquist plots for better visualization and easily interpret the results [59]. In order to relate the EIS spectrums to the physical and electrochemical processes taking place in the cell, an equivalent circuit model should be fitted to the impedance raw data. In this work, the EIS fittings are performed with Bio-Logic Zfit software and the fitting method is chosen as the "Randomize+Simplex" method with 1000 fitting and randomization iterations. The most suitable fit can be found with the best initial values; therefore, randomization is performed before minimization. In addition, the quality of the fittings is tested with the $\chi^2/|Z|$ where χ^2 shows the difference between the experimental and fitting values in Ω^2 and $|Z|$ is the modulus in Ω. So the minimization of the fit is done to obtain minimum $\chi^2/|Z|$ in Ω using Downhill simplex minimization method [60].

The fitting elements discussed in this work are listed in the Table 3.3.

Table 3.3. The EIS Fitting Elements Considered in This Work.

Circuit Element	**Faradaic Impedance**	**Nyquist Representation (-Im(Z) vs. Re(Z))**
Capacitor (C)	$\mathrm{Z(f)} = \frac{1}{\mathrm{C_1 i2\pi f}}$	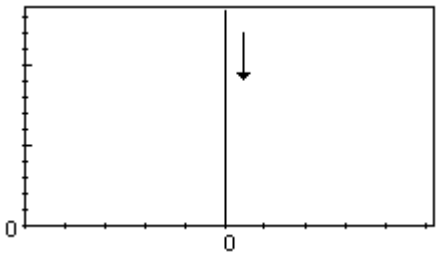
Constant Phase Element (CPE)	$\mathrm{Z(f)} = \frac{1}{\mathrm{Q_1(i2\pi f)^{\alpha_1}}}$	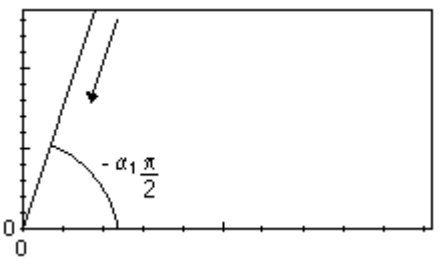

Table 3.3. The EIS Fitting Elements Considered in This Work. (cont.)

Circuit Element	Faradaic Impedance	Nyquist Representation (-Im(Z) vs. Re(Z))
Resistor	$Z(f) = R_1$	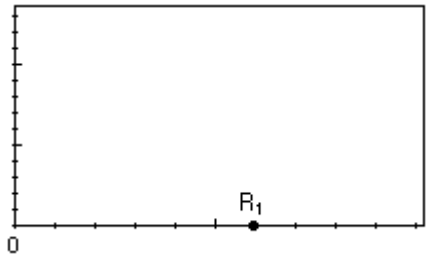
Warburg	$Z(f) = \frac{\sqrt{2}\sigma_1}{\sqrt{i2\pi f}}$	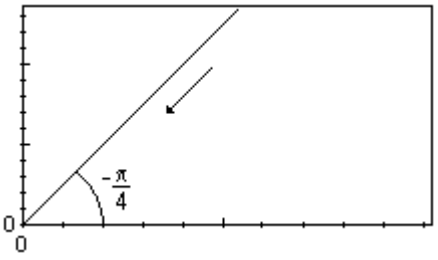

3.3.3. Stabilization of the Cells

When the EIS spectra were taken at a DOD immediately after discharging, unexpected profiles were obtained in the low frequencies. For example, the EIS spectrums in Figure 3.4 were taken immediately after discharging the cell for 30 minutes at 0.1 C rate. As can be seen in Figure 3.4, there are unexpected shapes at the low frequencies of the EIS spectra. According to the literature, these shapes may occur in the high frequencies and in that situation, they imply induction within the Li-S cell. However, for low and middle frequencies, these shapes show that, the cell is suffering from thermal and electrochemical instabilities [61], [62]. To eliminate these instabilities, the cells should be stabilized after each disruption. Therefore, the cells should be rested prior to the EIS measurements after each discharge period.

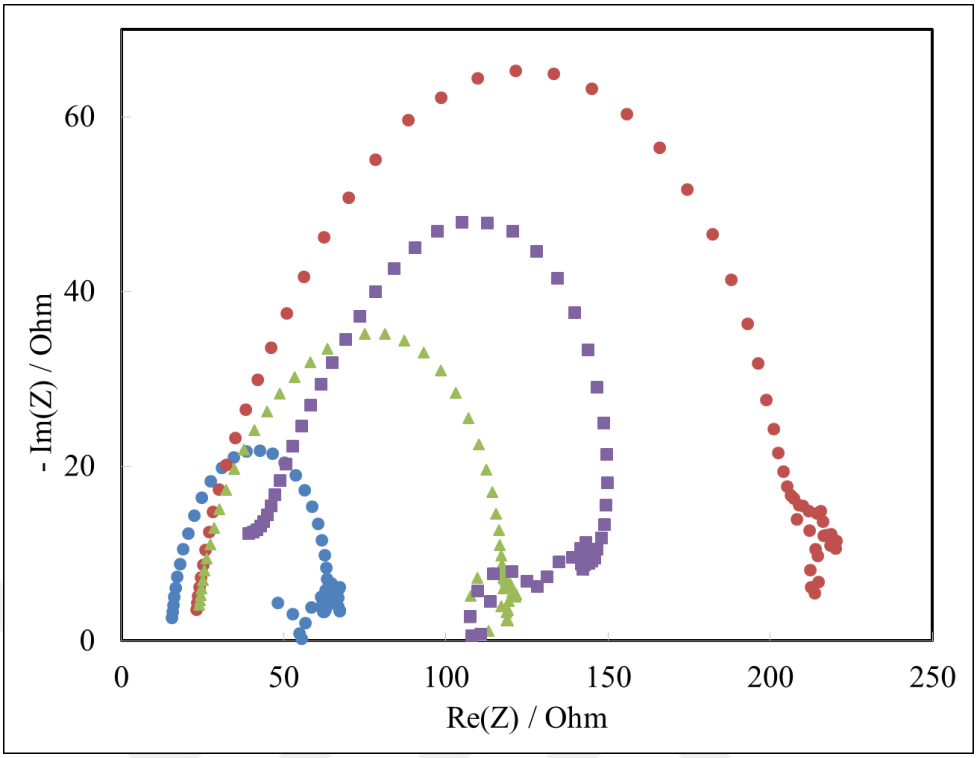

Figure 3.4. EIS spectrums immediately after discharges.

Cells are disturbed when they are discharged at a constant current. Hence, the unexpected shapes (red spectrum) are obtained in the middle and low frequency due to drifting when the impedance measurement is taken right after the discharge. It is shown that resting at OCV for 20 min is enough for the cells to stabilize. However, a smoother EIS spectrum is obtained for 30 minutes resting period. After that point, although the spectrums are smooth, relatively bigger semi-circles are obtained. In order to get the impedance at each DOD with a minimum amount of rest time, 30 minutes resting period is chosen. Therefore, for all of the DOD points, the cells are stabilized for 30 minutes before conducting the EIS measurements.

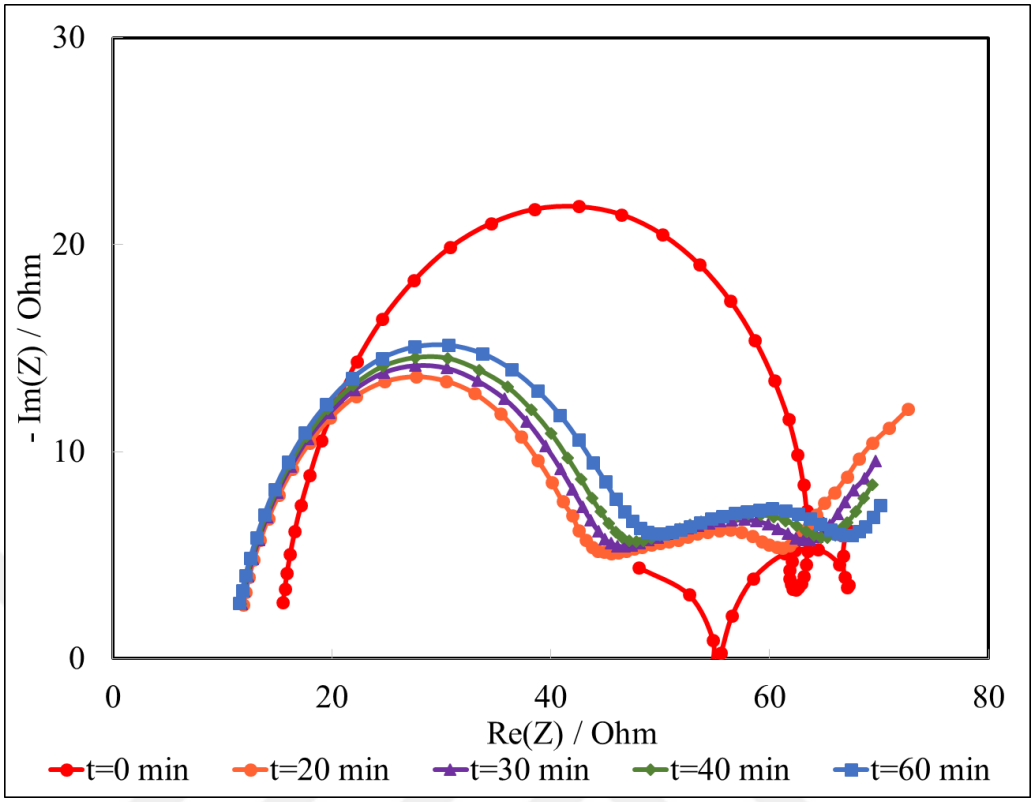

Figure 3.5. EIS Spectrum of the same Li-S cell after 30 min of discharge followed by various resting periods at OCV

4. RESULTS AND DISCUSSION

The results of the electrolyte-to-sulfur (E/S) and carbon-to-sulfur (C/S) ratio experiments are presented and their effect on the electrolyte, charge transfer and film resistances are discussed in this chapter of the thesis. First, calculations of DOD points for a cell are presented and the EIS spectrums of one representative cell is given for all DODs for each ratio. Next, these EIS results are compared in selected DOD points. Finally, the effect of E/S and C/S ratios and their change during discharge are discussed for each individual resistance.

4.1. Discharge Curves and Impedance Measurements

As stated in the experimental section, the discharge C rate is decided as C/10 in the experiments. Electrical vehicles spent different energies in different situations. For example, C/30 rate can be taken as the base discharge rate or C/100 for energy recovery while braking. C/10 can be adapted to real world as light acceleration and it is one of the highest C rate an EV needs [63]. In addition, C/10 rate is one of the most commonly used current rate in the literature [25], [64]–[66].

In Figure 4.1, the voltage profile of a Li-S cell discharged at C/10 can be seen. As can be seen from the cell voltage versus time graph in the figure, the cell is discharged with C/10 discharge rate for a certain time. It is important to have sufficient amount of data points for a cell. Therefore, the discharge intervals are kept short to ensure that data points are enough to represent the impedances of the cells. This is followed by the OCV resting period for 30 minutes. The EIS spectrums are then taken after each of these resting periods until the 1.5 V voltage is reached. The final EIS measurements are performed after reaching 1.5 V and waiting for another 30 min to get the impedance at fully discharged state of the battery.

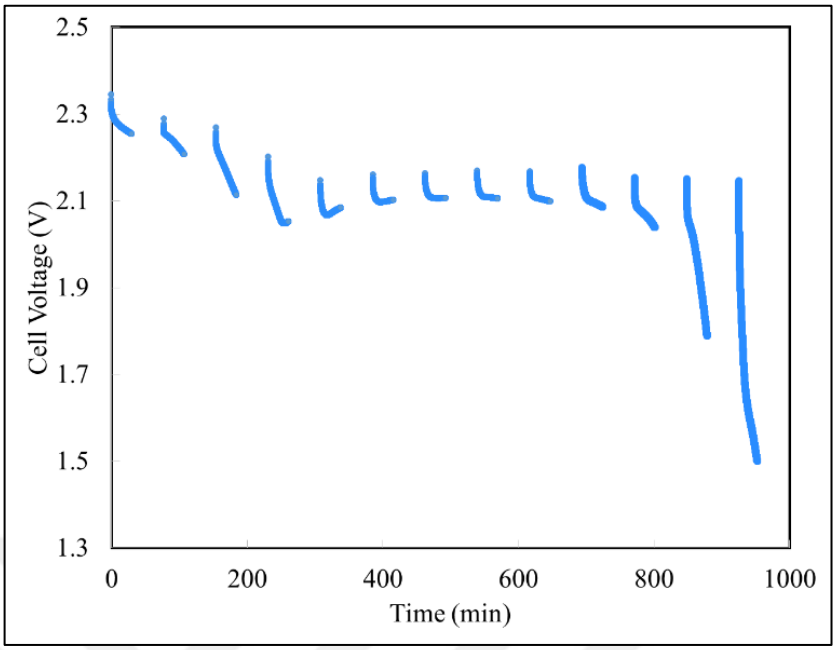

Figure 4.1. The discharge profile of a Li-S cell with C/S=1 and E/S=19 µl/mg at 0.1 C.

The cell voltage versus capacity graph for the same cell can be seen in Figure 4.1. In this study, the degree of discharge is calculated based on the capacity of the corresponding cell rather than the theoretical capacity, 1675 mAh/mg S, with the Equation (4.1). Therefore, obtained DODs are different for different cells even though they are discharged for similar intervals. For instance, for the cell in Figure 4.2, the obtained discharge capacity is 1080.6 mAh/gS and the capacity contribution of each interval is 83.8 mAh/gS, which is calculated for the discharge time of 30 min with 275.9 mAh current rate for the Li-S cell containing 1.65 mg of sulfur.

$$\text{DOD } \% = \frac{\text{Cell Obtained Capacity}}{\text{Cell Actual Capacity}} \text{x}100 \tag{4.1}$$

$$\text{DOD } \% = \frac{83.8 \text{ mAh/gS}}{1080.6 \text{ mAh/gS}} \text{x}100 = 8 \ \% \tag{4.2}$$

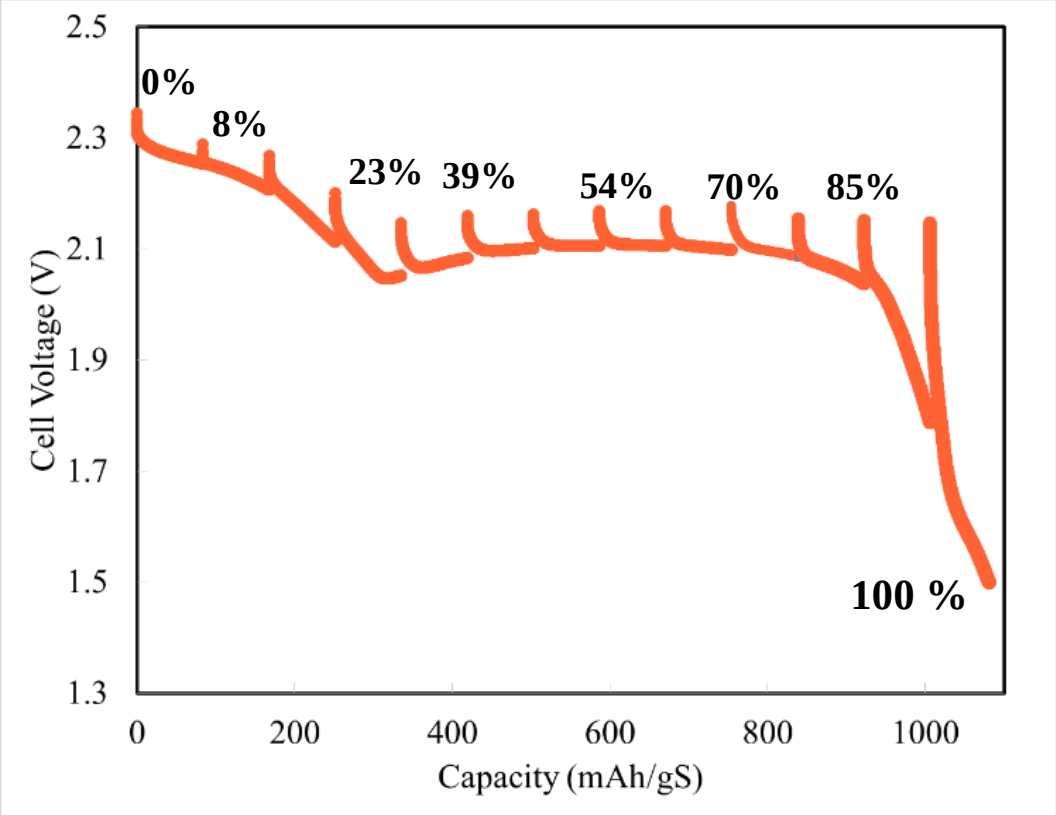

Figure 4.2. The discharge profile, which is based on cell capacity, of a Li-S cell with C/S=1 and E/S=19 µl/mg at 0.1 C. EIS measurements are conducted at each DOD shown in the figure.

The EIS spectrum of the Li-S cell with C/S=1 and E/S=19 µl/mg at 47% DOD shown in Figure 4.3. As it can be seen from the figure, there are 2 semi-circles in the high frequency region and one straight line in the low frequency region in the EIS spectrum for this point. The first semi-circle, the one on the left, is more obvious than the second one and the size of the first semi-circle is significantly higher than the size of the second one. However, in order to get the individual impedances, the experimental data should be fitted to an equivalent circuit. The equivalent circuit should represent the physical phenomenon taking place in the cell. With the proposed equivalent circuit, Z-fitting is carried out for this experimental data and the result is also given in the Figure 4.3.

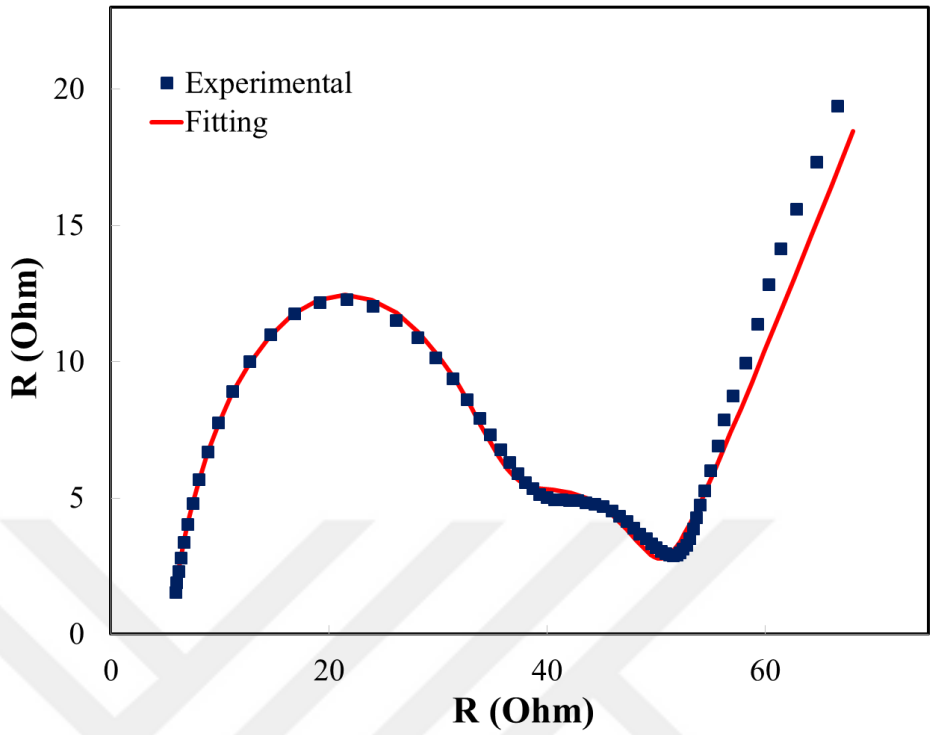

Figure 4.3. The EIS spectrum at 47 % DOD of the cell with E/S=19 µl/mg and C/S=1.

In EIS analysis, semi-circles are modelled with one constant phase element (Q) or capacitance and one resistance (R), which are in parallel to each other (Q//R or C//R). Since the cells are not at ideal conditions, a constant phase element is typically used rather than a capacitor [50]. As shown in Figure 4.3, we observed two semi-circles in most of the EIS spectrums, and therefore, two Q//R in series is proposed in the equivalent circuit. There are many examples of equivalent circuits which proposed two semi-circles in series in the literature and those support our proposed circuit [17], [35], [48], [67]. In the circuit, prior to Q//R, we used one resistance in the high frequency region. This represents the difference between y-axis and the beginning of the first semi-circle. In addition, a Warburg resistance (W) is used to simulate the linear line in the low frequency region (Figure 4.3). The proposed equivalent circuit diagram with four proposed circuit elements with a Nyquist plot are shown in the Figure 4.4.

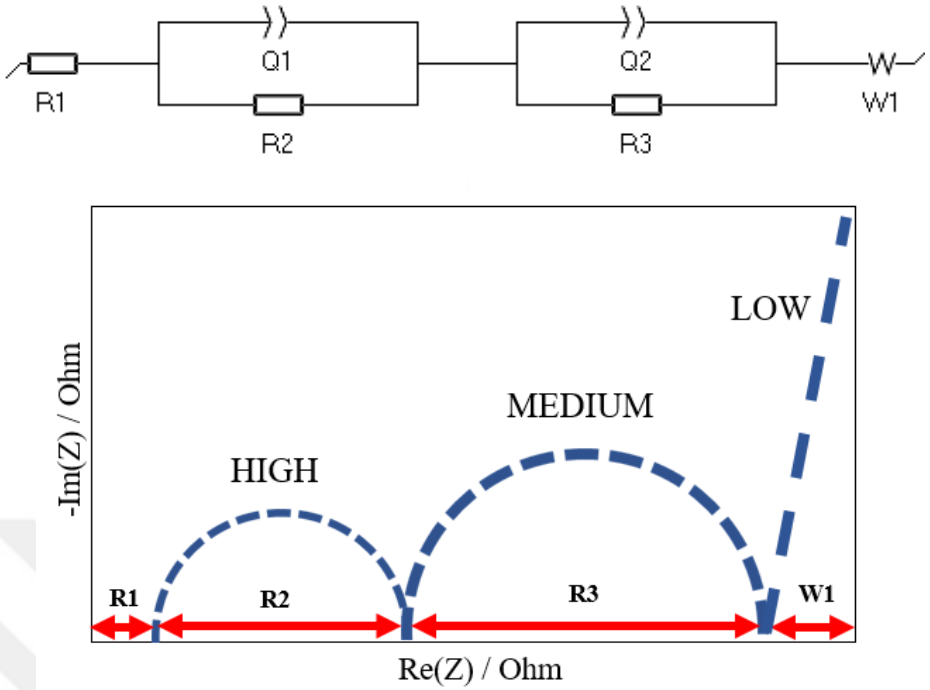

Figure 4.4. The proposed equivalent circuit for Z-fitting.

Using the proposed equivalent circuit model, EIS impedances are linked to the characteristic processes taking place in the Li-S cell. As a result, the corresponding resistances are extracted from the data after the identification of each of the resistances. When the previous studies in the literature are investigated in detail and the obtained spectrums are evaluated as a function of the degree of discharge, the circuit elements are defined as summarized in the Table 4.1.

Table 4.1. Summary of Resistances Attributed to Proposed Circuit Element.

R1	Electrolyte resistance
R2	Charge transfer resistance
R3	Non-conductive film resistance
W1	Warburg diffusion resistance

To sum up, there are 3 main resistances and one Warburg resistance in our cells. This equivalent circuit is used in fitting for all of the cells at each DOD. 3 replicate cells are made

for each E/S and C/S ratios and the average of the resistances obtained by fittings are taken as results.

4.2. The Effect of E/S Ratio on the EIS Results of Li-S Cells

4.2.1. The Effect DOD on the Cell Resistances for Different E/S Ratios

The EIS results of cells having E/S ratios of 34, 19, 12, 6 and 3 µl/mg are shown in the Figures 4.5-4.8, respectively. These results are shown here for one representative cell of each E/S ratio; the results of the replicate cells can be found in the Appendix A. As stated in the previous section, since DODs are calculated based on the cell's actual capacity, the DOD's obtained for the cells are different from each other.

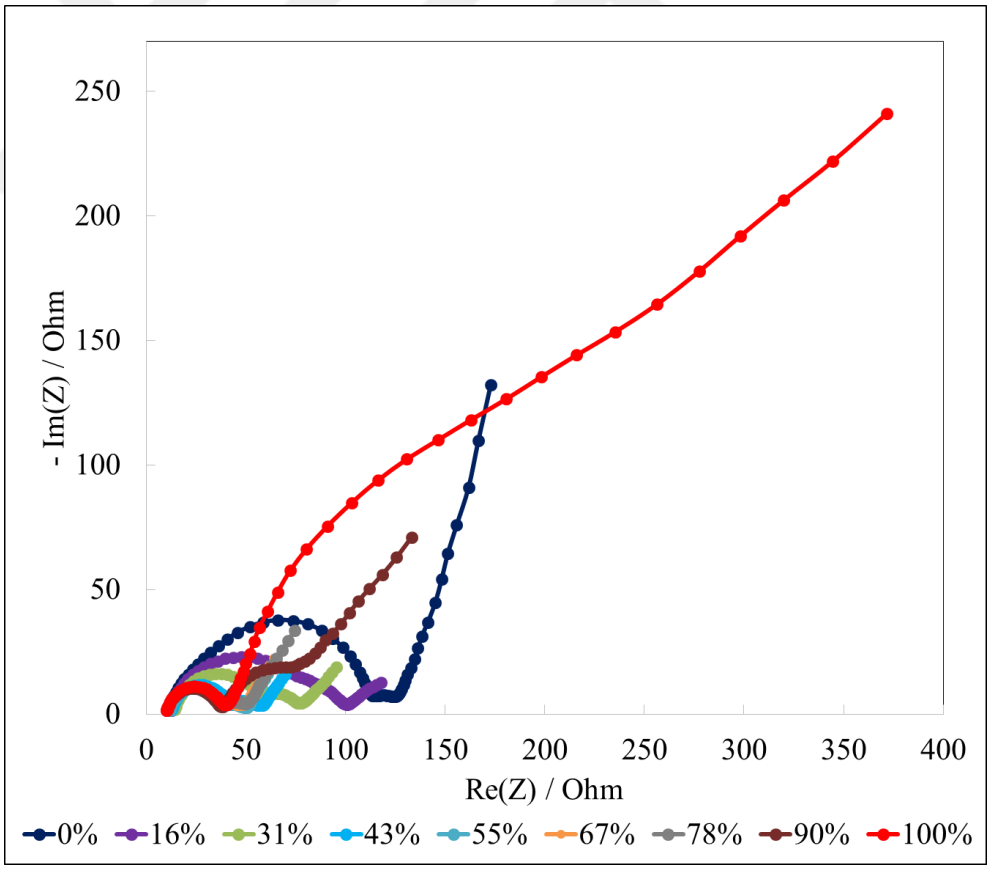

Figure 4.5. The EIS spectrums of the cell with E/S=34 µl/mg for different discharge depths.

In Figure 4.5, the EIS spectrum for E/S=34 µl/mg is shown. According to the figure, in the complete charge of the cell (DOD=0%), the semi-circle in the high frequency is much bigger than the semi-circle in the medium frequency suggesting that in the complete charge, charge transfer resistance is much higher than the film resistance. Up to a certain degree of discharge, the radius of the high frequency semi-circle is higher than the middle frequency semi-circle. However, with increasing DOD, the radius of the middle frequency semi-circle is increasing and towards the end of the discharge, the radius of the second semi-circle is much higher than the first one. This means that, towards the end of the discharge, film transfer resistance becomes more important and a more restricting factor.

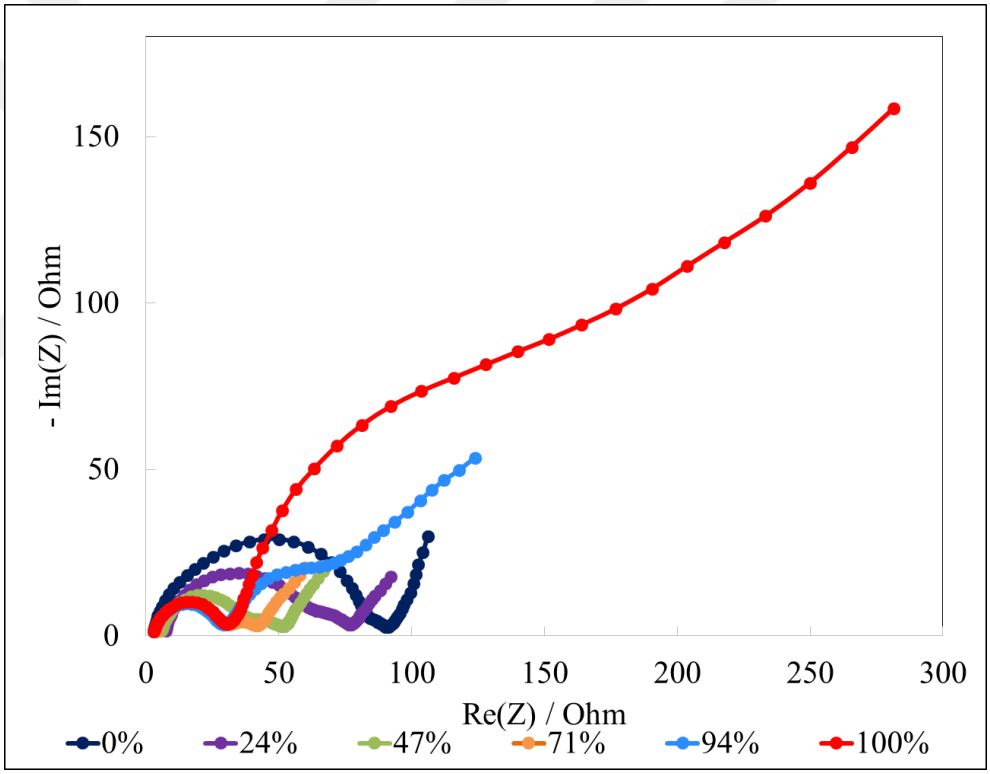

Figure 4.6. The EIS spectrums of the cell with E/S=19 µl/mg for different discharge depths.

The EIS spectrum for E/S=19 µl/mg is shown in Figure 4.6. Before discharging, i.e. at 0 % depth of discharge, the highest radius of the first semi-circle is obtained whereas the second semi-circle at that point is very small and it has the lowest radius compared to the others. After that point, the size of the first semi-circle is getting smaller until complete discharge, at which it has the minimum value. So, the charge transfer of the cell decreases

significantly starting from 0% DOD to 71 % DOD and after that point it stabilizes. On the other hand, the Li_2S/Li_2S_2 film resistance, has its highest values at 94 % and 100 % DODs.

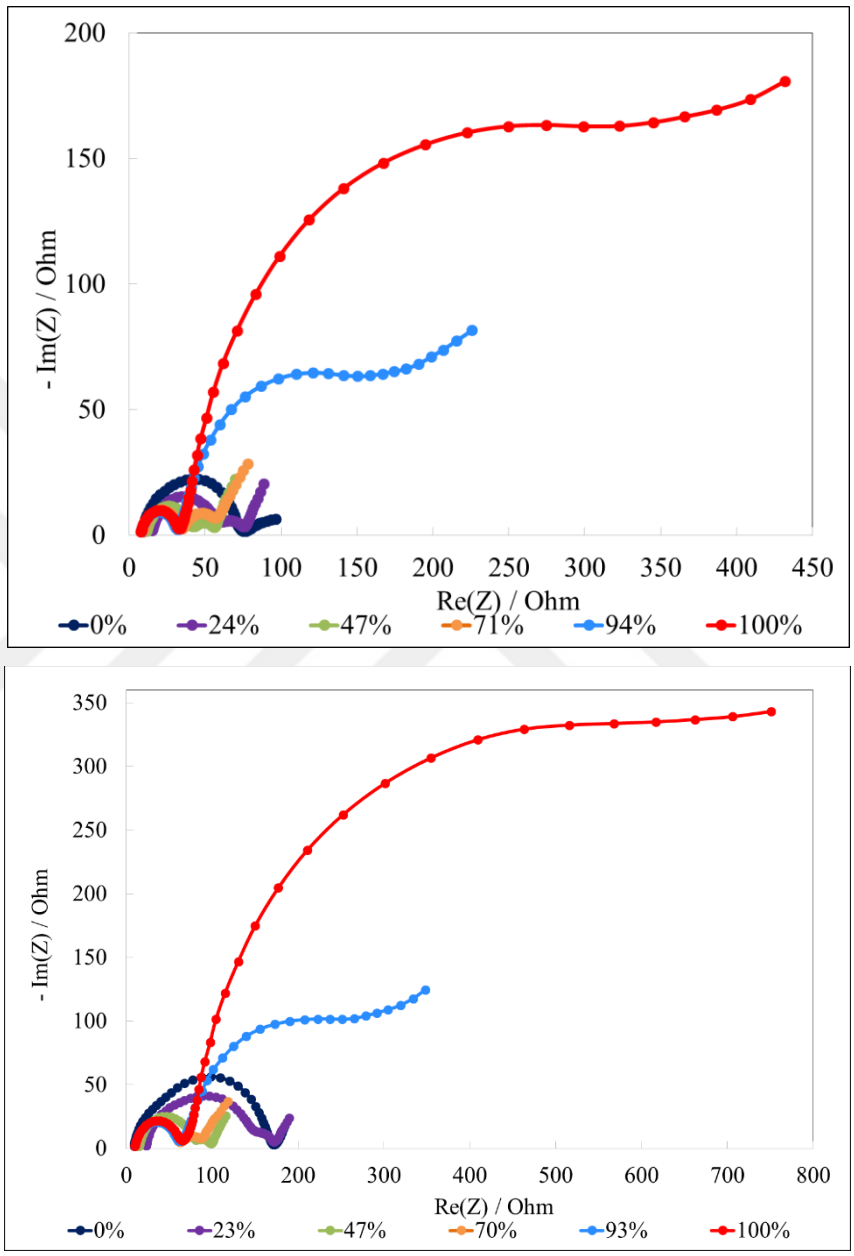

Figure 4.7. The EIS spectrums of the cell with E/S=12 µl/mg (top) and E/S=6 µl/mg(bottom) for different discharge depths.

The same trends are obtained with the E/S ratios of 12 and 6 µ/mg which are given in the Figure 4.7. For both of them, the high frequency semi-circles are bigger in the beginning of the discharge. However, the differences between the sizes of the semicircles after 24 %

DODs, are very small. After that point, the charge transfer resistances stabilize and reach to constant values. The semi-circles in the low frequency regions are only apparent in 93 % and 100 % DOD; as it can be seen in the figure, it is significantly higher at the complete discharge of the cell. So, the film transfer resistance has its maximum value at the complete discharge.

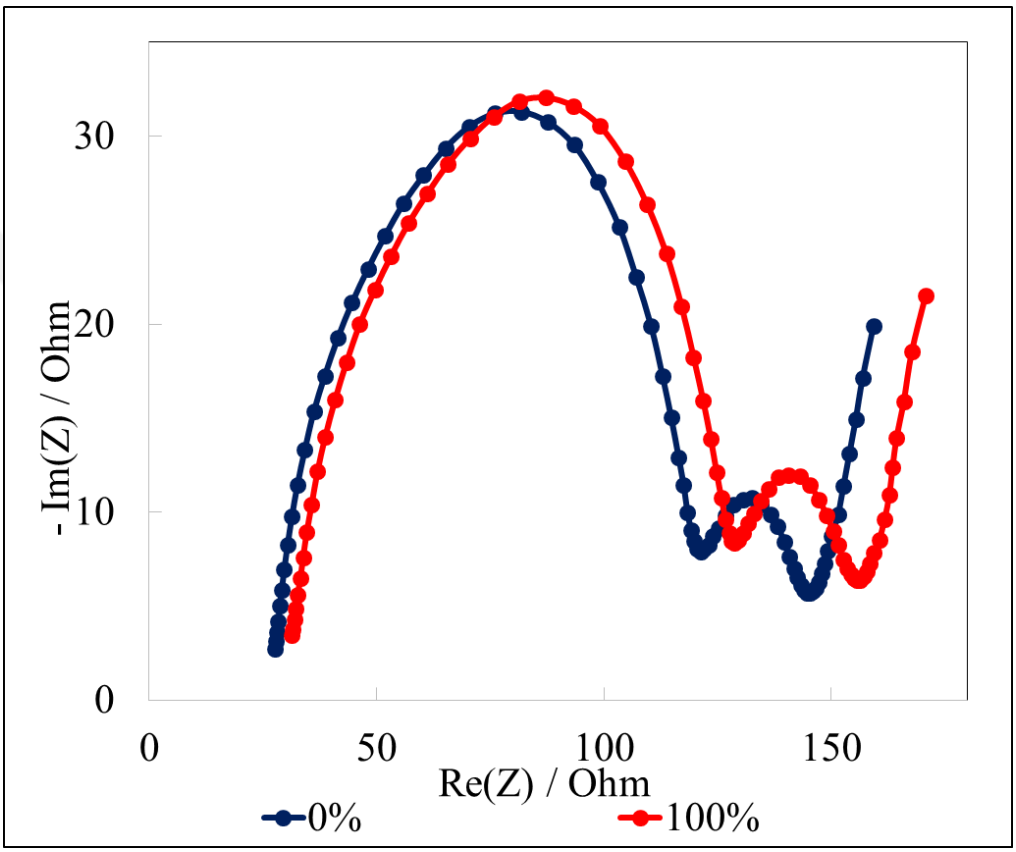

Figure 4.8. The EIS spectrums of the cell with E/S=3 µl/mg for different discharge depths.

Finally, Li-S cells with an E/S ratio of 3 µl/mg are prepared by adding 5 µl electrolyte to each cell. Since the electrolyte volume in the cell is very low, wetting problems occur and that decreases the discharge capacity significantly. Cells discharge within minutes rather than 10 hours. Therefore, there are only two points, at which the EIS measurements are taken, one at full charge and the other at full discharge. As can be seen from Figure 4.8, the same trends are obtained for both of the points and the magnitudes of the semi-circles are very close. Since the discharge time is very short, no significant change inside the cell occur and the resistances are close to each other.

4.2.2. The Effect of E/S Ratio on the Cell Resistances for Different DODs

In order to discuss the effect of E/S ratio on the cell resistance, the EIS results with different E/S ratios are compared for similar DODs (±5 %).

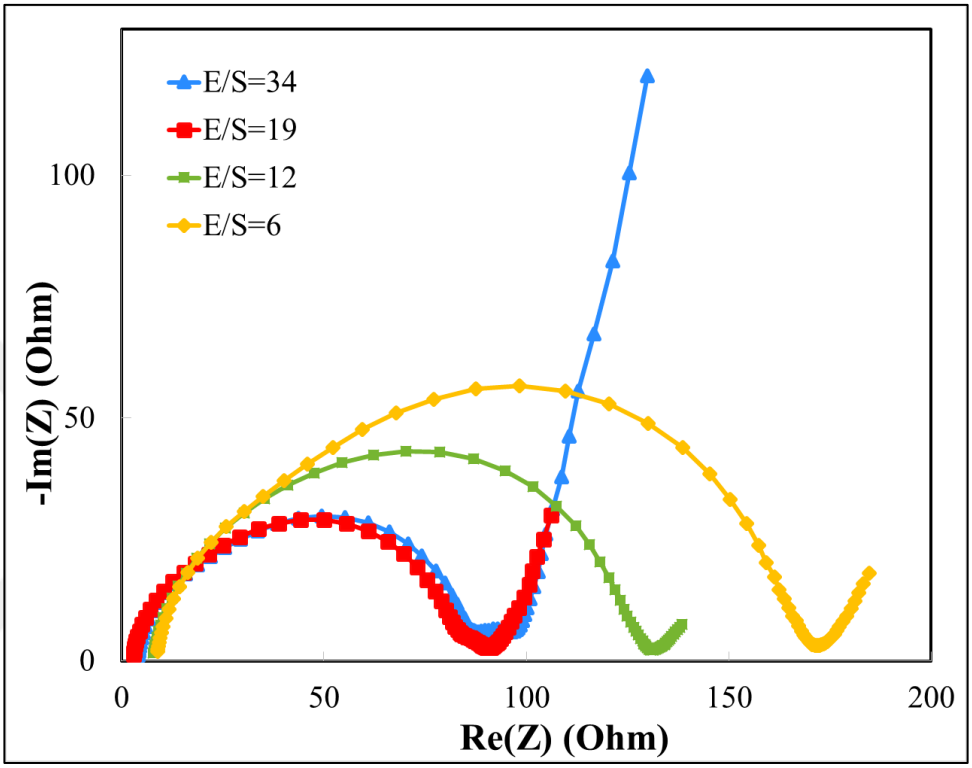

Figure 4.9. The effect of E/S ratio on the EIS spectrums at 0 % DOD.

The impedances for the cells with different E/S ratios in the complete charge state can be seen in Figure 4.9. As can be seen from the figure, the largest size of the first semi-circle is obtained for the cell with an E/S ratio of 6 µl/mg. Increasing the E/S ratio up to 19 µl/mg decreases the size of the high-frequency semi-circle significantly. However, there is not a distinct difference between 19 µl/mg and 34 µl/mg. Hence, the highest charge transfer resistance is obtained at the lowest E/S ratio. The second semi circles are not apparent for this degree of discharge. That means that for all E/S ratios, the charge transfer resistances are much higher than the film resistances at the beginning of discharge.

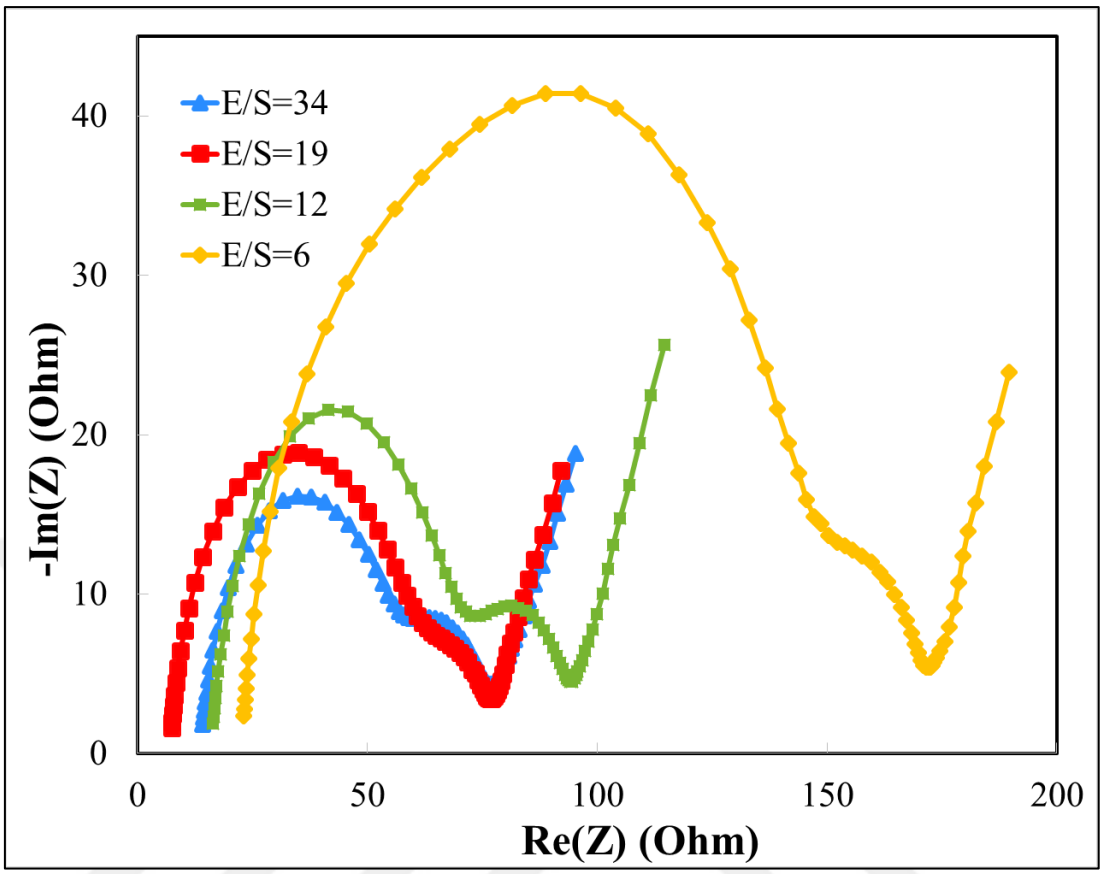

Figure 4.10. The effect of E/S ratio on the EIS spectrums at 20 % DOD.

The second point is chosen in the high voltage discharge plateau, where the solid sulfur transforms to long order polysulfides which are soluble in the electrolyte. As can be seen from Figure 4.10, for all of the E/S ratios, the first semi-circles are higher than the second semi-circles. The first semi-circles are getting smaller with increasing E/S ratio with the biggest one in the 6 µl/mg and the smallest one in the 34 µl/mg. 6 µl/mg also has the highest R1, electrolyte resistance, whereas 19 µl/mg has the lowest. Since this point is in the high discharge plateau, the second semi-circles which represent the film resistance due to insulating Li_2S formation are not completely formed. However, it can still be discussed that 6 µl/mg and 12 µl/mg have the highest film transfer resistance and the rest are very close to each other.

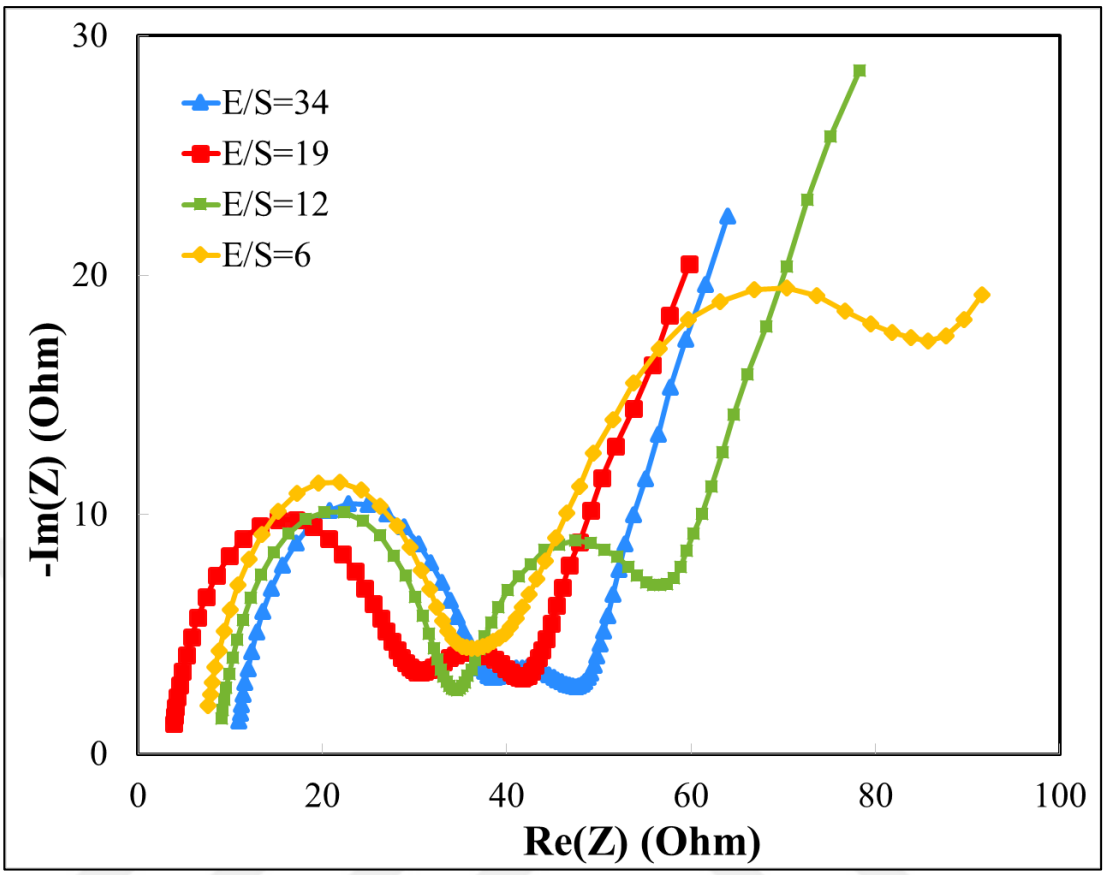

Figure 4.11. The effect of E/S ratio on the EIS spectrums at 70 % DOD.

The first noticeable difference between 20 % and 70 % degree of discharge, in Figure 4.11, is that the variation in the size of the high-frequency semi-circles for different E/S ratios get less apparent. R3's become more visible and complete semi-circles are obtained. The size of R3 is higher than the size of R2 for an E/S ratio of 6 µl/mg, whereas for 12 µl/mg the sizes of R2 and R3 are very close to each other. These may indicate that in the second voltage plateau, R3 becomes more dominant in the total resistance of the cell for low E/S ratios. Since R3 is the film resistance, this trend is expected. Similar to the previous results, the lowest resistances are obtained with the two highest E/S ratio. When we compare the R1 electrolyte resistances, there is no obvious trend with the E/S ratio. The sizes of R1's from the largest to the smallest are as follows; 34 µl/mg, 12 µl/mg, 6 µl/mg and 19 µl/mg.

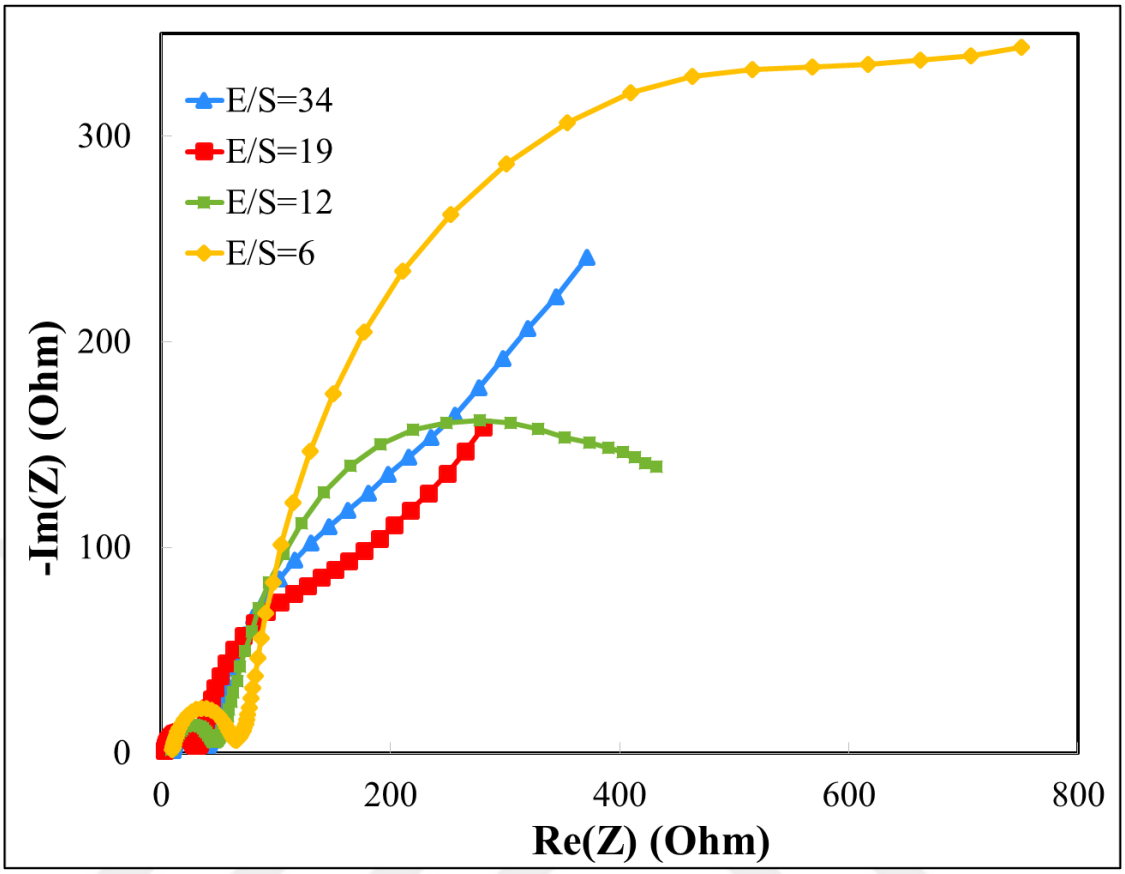

Figure 4.12. The effect of E/S ratio on the EIS spectrums at 100 % DOD.

Finally, the cells are compared for 100% DOD for different E/S ratios. The trends change completely at the complete discharge state in Figure 4.12. The R1s are very close to each other and their contributions to the total resistance are significantly smaller than R2 and R3. The R2s, which is the charge transfer resistance, were the most prominent resistances in the previous depth of discharges. However, in this case they are also smaller and they do not highly affect the total resistance, even though 6 µl/mg and 12 µl/mg still have the largest semi-circles. Finally, significant differences are obtained for the R3 film resistances. The R3 resistances are much bigger than R2 resistances for all of the cases. The sizes of R3s from the largest to the smallest are as follows; 6 µl/mg, 12 µl/mg, 34 µl/mg and 19 µl/mg. The fact that 19 µl/mg ratio has a smaller resistance than 34 µl/mg can be a sign that there is a limit of increasing the electrolyte volume to decrease the resistance.

These discussions show that the individual resistances of the cells are highly dependent on both the degree of discharge and the E/S ratio. In order to observe the trends in a more

obvious way, quantitative comparisons of the resistances as a function of the E/S ratio in the entire discharge region are made. In addition, R1, R2 and R3 are linked to the real resistances in a Li-S cell, which are the electrolyte, charge transfer and non-conductive layer resistances, respectively.

After fitting is applied to all of the three replicate cells for each E/S ratio and DOD, averages of the resistances are taken and the results are given in Table 4.2-Table 4.6.

Table 4.2. Average Fitting Results of E/S=34 µl/mg.

DOD (%)	R1 (Ω)	R2 (Ω)	R3 (Ω)
0	9	74	8
15	11	50	19
30	12	36	20
44	10	33	12
55	8	38	8
67	9	31	7
80	8	32	10
100	8	29	114

Table 4.3. Average Fitting Results of E/S=19 µl/mg.

DOD (%)	R1 (Ω)	R2 (Ω)	R3 (Ω)
0	4	80	11
23	7	51	15
46	6	35	12
69	4	32	18
91	4	34	58
100	4	32	140

Table 4.4. Average Fitting Results of E/S=12 µl/mg.

DOD (%)	R1 (Ω)	R2 (Ω)	R3 (Ω)
0	9	90	25
24	17	61	20
47	14	39	20
70	11	32	25
93	11	30	84
100	10	33	238

Table 4.5. Average Fitting Results of E/S=6 µl/mg.

DOD (%)	R1 (Ω)	R2 (Ω)	R3 (Ω)
0	7	184	22
23	19	116	25
41	16	72	29
72	9	39	43
87	8	40	87
100	8	41	475

Table 4.6. Average Fitting Results of E/S=3 µl/mg.

DOD (%)	R1 (Ω)	R2 (Ω)	R3 (Ω)
0	38	490	NP
100	48	246	108

The electrolyte, charge transfer and film resistances of various E/S ratios as a function of DOD are given Figure 4.13-Figure 4.16, respectively. The standard deviations are also reported to see the reproducibility of the results.

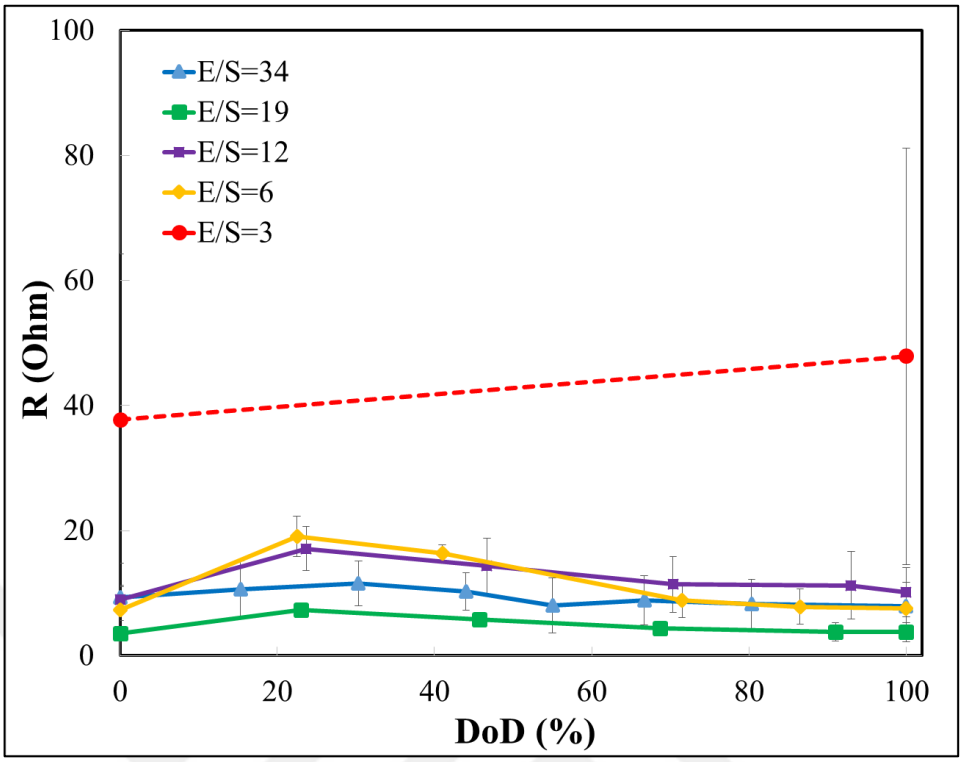

Figure 4.13. Effect of E/S ratio on the electrolyte resistance (R1) as a function of depth of discharge.

Figure 4.13 shows the results of R1 resistance at different degree of discharges for all of the E/S ratios. As can be seen from the figure, with the exception of 3 µl/mg, the same trend is obtained for different E/S ratios. For a E/S ratio of 3 µl/mg, since there are only 2 points, this trend is not observed. For all E/S ratios, the electrolyte resistances are increasing with increasing DOD up to 25-30 % DOD and then they start to decrease after that maximum point until the end of discharge. These trends support that R1 resistance can be defined as the electrolyte Ohmic resistance.

In the high voltage plateau, only high order polysulfides are present in the electrolyte. The reason of this maximum resistance point is the formation of high order polysulfides in the transition between the high voltage plateau to the low voltage plateau. These high order polysulfides increase the viscosity of the electrolyte, and therefore the Ohmic resistance [35]. Further reduction of these polysulfides in the second discharge plateau results in shorter polysulfides and non-soluble discharge products. Following that, the Ohmic resistance of the electrolyte decreases [50].

As can be seen from Figure 4.13, E/S ratio affects the electrolyte resistance significantly. 19 µl/mg ratio shows the lowest resistance whereas 3 µl/mg shows the highest electrolyte resistance. For 3 µl/mg, since the electrolyte volume is very limited, wetting problems occur, which limits the ionic conductivity and thus increases the electrolyte resistance. Increasing E/S ratio from 3 µl/mg to 19 µl/mg, decreases the cell resistance for all of the depth of discharges. However, 34 µl/mg has higher resistances than 19 µl/mg. This shows that there is an optimum point to increase the electrolyte volume to decrease the electrolyte resistance. It is stated in the literature that increasing electrolyte amount too much may trigger the polysulfide shuttle mechanism [30]. Reoccurrence of the high ordered polysulfides may increase the electrolyte resistance along the discharge region again.

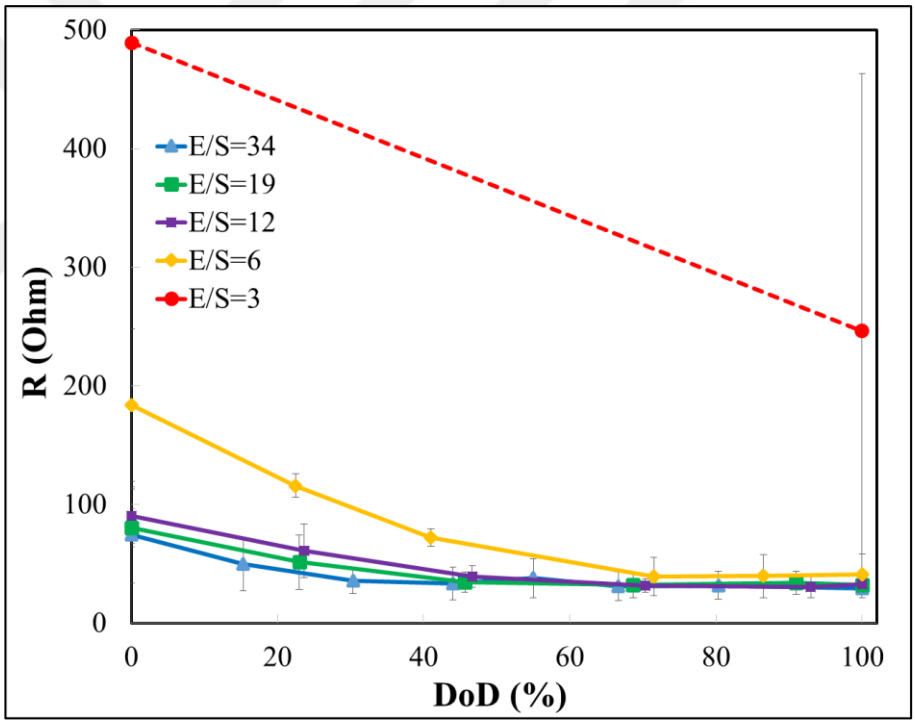

Figure 4.14. Effect of E/S ratio on the charge transfer resistance (R2) as a function of the depth of discharge.

In Figure 4.14 the effect of E/S ratio on R2, which is defined as the charge transfer resistance, is shown. 3 µl/mg has the highest charge transfer resistance, which is expected due to the limited polysulfide solubility at low E/S ratios hindering the reaction mechanisms, and thus results in low capacity. As can be seen from the figure, R2 is decreasing continuously until 40 % degree of discharge. The charge transfer resistances are very close

for 34, 19 and 12 µl/mg ratios after that point. However, for an E/S ratio of 6 µl/mg, since the electrolyte volume is limited, the reactions are more sluggish compared to the other ratios. After the complete dissolution of sulfur, charge transfer resistance of E/S ratio of 6 µl/mg becomes closer to the other E/S ratios. For degree of discharges higher than 70%, resistances are almost constant for these E/S ratios. These results propose that E/S ratios may not affect the charge transfer resistance after 70 % degree of discharge. This suggests that E/S ratio has a more critical impact on the reaction kinetics in the high voltage plateau.

For all E/S ratios, the charge transfer resistance is decreasing along the discharge as seen in Figure 4.14. The reason for this trend is as follows; at the beginning of the discharge sulfur is mostly in the solid form and since sulfur is electronically insulated, it blocks the electron transfer [35], [48], [50]. In addition, the reactions in the first discharge plateau ($S \rightarrow Li_2S_x$ ($8 \geq x \geq 4$)) are more sluggish compared to the second discharge plateau ($Li_2S_{x1} \rightarrow Li_2S_{x2}$ ($8 \geq x_1 > x_2 \geq 4$) and $Li_2S_y \rightarrow Li_2S$). These may explain the higher charge transfer resistances observed at the beginning of the discharge [48].

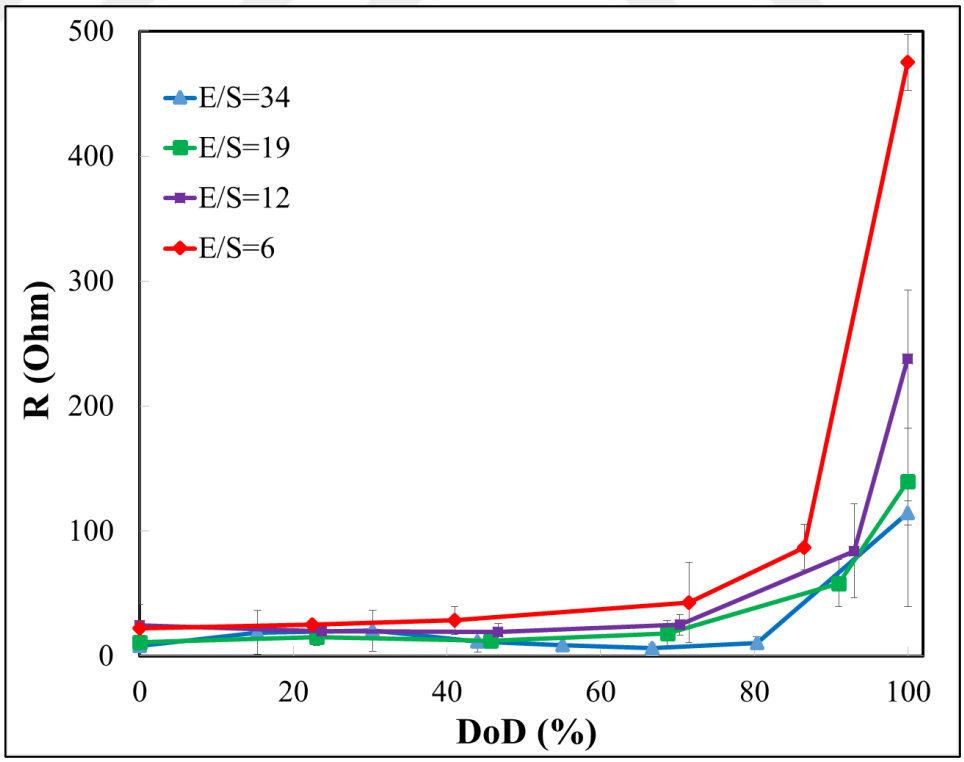

Figure 4.15. Effect of E/S ratio on the film resistance (R3) as a function of the depth of discharge.

The semi-circle in the middle frequency represents the solid film resistance occurred on the cathode surface towards the end of discharge. Hence, R3 is defined as the non-conductive film layer resistance, which is shown in the Figure 4.15. First of all, for all E/S ratios the same trend is observed. The film resistance is almost constant until 70% DOD, however at higher DODs, the obtained resistances are increasing rapidly and the differences between the E/S ratios are becoming more significant. Since Li_2S is the final product of the discharge process, this trend is expected [48], [50].

Contrary to the charge transfer resistance, the film resistance starts to increase after 40 % DOD and the impact of E/S ratio on the film resistance becomes more visible. When we consider only high DODs, 34 µl/mg has the lowest and 6 µl/mg has the highest film resistance. This result shows that the E/S ratio significantly affects the precipitation reactions.

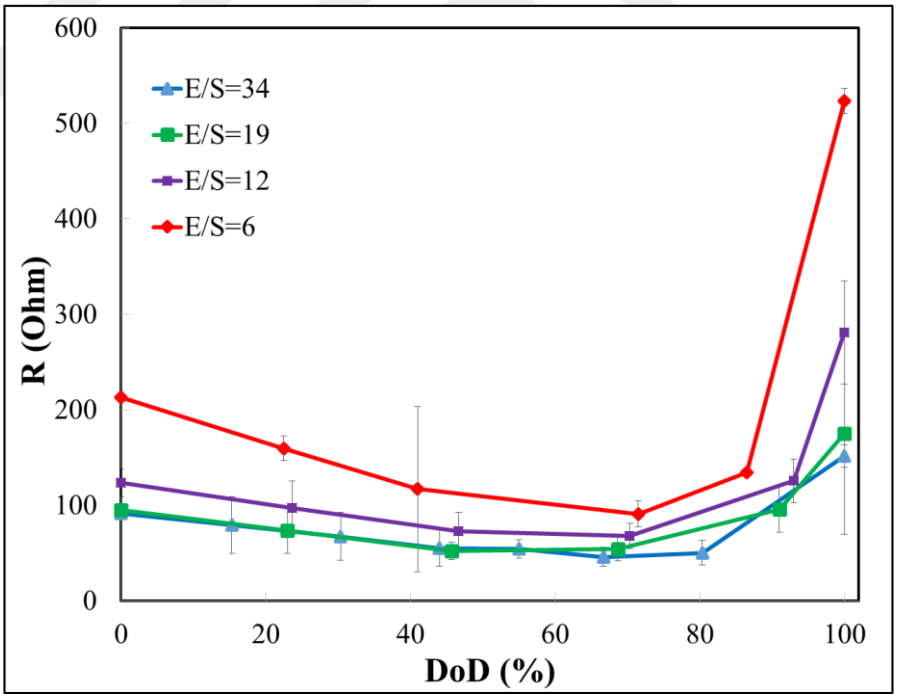

Figure 4.16. Effect of E/S ratio on the total cell resistance as a function of the depth of discharge.

Finally, the variation of the total cell resistances as a function of the E/S ratios is given in Figure 4.16. It is clear that, E/S ratio influences the cell resistance considerably. It is seen

that the highest total resistance is obtained with the lowest E/S ratio, 6 µl/mg. Increasing the E/S ratio from 6 µl/mg to 19 µl/mg decreases the cell resistance especially at the beginning and the end of discharge. However, further increase of the E/S ratio to 34 µl/mg slightly improves the cell resistance towards the end of discharge.

To sum up, the highest resistances are obtained with the lowest E/S ratio because of inadequate wetting of the sulfur cathode, sluggish reaction kinetics and enhanced polysulfide shuttle mechanism due to insufficient electrolyte volume. However, increasing the electrolyte volume decreases the cell resistance only up to a point; any further increase in the E/S ratio gives similar resistance results.

4.3. The Effect of C/S Ratio on the EIS Results of Li-S Cells

4.3.1. The Effect DOD on the Cell Resistances for Different C/S ratios

The EIS spectrums for C/S ratios of 0.3, 0.5, 2 and 3.5 are shown in Figures 4.17-4.20, respectively. To see the dependence of the EIS results on the degree of discharge, these plots are discussed first. For all of the C/S ratios, similar trends are obtained for both charge transfer and film resistances.

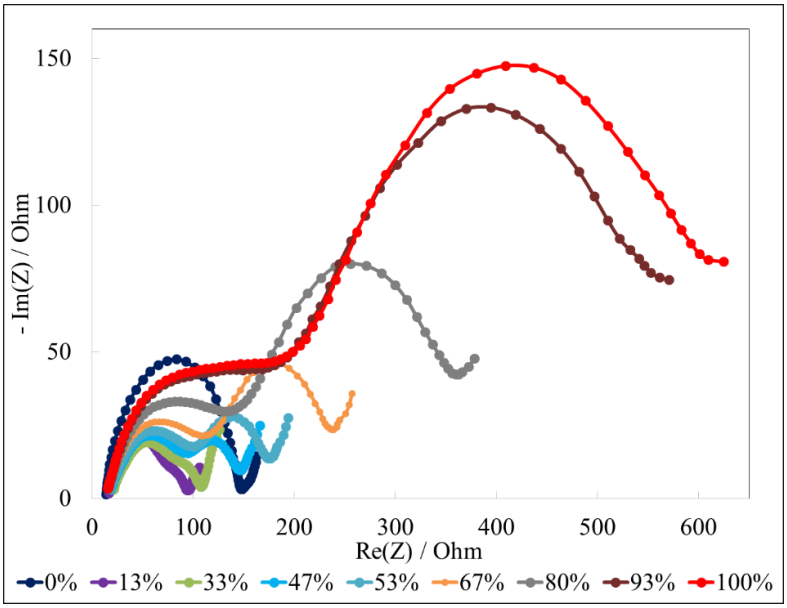

Figure 4.17. The EIS spectrums of the cell with C/S=0.3 for different discharge depths.

The EIS spectrums in the various depths of discharge for the cells having a C/S ratio of 0.3 are shown in Figure 4.17. As can be seen from the figure, there are two semi-circles in all of the spectrums. The first semi-circle has the highest value in the complete charge, however it gets smaller towards the end of discharge. On the other hand, the second semi-circle is getting bigger with increasing discharge depth. So, when the cell is discharging, its charge transfer resistance is decreasing whereas film transfer resistance is increasing.

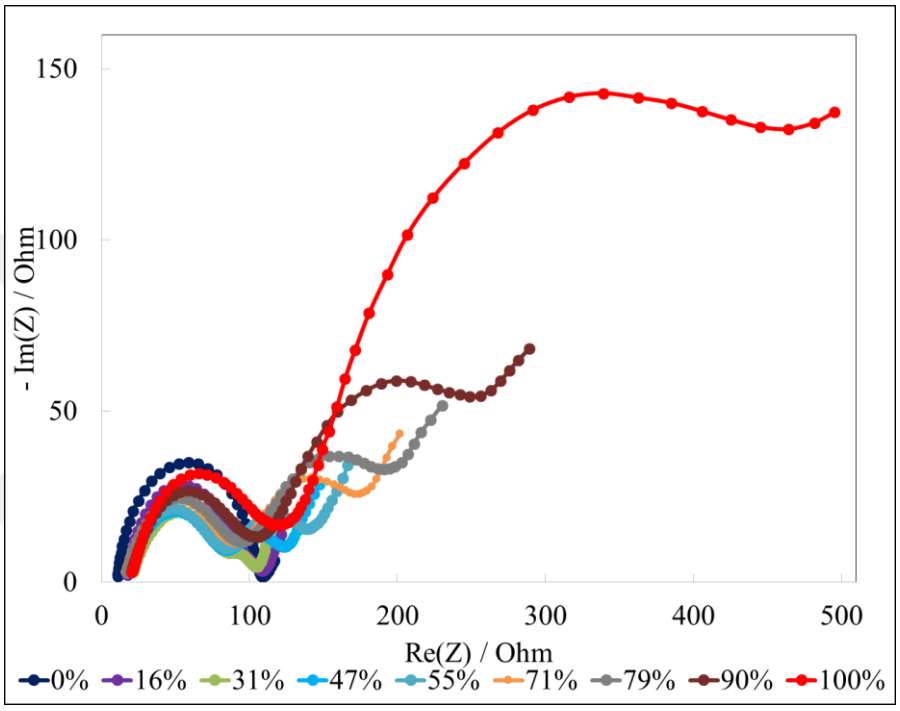

Figure 4.18. The EIS spectrums of the cell with C/S=0.5 for different discharge depths.

When the EIS spectrums of cells with a C/S ratio of 0.5 is considered, which is given in Figure 4.18, we see that the size of the first semi-circles decreases until 55 % DOD and increases again after that point. Whereas the size of the second semi-circle, which represents the film resistance, constantly increases. The largest semi-circle is obtained for the second semi-circle at complete discharge state. It shows that, the most important resistance in this cell is the film resistance, especially towards the end of discharge. The same discussions are also valid for the Li-S cells with a C/S ratio of 2, as shown in Figure 4.19.

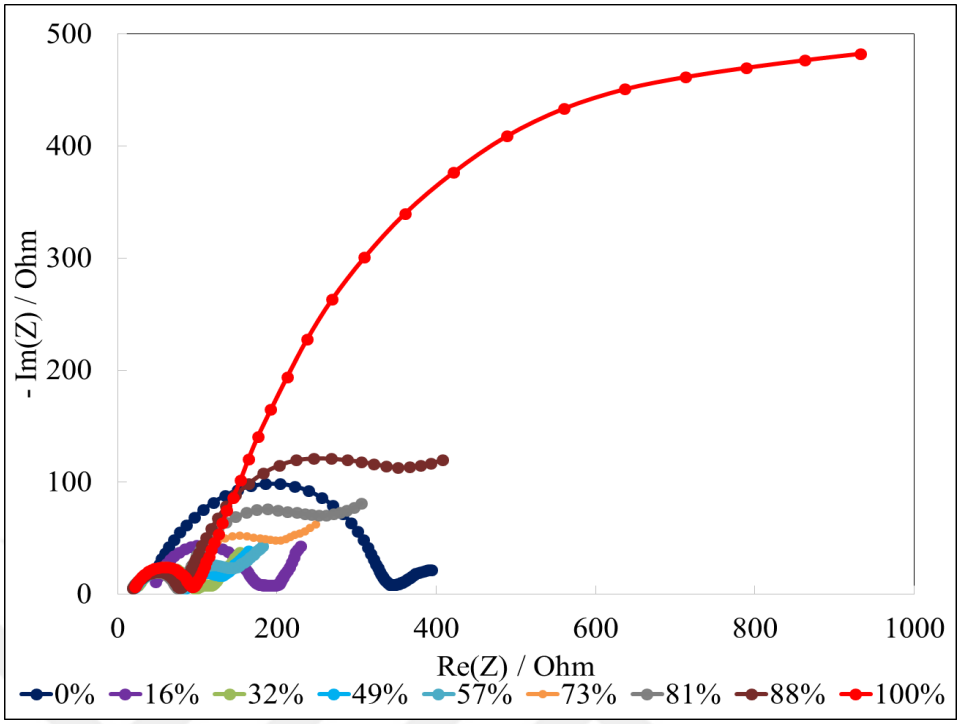

Figure 4.19. The EIS spectrums of the cell with C/S=2 for different discharge depths.

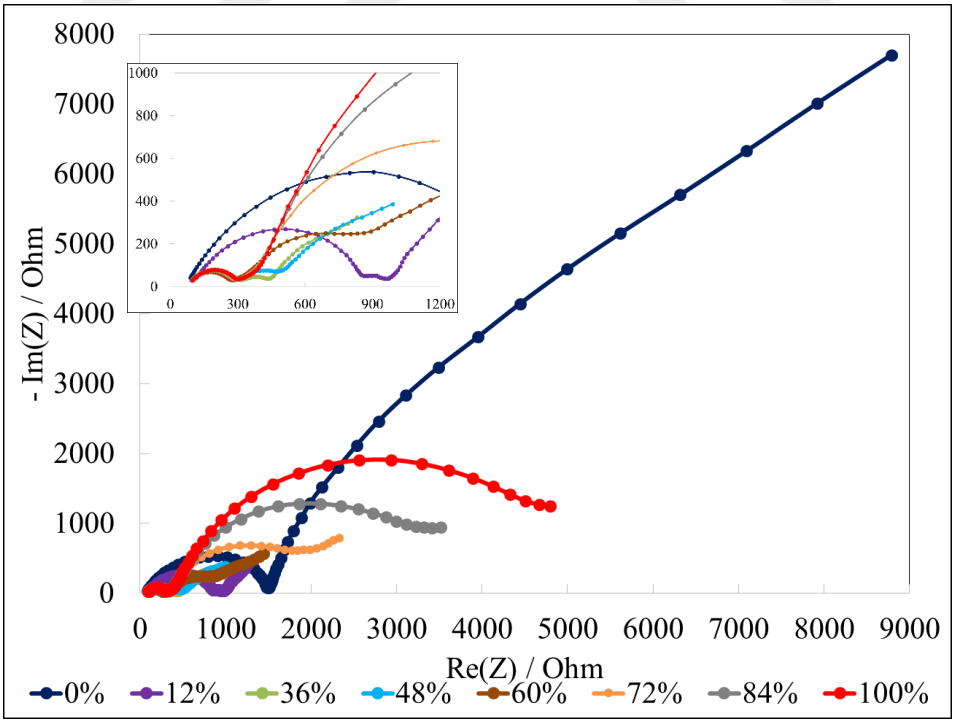

Figure 4.20. The EIS spectrums of the cell with C/S=3.5 for different discharge depths.

The semi-circles are much bigger in this C/S ratio compared to the other C/S ratios and the highest magnitudes of resistances are obtained in the C/S ratio of 3.5, Figure 4.20. The charge transfer resistances continuously increase and film resistances increases towards the end of the discharge similar to other results.

4.2.2. The Effect of C/S Ratio on the Cell Resistances for Different DODs

In this section the impedance spectrums are compared for the cells having C/S ratios of 3.5, 2.0, 1.0, 0.5 and 0.3 for similar discharge depths within ±5 % DODs.

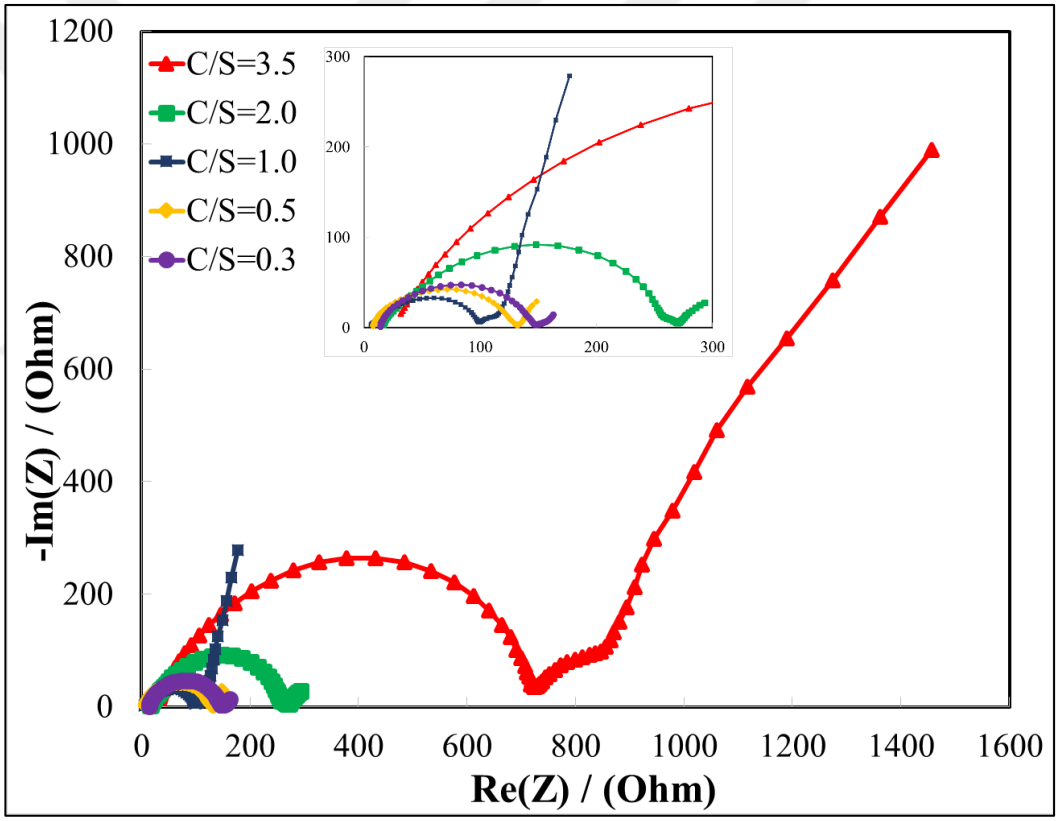

Figure 4.21. The effect of C/S ratio on the EIS spectrums at 0 % DOD.

First, the spectrums at the beginning of the discharge are shown for different C/S ratios in Figure 4.21. The highest impedance is obtained with the highest carbon content. In addition, the second semi-circle is apparent only in that C/S ratio. Even though C/S ratio of 2 has a higher impedance than the ratios of 1, 0.5 and 0.3, it is much smaller when it is compared with the 3.5 C/S ratio. When the lower C/S ratios are considered, it is clear that

the first semi-circle has the smallest radius for a C/S ratio of 1. On the other hand, the results are very close for the C/S ratios of 0.5 and 0.3.

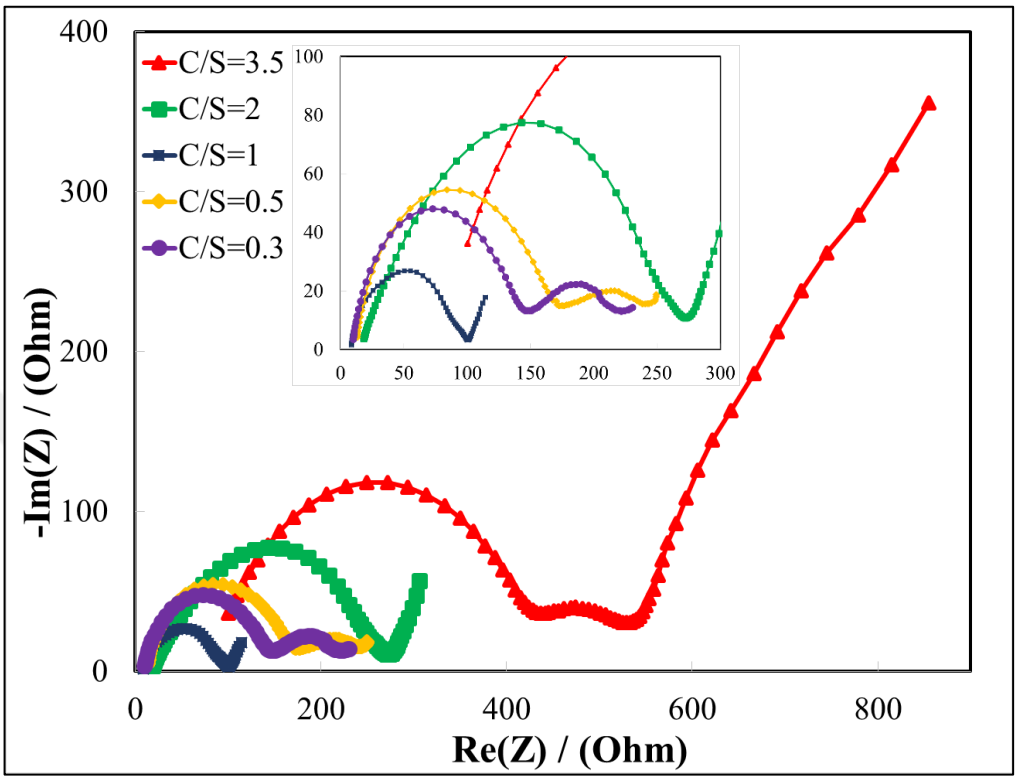

Figure 4.22. The effect of C/S ratio on the EIS spectrums at 20 % DOD.

The trend is the same for 20 % DOD, which is in the first discharge plateau, as shown in Figure 4.22. The highest charge transfer resistances are obtained for the ratios of 3.5 and 2, whereas the lowest is observed for the ratio of 1. On the other hand, the film resistances are much clearer compared to 0 % DODs. C/S ratio of 1 showed the lowest resistance by having the smallest semi-circles. Although C/S ratio of 0.5 shows a higher resistance than 0.3, their values are very close to each other.

In the second voltage plateau, Figure 4.23, similar to the previous DODs the highest impedance is obtained with the C/S ratio of 3.5 for both charge transfer and film resistances and the lowest for C/S=1. Contrary to the results in 20 % DOD, C/S=0.3 has the second highest charge transfer resistance, whereas the charge transfer resistances of 0.5 and 2 are very close to each other. In addition, the electrolyte resistance is significantly higher in the highest C/S ratio, while it is much lower in the C/S ratio of 1.

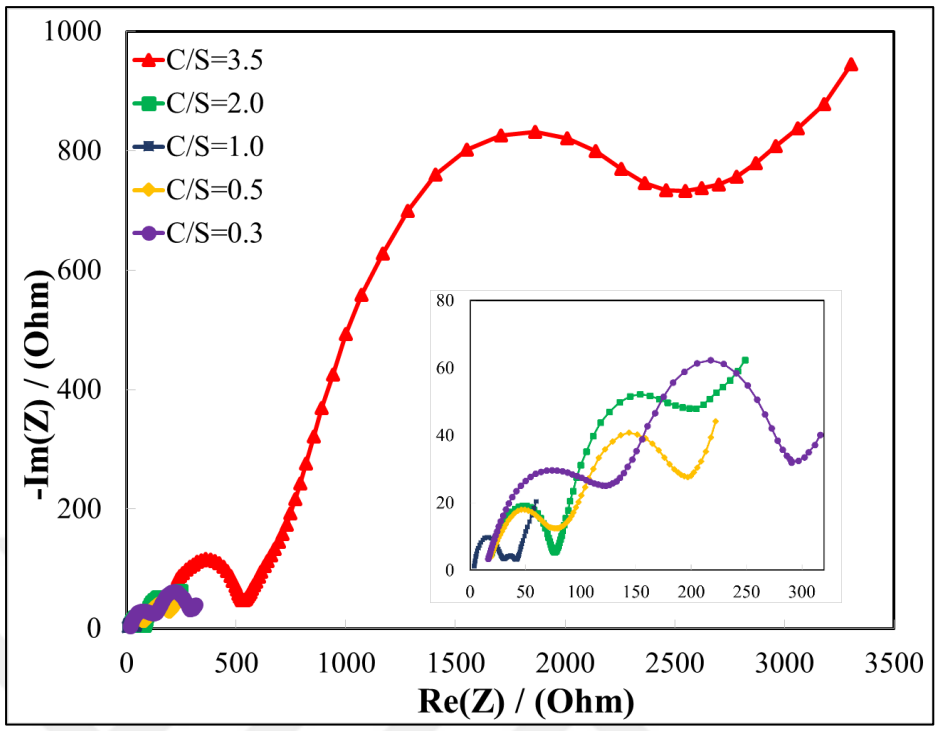

Figure 4.23. The effect of C/S ratio on the EIS spectrums at 70 % DOD.

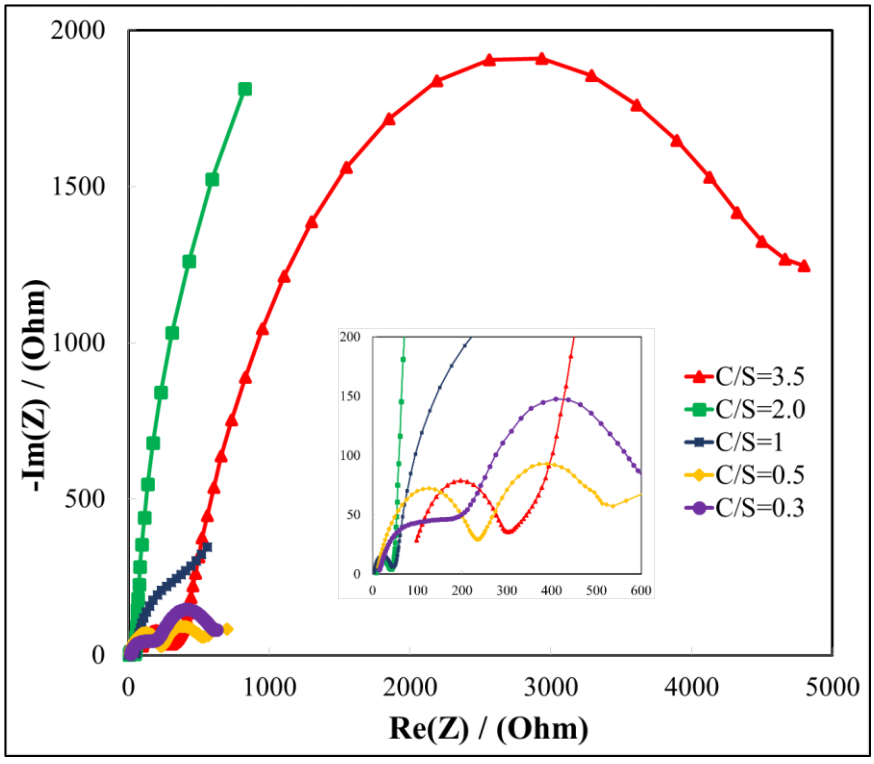

Figure 4.24. The effect of C/S ratio on the EIS spectrums at 100 % DOD.

Finally, EIS results for different C/S ratios at the complete discharge are compared in Figure 4.24. C/S ratio of 3.5 has the highest impedance for both charge transfer and film resistances. The lowest charge transfer resistance is obtained for C/S ratios of 1 and 2, and smaller carbon contents lead to a higher charge transfer resistance.

The same procedure discussed for the investigation of the effect of E/S ratio is also followed for the determination of C/S ratio influence on the cell resistances. Three replicates of a cell for each C/S ratio are prepared and the averages of these three cells resistances are taken into consideration. The tables presenting the average fitting results of the resistances for each C/S ratio are listed below (Tables 4.7-4.10). The results of C/S ratio of 1 is not tabulated again in this part since it is already presented in Table 4.3.

Table 4.7. Average Fitting Results of C/S=0.3.

DOD (%)	R1 (Ω)	R2 (Ω)	R3 (Ω)
0	8	118	24
14	10	72	66
25	12	79	61
32	13	79	61
45	11	122	64
59	10	126	138
71	9	179	181
79	9	178	242
91	8	202	424
100	8	220	568

Table 4.8. Average Fitting Results of C/S=0.5.

DOD (%)	R1 (Ω)	R2 (Ω)	R3 (Ω)
0	7	108	10
28	18	96	47
45	18	109	78

Table 4.8. Average Fitting Results of C/S=0.5. (cont.)

DOD (%)	R1 (Ω)	R2 (Ω)	R3 (Ω)
58	16	102	97
73	14	126	128
88	15	144	196
100	14	130	273

Table 4.9. Average Fitting Results of C/S=2.

DOD(%)	R1 (Ω)	R2 (Ω)	R3 (Ω)
0	20	215	69
16	25	223	20
34	19	183	27
58	17	181	55
74	17	174	78
90	27	224	177
100	31	296	1887

Table 4.10. Average Fitting Results of C/S=3.5.

DOD(%)	R1 (Ω)	R2 (Ω)	R3 (Ω)
0	84	1344	1517
12	98	478	392
23	88	407	107
37	84	289	217
48	86	247	394
59	81	258	814
71	69	294	1542
82	63	319	2458
94	61	339	4010
100	47	225	4895

To illustrate the change of C/S ratio throughout discharge and to see the effect C/S on the individual resistances, these tables are plotted into line graphs.

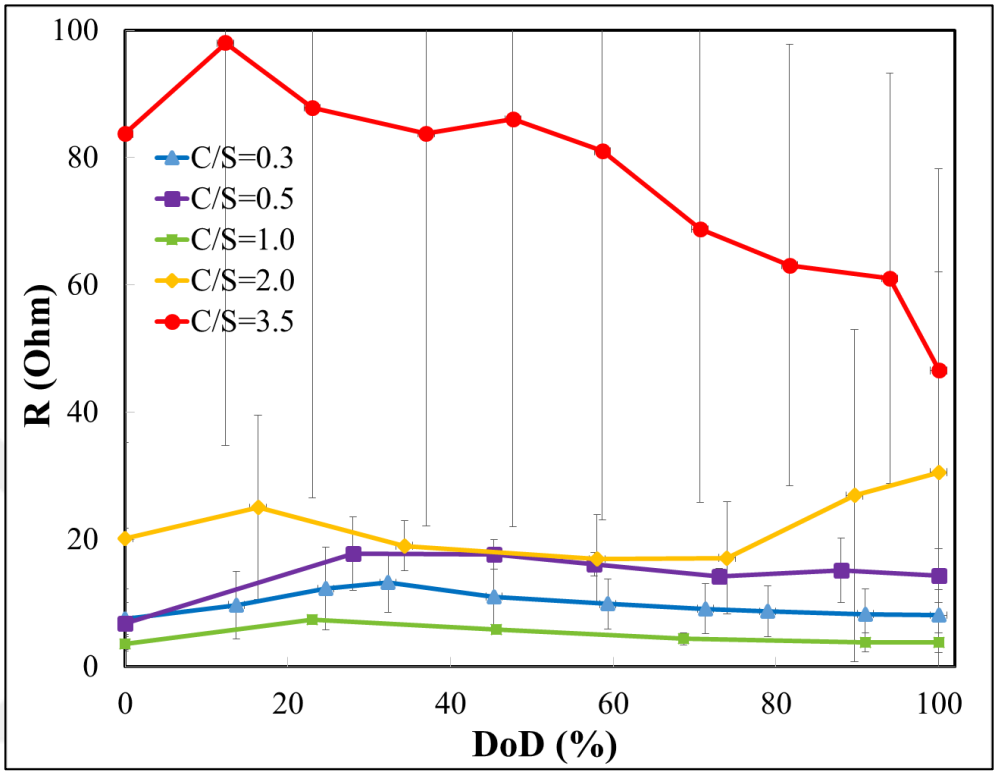

Figure 4.25. Effect of C/S ratio on the electrolyte resistance (R1) as a function of discharge depth.

The effect of C/S ratio on the electrolyte resistance is given in Figure 4.25. The trend is similar for all of the C/S ratios. Similar to the E/S results, the electrolyte resistance increases to a maximum value near the end of the first discharge plateau and then decrease until the end of discharge. However, this decrease with the C/S=3.5 is more prominent than the others. This may be explained with the insufficient amount of electrolyte that can penetrate into the carbon surface since the surface area significantly increases at very high carbon amounts. Since the carbon amount is too high, the electrolyte may not wet the surfaces with the active materials. That may increase the electrolyte resistance.

The figure clearly shows that decreasing the C/S ratio to 1 decreases the electrolyte resistance in the cell significantly, whereas, any further decrease in the carbon amount leads

to an increase in the cell resistance. This show that C/S=1 ratio provides an optimum condition for the electrolyte conductivity at an E/S ratio of 19 mL/gS.

In addition, the standard deviation for C/S=3.5 is too high. This can stem from the inhomogeneity of the sulfur distribution on the carbon particles. Since, sulfur constitutes only 20 wt.% of the cathode and only mechanical mixing is applied to the cathode, there is a high chance that it is not distributed on the carbon particles uniformly.

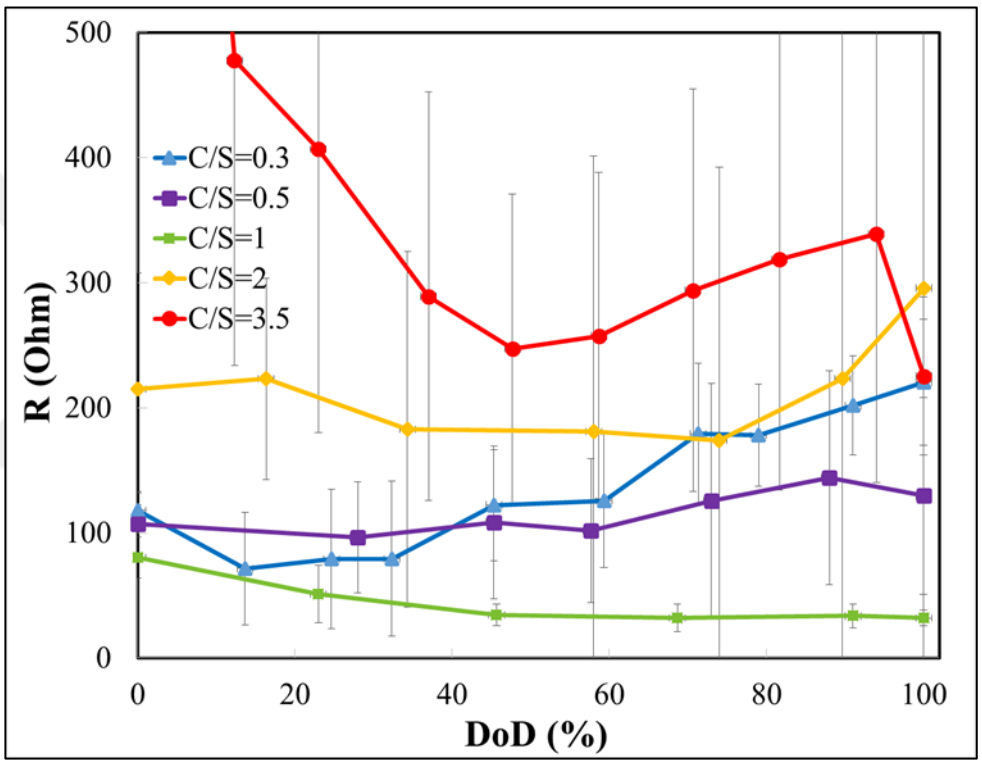

Figure 4.26. Effect of C/S ratio on the charge transfer resistance (R2) as a function of discharge depth.

The effect of C/S ratio on the charge transfer resistance is given in Figure 4.26. As seen in the figure, the minimum resistance is obtained for a C/S ratio of 1 for all of DODs. A common trend is not observed for the C/S ratios. For a C/S ratio of 0.3, the charge transfer resistance constantly increases whereas for a C/S ratio of 1, it decreases along the discharge. For C/S=3.5 ratio, it reduces until 50 % of discharge and increases again. However, it gets its minimum value in the complete discharge of the cell with a rapid decrease between 90-100 % DOD. For a C/S ratio of 2, it decreases until 80 % DOD and increases again after that

point. Even though it is hard to generalize the trend of the effect of DOD on R2 for different C/S ratios, the impact of C/S ratio on the charge transfer resistance is highly clear; there is an optimum C/S ratio that minimizes the charge transfer resistance. This can be explained with the nature of the sulfur cathode.

Carbon is added into the cathode in order to improve the electronic conductivity and to provide an electrochemically active space. Therefore, the pore size and surface area of the carbon is very important. However, the carbon black used in this cathode has 62 m^2/g specific surface area and 0.04 μm particle size according to MTI information sheet. The low amount of specific surface area and low porosity can result in accumulation of large sulfur particles on the carbon surface leading to a poorer electronic conductivity. Due to this reason, the reproducibility of the results may decrease. In these respects, it can be said that the highest charge transfer resistance is obtained with the C/S=3.5 and the lowest with the C/S=1.

According to the literature, the sulfur utilization decreases at lower C/S ratios because excess sulfur on the carbon decreases the electronic conductivity [38]. In addition, low C/S ratios suffer from poor electronic conductivity, hence it causes slower reaction kinetics and higher resistances. However, we observed an opposite trend. This may be due to low S loadings in the cathode at high C/S ratios; since the cathode thickness is kept constant in these experiments increasing C/S corresponds to a decrease in the active material amount. This may be the reason of the high charge transfer resistance in the cell. Furthermore, Duo *et al.* (2011) suggested that good electronic conductivity can be achieved by trapping and connecting sulfur particles on the cathode matrix [41]. Hence, the isolated sulfur aggregates may increase the charge transfer resistance for the C/S=3.5.

Similar to the other results, the lowest film transfer resistance is obtained with the C/S ratio of 1 and the highest for the C/S ratio of 3.5. It is shown in Figure 4.27 that, decreasing C/S ratio below 1 increases the film transfer resistances. Except the complete discharge and charge points, the second lowest resistance is obtained with a C/S ratio of 2. This is an indication to show that both sulfur and carbon shortages in the cathode significantly increase the film transfer resistances especially in the complete discharge state.

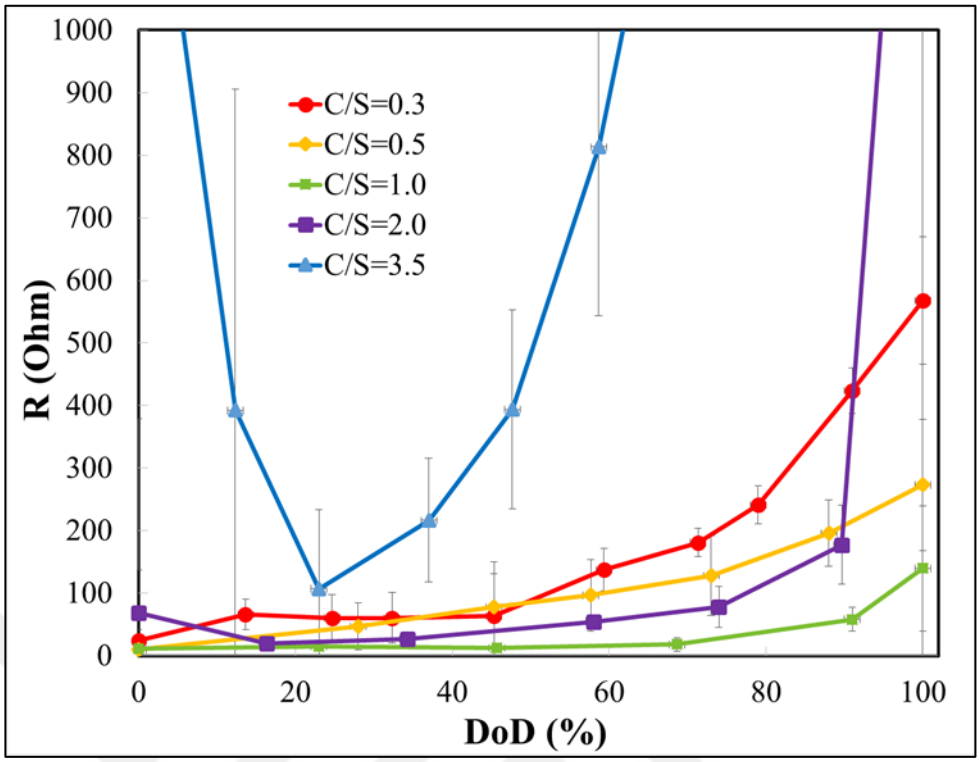

Figure 4.27. Effect of C/S ratio on the film resistance (R3) as a function of discharge depth.

Film transfer resistance is defined as the resistance of solid Li_2S film on the carbon surface due to Li_2S insulating behavior. It can be interpreted that, when the carbon amount is low, i.e. for C/S=0.3 and C/S=0.5, there is not enough surface for Li_2S solid product deposition. In this case, the active area for PS adsorption and Li_2S deposition is the limiting factor rather than the sulfur utilization [68]. Hence, the Li_2S film grows thicker and that may increase the film resistance. On the other hand, at high C/S ratios, explanation to this may stem from the presence of too low sulfur in the carbon surface and isolation of the sulfur particles [41]. Therefore, carbon surface partly contributes to the electrochemical reactions and that may increase the cell resistance. When the carbon and sulfur amounts are equal to each other, a homogenous film will occur on the surface and a lower resistance is obtained all over the cathode surface.

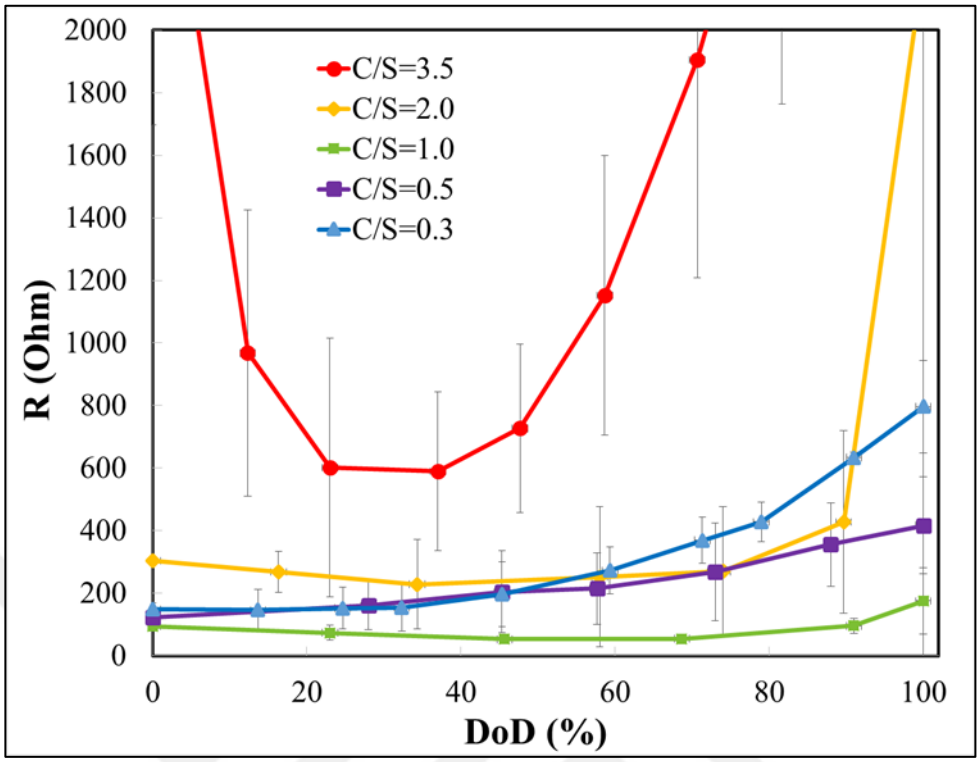

Figure 4.28. Effect of C/S ratio on the total resistance as a function of discharge depth.

Finally, the effect of C/S ratio on the total cell resistance is given in

Figure 4.28. It is clear that C/S ratio affects the cell resistance significantly. Moreover, the cell resistances depend on the discharge state of the cells in a great manner. Cells with a C/S ratio of 3.5 experience the highest resistance for all DODs whereas C/S ratio of 1 shows the lowest resistance for any discharge depth. This shows that, there is an optimum C/S ratio in which the cells suffer less from all forms of kinetic and transport resistances.

5. CONCLUSIONS

5.1. Conclusions

The aim of this thesis is to determine the effect of electrolyte to sulfur (E/S) and carbon to sulfur (C/S) ratios on the reaction and degradation mechanisms of Li-S batteries depending on discharge state of the cells using electrochemical impedance spectroscopy. First, cell elements are decided by choosing the most conventional cathode, anode, separator and electrolyte chemistries. Li metal for the anode, a polymeric material for the separator, elemental sulfur, carbon black and PVDF binder for the cathode are combined with the DOL:DME electrolyte containing 1 M LiTFSI and 0.1 M $LiNO_3$ to construct the cells. The effect of E/S ratio and C/S ratio on the cell resistances are tested with these cells by keeping one of the ratio and the cathode thickness constant. The most important resistances for these cells are decided as the electrolyte, the charge transfer and the film resistances.

The effect of E/S ratio on these resistances are tested with Li-S cells having C/S=1 and E/S ratios of 34 µl/mg, 19 µl/mg, 12 µl/mg, 6 µl/mg and 3 µl/mg. Electrolyte resistance shows a maximum point around ~25 % DOD and after that point it decreases and reaches to similar values at the 0 % DOD. This is explained by the change in the electrolyte viscosity due to transition from high order to the low order polysulfides. This trend is obtained for all of the E/S ratios except 3 µl/mg due to too lean electrolyte volume. After 3 µl/mg, the highest electrolyte resistance is obtained with an E/S ratio of 6 µl/mg and the lowest resistance at 19 µl/mg . A similar trend, in which there is a significant decrease until nearly half of the discharge and constant resistance after that, is obtained with the charge transfer resistance for all of the E/S conditions. This is attributed to the presence of solid sulfur and more complex reactions in the beginning of discharge. Significantly high resistance is obtained for cells with 3 µl/mg. The second highest resistance is obtained for cells with 6 µl/mg. There is no distinct difference between the resistances for the other E/S ratios. Lastly, the film resistance showed an opposite trend with the charge transfer resistance; towards the end of discharge, the resistances start to distinguish and a significant increase in the resistances is obtained after 70 % DOD. This is due to the formation of Li_2S and their deposition on the cathode surface. The thickest film, therefore the highest film resistance is obtained with 6

µl/mg. The values of E/S=19 µl/mg and E/S=34 µl/mg are very close to each other. To sum up, when the total cell resistances are considered, a trend that shows a decrease up to ~70% DOD and then a significant increase near the end of discharge is obtained for all of the E/S ratio. The highest total resistance is obtained for an E/S ratio of 6 µl/mg and it shows that limited amount of electrolyte increases the cell resistance. However, 19 µl/mg is the limiting E/S ratio to decrease the total resistance and for higher E/S ratios, the cell resistance do not change.

On the other hand, for studying the effect of C/S ratio on the cell resistance, the cells are prepared by keeping the E/S ratio constant at 19 µl/mg with C/S ratios of 3.5, 2.0, 1.0, 0.5 and 0.3 C/S. Similar discussions are also made for the effect of C/S ratios on cell resistances. The highest electrolyte, charge transfer and film resistances are obtained with C/S=3.5. This is explained by the insufficient amount of sulfur and isolation of these sulfur particles on the carbon surface. Similarly, low C/S ratios also have high resistances due to insufficient electrochemical active area and poor conductivity. Although, film transfer resistances steeply increase towards the end of discharge due to Li_2S formation, different trends of charge transfer resistances are observed for different C/S ratios. When the total cell resistance is considered, it is recommended to use C/S=1 to have the minimum amount of cell resistance and to minimize the handicap between sulfur loading and sulfur utilization.

To conclude, it is seen that both E/S ratio and C/S ratio affect the individual resistances considerably and these resistances depend on the discharge state of the batteries. The analysis concludes that for the investigated system an optimum E/S ratio of 19 µl/mg and C/S ratio of 1 provide the minimum cell resistance.

5.2. Recommendations

Considering the discussions made in this thesis, there are some experimental suggestions that can be worth to consider for the future studies of the effect of E/S and C/S ratio on the resistances. These recommendations are as follows;

- As it is stated before, the optimum C/S and E/S ratio depend on the materials of cell construction. Therefore, different cathode chemistries can be used such as carbon

nanotubes rather than carbon black or TEGDME as electrolyte solvent. In addition, polysulfide additives can be added to electrolyte, to investigate the catholyte effect on cell resistances.

- Other than using different chemistries, the cathode preparation method can be changed. In the literature, the carbon black and sulfur composite is widely prepared with thermal treatment, to increase binding between sulfur and carbon. Hence, these cathodes can be prepared and all of the analysis can be repeated with this new cathode. In addition, the polymer separator can be replaced with modified separators.
- Cathode thickness is another important parameter that affects the cell resistance and sulfur loading. Hence, cathodes with various thicknesses can be prepared.
- Resistances are measured only in the initial cycle. However, some cells may need an activation cycle with a lower C rate. Hence, the same experiments can be carried out at different cycle numbers.
- Since an electric car spends different energies for acceleration, deceleration or breaking, rate capability of these cells are the other important performance criteria.
- Therefore, the impedances at the different C rates of the same cell can be investigated.
- Other than the impedance experiments, cycling can be carried out to see the stability of the cells.
- Finally, an electrochemical model can be developed to predict the cell resistances at various degree of discharges.

REFERENCES

1. C. Liu, Z. G. Neale, and G. Cao, “Understanding electrochemical potentials of cathode materials in rechargeable batteries”, *Materials Today* , vol. 19, no. 2. Elsevier Ltd , Oxford , pp. 109–123, 2016.

2. B. H. Strauss, S. Kulp, and A. Levermann, “Carbon choices determine US cities committed to futures below sea level”, *Proceedings of the National Academy of Sciences* , vol. 112, no. 44. National Acad Sciences , Washington , pp. 13508–13513, 2015.

3. S. Shafiee and E. Topal, “When will fossil fuel reserves be diminished?”, *Energy Policy*, vol. 37, no. 1, pp. 181–189, 2009.

4. L. Suganthi and A. A. Samuel, “Energy models for demand forecasting—A review”, *Renewable and Sustainable Energy Reviews* , vol. 16, no. 2. Elsevier Ltd, Oxford, pp. 1223–1240, 2012.

5. M. S. Guney and Y. Tepe, “Classification and assessment of energy storage systems”, *Renew. Sustain. Energy Rev.*, vol. 75, pp. 1187–1197, 2017.

6. S. Ould Amrouche, D. Rekioua, T. Rekioua, and S. Bacha, “Overview of energy storage in renewable energy systems”, *International Journal of Hydrogen Energy* , vol. 41, no. 45. Elsevier Ltd , Oxford , pp. 20914–20927, 2016.

7. M. Gao, S.-Y. Pan, W.-C. Chen, and P.-C. Chiang, “A cross-disciplinary overview of naturally derived materials for electrochemical energy storage”, *Mater. Today Energy*, vol. 7, pp. 58–79, 2018.

8. P. G. Bruce, S. A. Freunberger, L. J. Hardwick, and J.-M. Tarascon, “Li-O2 and Li-S batteries with high energy storage”, *Nature materials* , vol. 11, no. 1. Nature Publishing Group , England , pp. 19–29.

9. X. Ji and L. F. Nazar, “Advances in Li-S batteries”, *Journal of Materials Chemistry* , vol. 2, no. 44. Royal Soc Chemistry , Cambridge , pp. 9821–9826, 2010.

10. M. Hagen, D. Hanselmann, K. Ahlbrecht, R. Maça, D. Gerber, and J. Tübke, “Lithium-Sulfur Cells: The Gap between the State-of-the-Art and the Requirements for High Energy Battery Cells”, *Advanced Energy Materials* , vol. 5, no. 16. Wiley-V C H Verlag GMBH , Weiheim , 2015.

11. S. Chung, C. Chang, A. Manthiram, and A. Univ. of Texas at Austin TX (United States), “Progress on the Critical Parameters for Lithium–Sulfur Batteries to be Practically Viable”, *Advanced Functional Materials* , vol. 28, no. 28. Wiley-V C H Verlag GMBH , Weiheim , p. 1801188–n/a, 2018.

12. Y. Liu *et al.*, “An Artificial Solid Electrolyte Interphase with High Li-Ion Conductivity, Mechanical Strength, and Flexibility for Stable Lithium Metal Anodes”, *Adv. Mater.*, vol. 29, no. 10, 2017.

13. J. Scheers, S. Fantini, and P. Johansson, “A review of electrolytes for lithium–sulphur batteries”, *J. Power Sources*, vol. 255, pp. 204–218, 2014.

14. A. Manthiram, S. Chung, and C. Zu, “Lithium–Sulfur Batteries: Progress and Prospects”, *Advanced Materials* , vol. 27, no. 12. Wiley-V C H Verlag GMBH , Weiheim , pp. 1980–2006, 2015.

15. W. Xue *et al.*, “Gravimetric and volumetric energy densities of lithium-sulfur batteries”, *Curr. Opin. Electrochem.*, vol. 6, no. 1, pp. 92–99, 2017.

16. S. Urbonaite, T. Poux, and P. Novák, “Progress Towards Commercially Viable Li–S Battery Cells”, *Adv. Energy Mater.*, vol. 5, no. 16, 2015.

17. J. Liang, Z.-H. Sun, F. Li, and H.-M. Cheng, “Carbon materials for Li–S batteries: Functional evolution and performance improvement”, *Energy Storage Mater.*, vol. 2, pp. 76–106, 2016.

18. S. S. Zhang, “Liquid electrolyte lithium/sulfur battery: Fundamental chemistry, problems, and solutions”, *J. Power Sources*, vol. 231, pp. 153–162, 2013.

19. A. F. Hofmann, D. N. Fronczek, and W. G. Bessler, “Mechanistic modeling of polysulfide shuttle and capacity loss in lithium–sulfur batteries”, *Journal of Power Sources* , vol. 259. Elsevier B.V , Amsterdam , pp. 300–310, 2014.

20. D. N. Fronczek and W. G. Bessler, “Insight into lithium–sulfur batteries: Elementary kinetic modeling and impedance simulation”, *J. Power Sources*, vol. 244, pp. 183–188, 2013.

21. S. Risse, S. Angioletti-Uberti, J. Dzubiella, and M. Ballauff, “Capacity fading in lithium/sulfur batteries: A linear four-state model”, *Journal of Power Sources* , vol. 267. Elsevier B.V , Amsterdam , pp. 648–654, 2014.

22. T. Zhang, M. Marinescu, L. O’Neill, M. Wild, and G. Offer, “Modeling the voltage loss mechanisms in lithium-sulfur cells: the importance of electrolyte resistance and precipitation kinetics”, *Physical Chemistry Chemical Physics* , vol. 17, no. 35. Royal Soc Chemistry , Cambridge , pp. 22581–22586, 2015.

23. K. Kumaresan, Y. Mikhaylik, and R. E. White, “A mathematical model for a lithium-sulfur cell”, *Journal of the Electrochemical Society* , vol. 155, no. 8. Electrochemical Soc Inc , Pennington , pp. A576–A582, 2008.

24. A. Fotouhi, D. J. Auger, L. O’Neill, T. Cleaver, and S. Walus, “Lithium-Sulfur Battery Technology Readiness and Applications-A Review”, *Energies* , vol. 10, no. 12. MDPI AG , Basel , p. 1937, 2017.

25. S. Urbonaite and P. Novák, “Importance of ‘unimportant’ experimental parameters in Li–S battery development”, *J. Power Sources*, vol. 249, pp. 497–502, 2014.

26. A. Gupta and S. Sivaram, “Separator Membranes for Lithium–Sulfur Batteries: Design Principles, Structure, and Performance”, *Energy Technol.*, vol. 7, no. 6, p.

1800819, 2019.

27. Y. Diao, K. Xie, S. Xiong, and X. Hong, “Shuttle phenomenon – The irreversible oxidation mechanism of sulfur active material in Li–S battery”, *J. Power Sources*, vol. 235, pp. 181–186, 2013.

28. Y. V Mikhaylik and J. R. Akridge, “Polysulfide shuttle study in the Li/S battery system”, *Journal of the Electrochemical Society* , vol. 151, no. 11. Electrochemical Soc Inc, Pennington, pp. A1969–A1976, 2004.

29. W. Xu *et al.*, “Lithium metal anodes for rechargeable batteries”, *Energy Environ. Sci.*, vol. 7, no. 2, pp. 513–537, 2014.

30. J.-W. Choi, J.-K. Kim, G. Cheruvally, J.-H. Ahn, H.-J. Ahn, and K.-W. Kim, “Rechargeable lithium/sulfur battery with suitable mixed liquid electrolytes”, *Electrochim. Acta*, vol. 52, no. 5, pp. 2075–2082, 2007.

31. N. Erisen, N. B. Emerce, S. C. Erensoy, and D. Eroglu, “Modeling the effect of key cathode design parameters on the electrochemical performance of a lithium-sulfur battery”, *International Journal of Energy Research* . 2018.

32. N. B. Emerce and D. Eroglu, “Effect of Electrolyte-to-Sulfur Ratio in the Cell on the Li-S Battery Performance”, *Journal Of The Electrochemical Society* , vol. 166, no. 8. Electrochemical Soc Inc , Pennington , pp. A1490–A1500, 2019.

33. Z.-L. Xu, J.-K. Kim, and K. Kang, “Carbon nanomaterials for advanced lithium sulfur batteries”, *Nano Today*, vol. 19, pp. 84–107, 2018.

34. W. Wang *et al.*, “The electrochemical performance of lithium–sulfur batteries with LiClO4 DOL/DME electrolyte”, *Journal of Applied Electrochemistry* , vol. 40, no. 2. Springer Netherlands , Dordrecht , pp. 321–325, 2010.

35. Z. Deng, Z. Zhang, Y. Lai, J. Liu, J. Li, and Y. Liu, “Electrochemical impedance

spectroscopy study of a lithium/sulfur battery: Modeling and analysis of capacity fading", *Journal of the Electrochemical Society* , vol. 160, no. 4. Electrochemical Soc Inc, Pennington , pp. A553–A558, 2013.

36. B. Jin, J.-U. Kim, and H.-B. Gu, "Electrochemical properties of lithium–sulfur batteries", *J. Power Sources*, vol. 117, no. 1, pp. 148–152, 2003.

37. D. Eroglu, K. R. Zavadil, and K. G. Gallagher, "Critical link between materials chemistry and cell-level design for high energy density and low cost lithium-sulfur transportation battery", *Journal of the Electrochemical Society* , vol. 162, no. 6. Electrochemical Soc Inc, Pennington , pp. A982–A990, 2015.

38. S.-R. Chen *et al.*, "Ordered mesoporous carbon/sulfur nanocomposite of high performances as cathode for lithium–sulfur battery", *Electrochim. Acta*, vol. 56, no. 26, pp. 9549–9555, 2011.

39. N. Ding, S. W. Chien, T. S. A. Hor, Z. Liu, and Y. Zong, "Key parameters in design of lithium sulfur batteries", *J. Power Sources*, vol. 269, pp. 111–116, 2014.

40. J. Gao and H. D. Abruña, "Key parameters governing the energy density of rechargeable Li/S batteries", *Journal of Physical Chemistry Letters* , vol. 5, no. 5. Amer Chemical Soc , Washington , pp. 882–885, 2014.

41. D. Li, F. Han, S. Wang, F. Cheng, Q. Sun, and W.-C. Li, "High sulfur loading cathodes fabricated using peapodlike, large pore volume mesoporous carbon for lithium-sulfur battery", *ACS Applied Materials and Interfaces* , vol. 5, no. 6. Amer Chemical Soc , Washington , pp. 2208–2213, 2013.

42. J.-W. Park *et al.*, "Effect of sulfur content in a sulfur-activated carbon composite on the electrochemical properties of a lithium/sulfur battery", *Materials Research Bulletin* , vol. 69. Elsevier Ltd , Oxford , pp. 24–28, 2015.

43. J. Brückner, S. Thieme, H. T. Grossmann, S. Dörfler, H. Althues, and S. Kaskel,

"Lithium–sulfur batteries: Influence of C-rate, amount of electrolyte and sulfur loading on cycle performance", *Journal of Power Sources* , vol. 268. Elsevier B.V , Amsterdam , pp. 82–87, 2014.

44. F. Y. Fan and Y. M. Chiang, "Electrodeposition Kinetics in Li-S Batteries: Effects of Low Electrolyte/Sulfur Ratios and Deposition Surface Composition", *Journal Of The Electrochemical Society* , vol. 164, no. 4. Electrochemical Soc Inc, Pennington , pp. A917–A922, 2017.

45. M. Hagen, P. Fanz, and J. Tübke, "Cell energy density and electrolyte/sulfur ratio in Li–S cells", *Journal of Power Sources* , vol. 264. Elsevier B.V , Amsterdam , pp. 30–34, 2014.

46. S. S. Zhang, "Improved Cyclability of Liquid Electrolyte Lithium/Sulfur Batteries by Optimizing Electrolyte/Sulfur Ratio", *Energies* , vol. 5, no. 12. 2012.

47. J. Zheng *et al.*, "How to obtain reproducible results for lithium sulfur batteries?", *Journal of the Electrochemical Society* , vol. 160, no. 11. E Electrochemical Soc Inc, Pennington , pp. A2288–A2292, 2013.

48. L. Yuan, X. Qiu, L. Chen, and W. Zhu, "New insight into the discharge process of sulfur cathode by electrochemical impedance spectroscopy", *Journal of Power Sources* , vol. 189, no. 1. Elsevier B.V , Amsterdam , pp. 127–132, 2009.

49. C. Barchasz, J.-C. Leprêtre, F. Alloin, and S. Patoux, "New insights into the limiting parameters of the Li/S rechargeable cell", *Journal of Power Sources* , vol. 199. Elsevier B.V , Amsterdam , pp. 322–330.

50. N. A. Cañas, K. Hirose, B. Pascucci, N. Wagner, K. A. Friedrich, and R. Hiesgen, "Investigations of lithium–sulfur batteries using electrochemical impedance spectroscopy", *Electrochimica Acta* , vol. 97. Elsevier Ltd , Oxford , pp. 42–51, 2013.

51. J. Yan, X. Liu, and B. Li, "Capacity fade analysis of sulfur cathodes in lithium– sulfur

batteries", *Advanced Science* , vol. 3, no. 12. Wiley , Hoboken , p. 1600101, 2016.

52. K. Sun, H. Liu, and H. Gan, "Cathode Loading Effect on Sulfur Utilization in Lithium–Sulfur Battery", *J. Electrochem. Energy Convers. Storage*, vol. 13, no. 2, pp. 21002–21009, Oct. 2016.

53. V. S. Kolosnitsyn, E. V Kuzmina, E. V Karaseva, and S. E. Mochalov, "A study of the electrochemical processes in lithium–sulphur cells by impedance spectroscopy", *J. Power Sources*, vol. 196, no. 3, pp. 1478–1482, 2011.

54. K. Li, B. Wang, D. Su, J. Park, H. Ahn, and G. Wang, "Enhance electrochemical performance of lithium sulfur battery through a solution-based processing technique", *J. Power Sources*, vol. 202, pp. 389–393, 2012.

55. J. Conder, C. Villevieille, S. Trabesinger, P. Novák, L. Gubler, and R. Bouchet, "Electrochemical impedance spectroscopy of a Li–S battery: Part 1. Influence of the electrode and electrolyte compositions on the impedance of symmetric cells", *Electrochim. Acta*, vol. 244, pp. 61–68, 2017.

56. Y. Li, H. Zhan, S. Liu, K. Huang, and Y. Zhou, "Electrochemical properties of the soluble reduction products in rechargeable Li/S battery", *J. Power Sources*, vol. 195, no. 9, pp. 2945–2949, 2010.

57. W. Ahn, K.-B. Kim, K.-N. Jung, K.-H. Shin, and C.-S. Jin, "Synthesis and electrochemical properties of a sulfur-multi walled carbon nanotubes composite as a cathode material for lithium sulfur batteries", *J. Power Sources*, vol. 202, pp. 394–399, 2012.

58. D. Andre, M. Meiler, K. Steiner, C. Wimmer, T. Soczka-Guth, and D. U. Sauer, "Characterization of high-power lithium-ion batteries by electrochemical impedance spectroscopy. I. Experimental investigation", *J. Power Sources*, vol. 196, no. 12, pp. 5334–5341, 2011.

59. D. Andre, M. Meiler, K. Steiner, C. Wimmer, T. Soczka-Guth, and D. U. Sauer, “Characterization of high-power lithium-ion batteries by electrochemical impedance spectroscopy. I. Experimental investigation”, *J. Power Sources*, vol. 196, no. 12, pp. 5334–5341, 2011.

60. EC-Lab Software User's Manual, https://mmrc.caltech.edu/BioLogic%20Echem/ECLab%20Manuals/ECLab%20software%20user's%20manual.pdf, accessed in June 2019.

61. A. Barai, G. H. Chouchelamane, Y. Guo, A. McGordon, and P. Jennings, “A study on the impact of lithium-ion cell relaxation on electrochemical impedance spectroscopy”, *J. Power Sources*, vol. 280, pp. 74–80, 2015.

62. H. Dai, B. Jiang, and X. Wei, “Impedance Characterization and Modeling of Lithium-Ion Batteries Considering the Internal Temperature Gradient”, *Energies* , vol. 11, no. 1. 2018.

63. J. Bell *et al.*, “Plateau targeted conditioning: An additive-free approach towards robust SEI formation in Li-S batteries for enhanced capacity and cycle life”, *Nano Energy* , vol. 49. Elsevier Science BV , Amsterdam , pp. 498–507, 2018.

64. W.-H. Li *et al.*, “Highly Improved Cycling Stability of Anion De-/Intercalation in the Graphite Cathode for Dual-Ion Batteries”, *Adv. Mater.*, vol. 31, no. 4, p. 1804766, 2019.

65. S. Choi, J. Song, C. Wang, S. Park, and G. Wang, “Multifunctional Free-Standing Gel Polymer Electrolyte with Carbon Nanofiber Interlayers for High-Performance Lithium–Sulfur Batteries”, *Chem. – An Asian J.*, vol. 12, no. 13, pp. 1470–1474, 2017.

66. Y.-P. Xie *et al.*, “Natural nitrogen-doped multiporous carbon from biological cells as sulfur stabilizers for lithium–sulfur batteries”, *Chinese Chem. Lett.*, vol. 28, no. 4, pp. 738–742, 2017.

67. Y. Deng, H. Xu, Z. Bai, B. Huang, J. Su, and G. Chen, “Durable polydopamine-coated porous sulfur core–shell cathode for high performance lithium–sulfur batteries”, *J. Power Sources*, vol. 300, pp. 386–394, 2015.

68. A. Schneider, C. Suchomski, H. Sommer, J. Janek, and T. Brezesinski, “Free-standing and binder-free highly N-doped carbon/sulfur cathodes with tailorable loading for high-areal-capacity lithium-sulfur batteries”, *Journal of Materials Chemistry A* , vol. 3, no. 41. Royal Soc Chemistry , Cambridge , pp. 20482–20486, 2015.

APPENDIX A: REST OF THE EIS SPECTRUMS OF E/S EXPERIMENTS

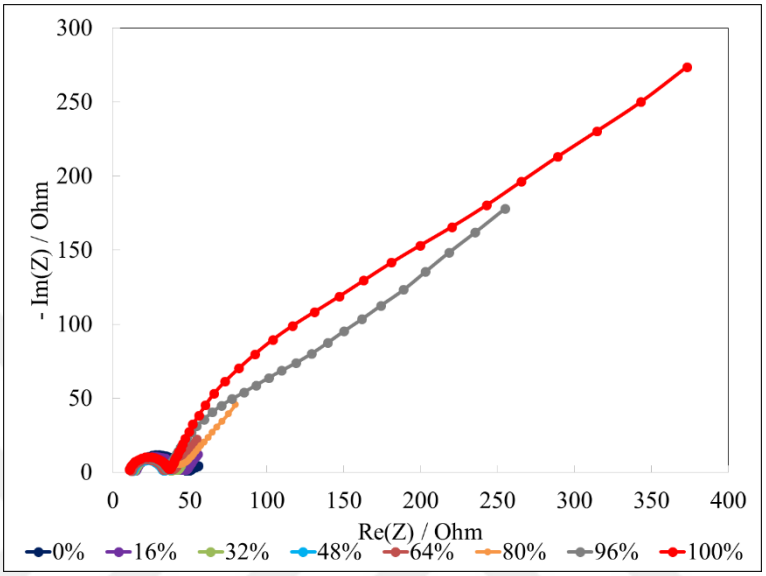

Figure A.1. The EIS spectrums of the cell with a E/S=34 µl/mg for several discharge points for the second cell.

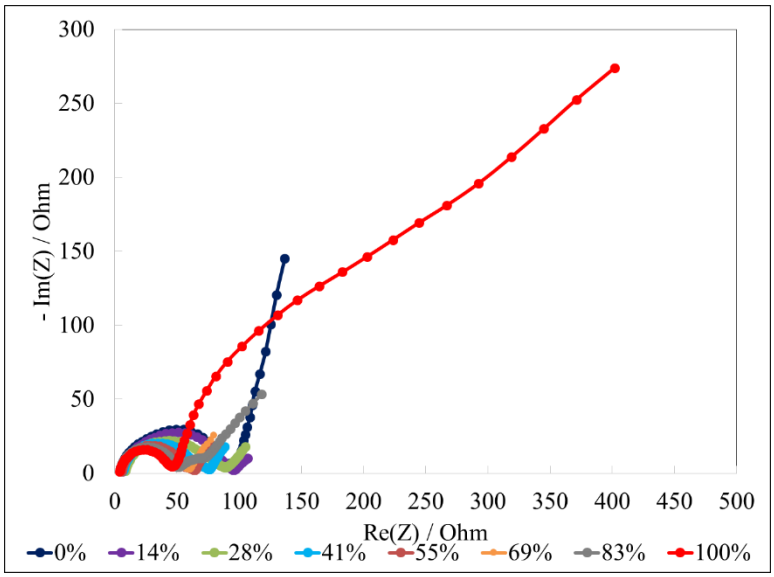

Figure A.2. The EIS spectrums of the cell with a E/S=34 µl/mg for several discharge points for the third cell.

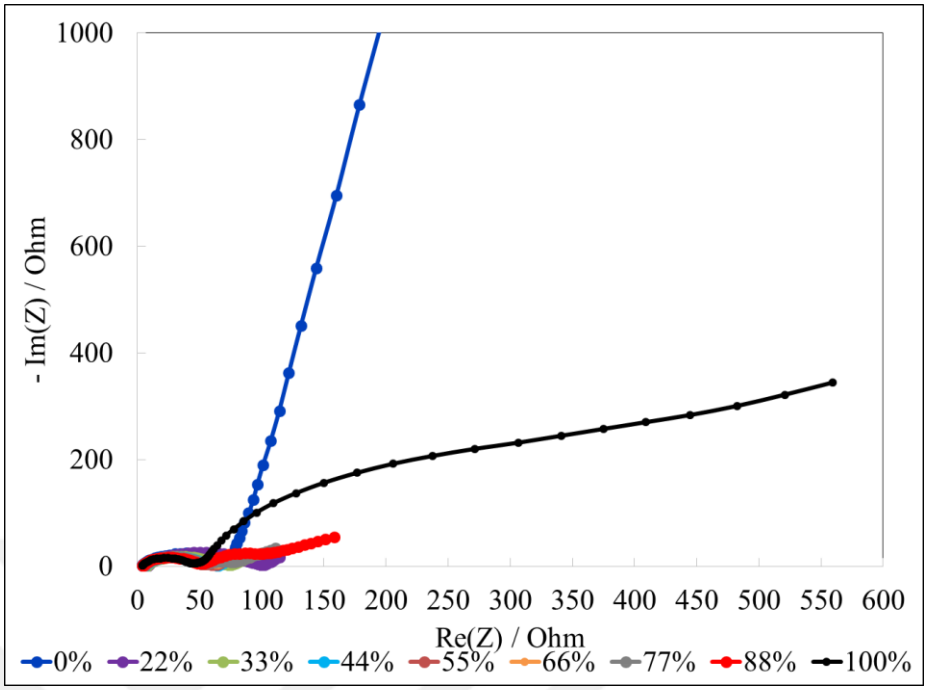

Figure A.3. The EIS spectrums of the cell with a E/S=19 µl/mg for several discharge points for the second cell.

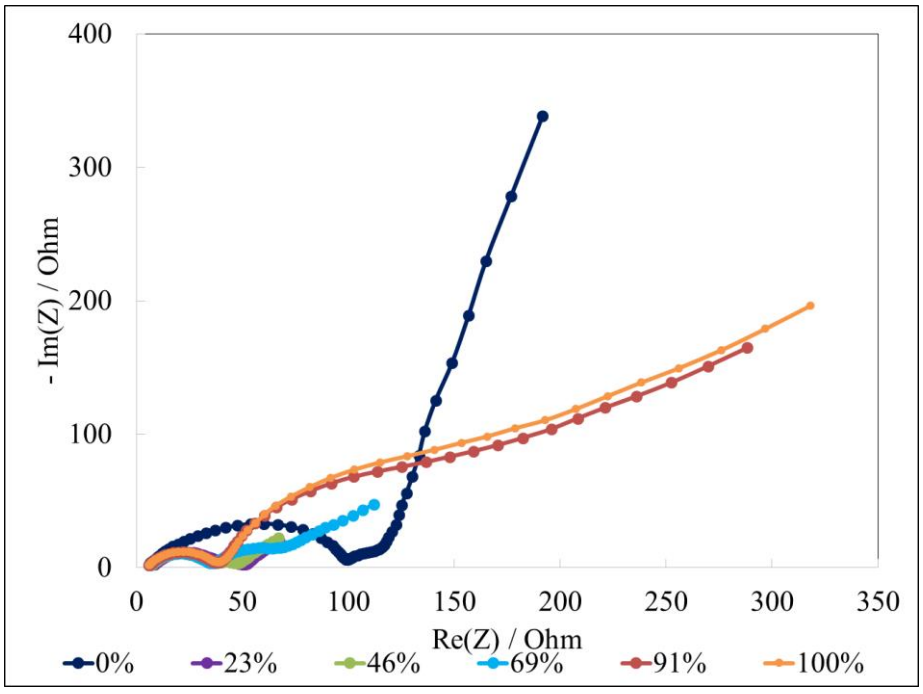

Figure A.4. The EIS spectrums of the cell with a E/S=19 µl/mg for several discharge points for the third cell.

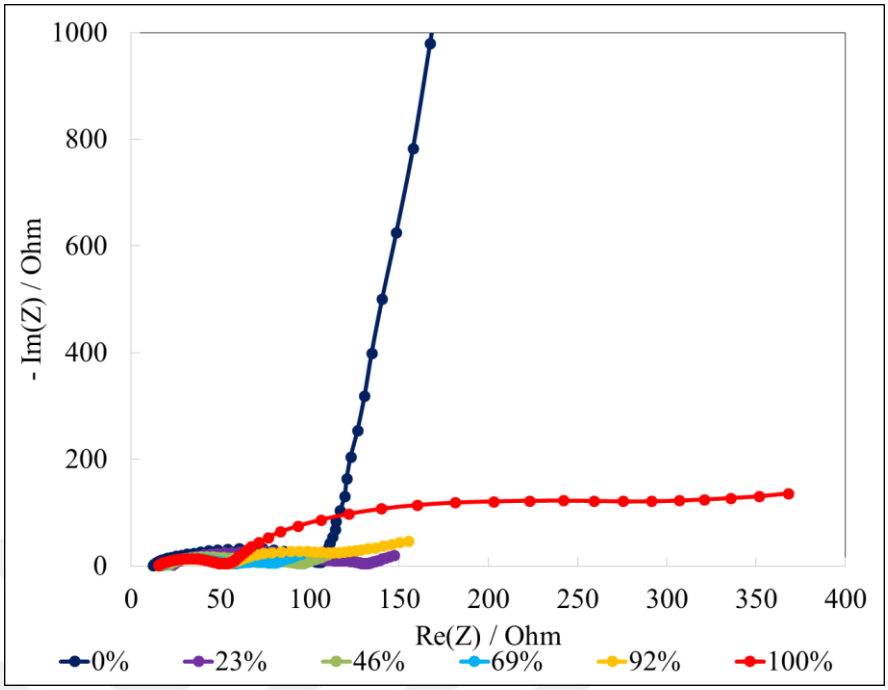

Figure A.5. The EIS spectrums of the cell with a E/S=12 µl/mg for several discharge points for the second cell.

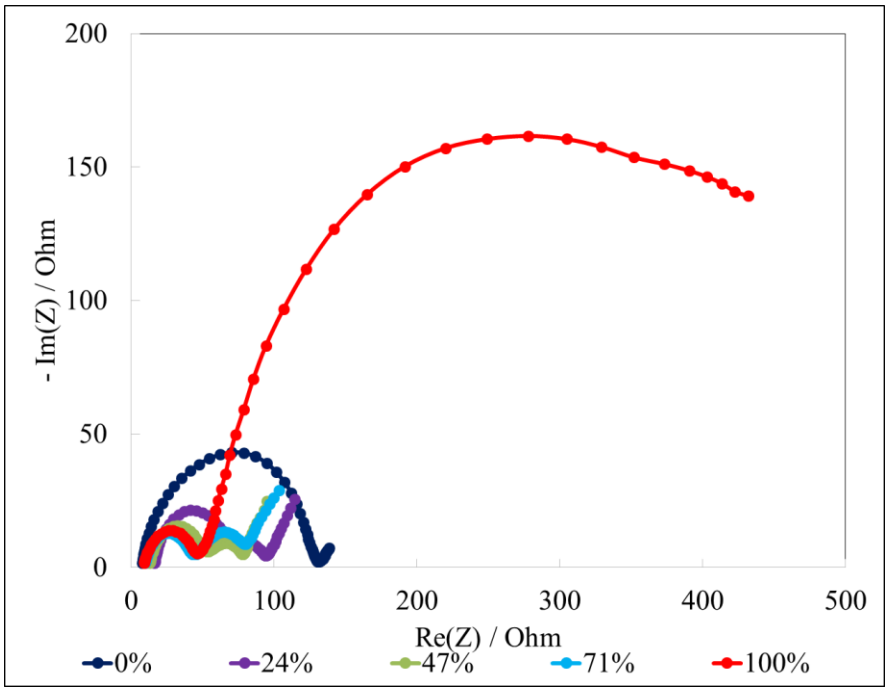

Figure A.6. The EIS spectrums of the cell with a E/S=12 µl/mg for several discharge points for the third cell.

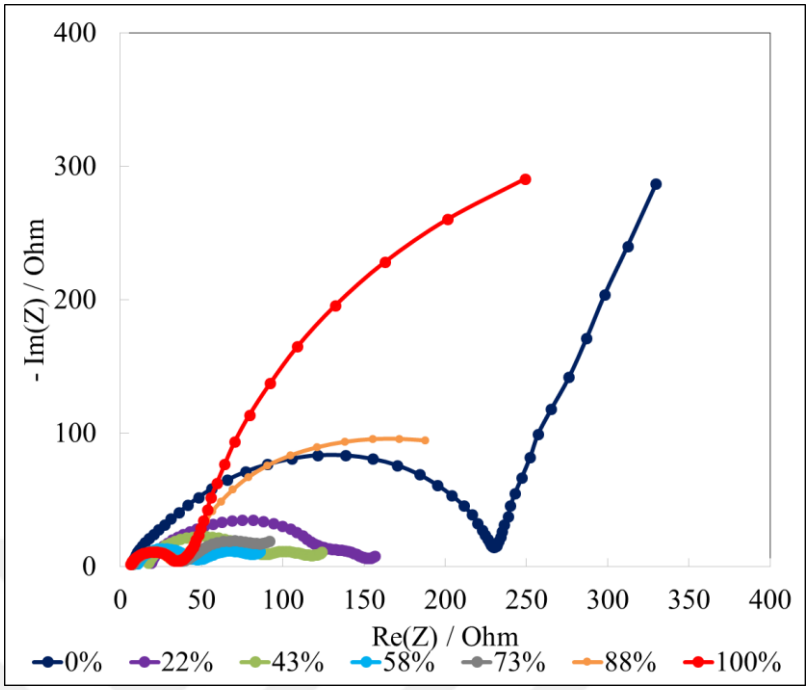

Figure A.7. The EIS spectrums of the cell with a E/S=6 µl/mg for several discharge points for the second cell.

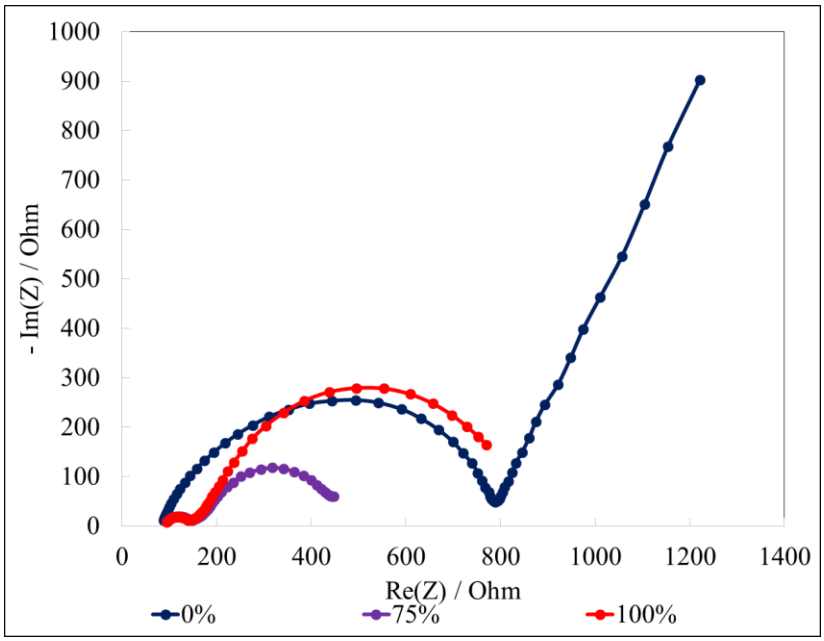

Figure A.8. The EIS spectrums of the cell with a E/S=6 µl/mg for several discharge points for the third cell.

APPENDIX B: REST OF THE EIS SPECTRUMS OF C/S EXPERIMENTS

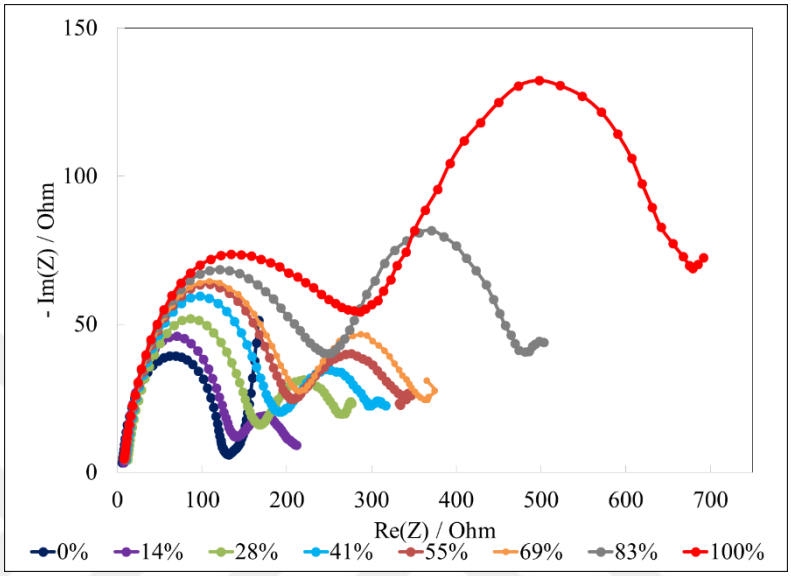

Figure B.1. The EIS spectrums of the cell with a C/S=0.3 for several discharge points for the second cell.

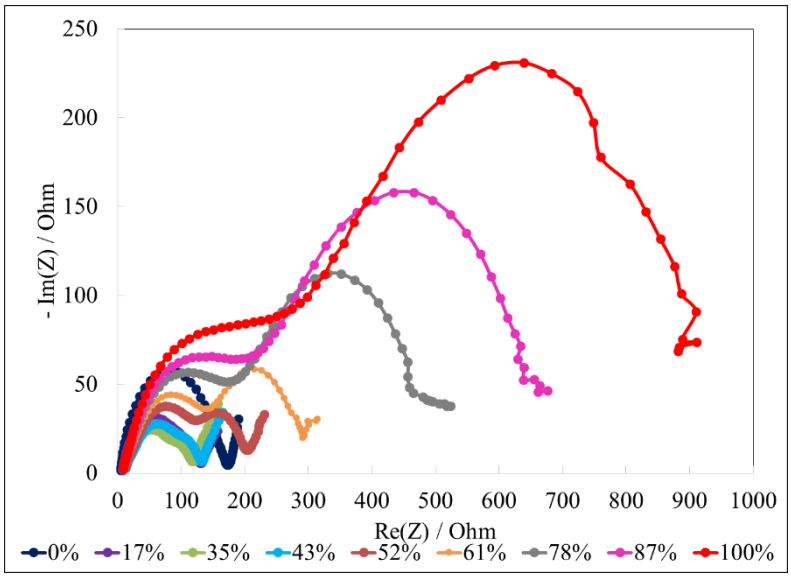

Figure B.2. The EIS spectrums of the cell with a C/S=0.3 for several discharge points for the third cell.

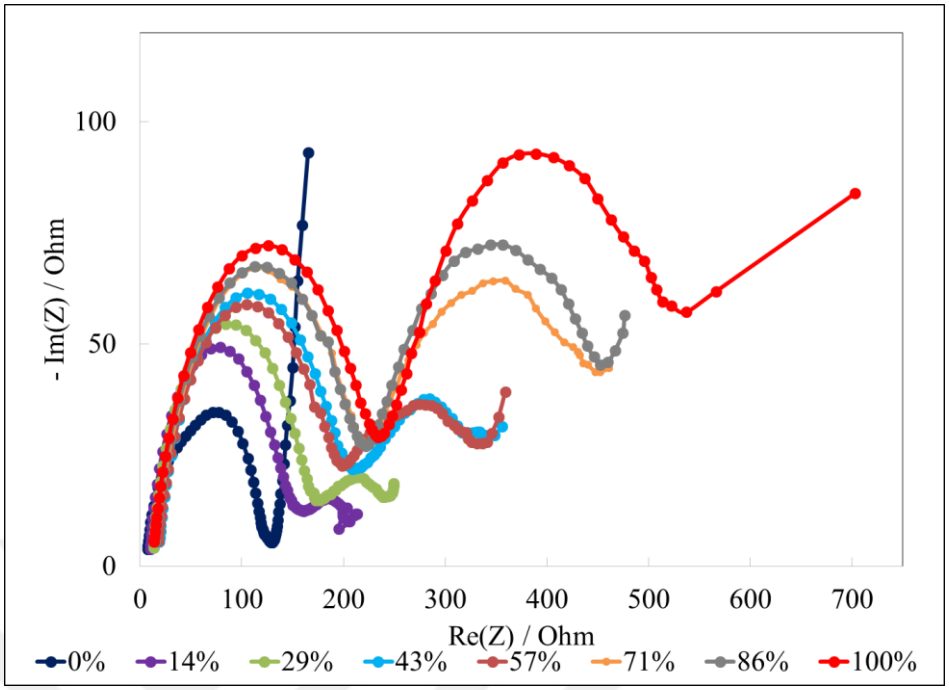

Figure B.3. The EIS spectrums of the cell with a C/S=0.5 for several discharge points for the second cell.

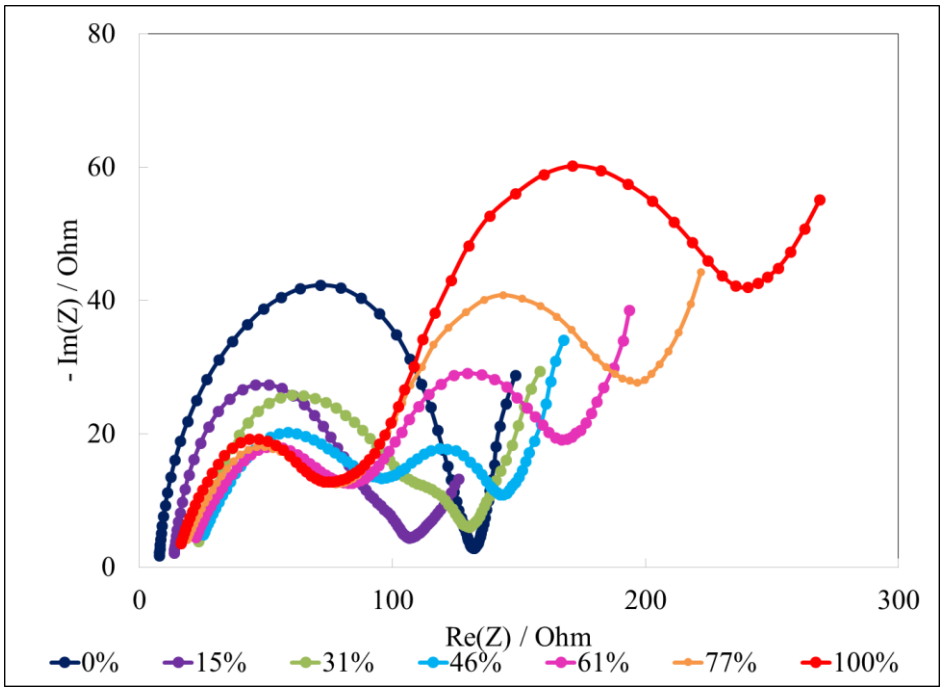

Figure B.4. The EIS spectrums of the cell with a C/S=0.5 for several discharge points for the third cell.

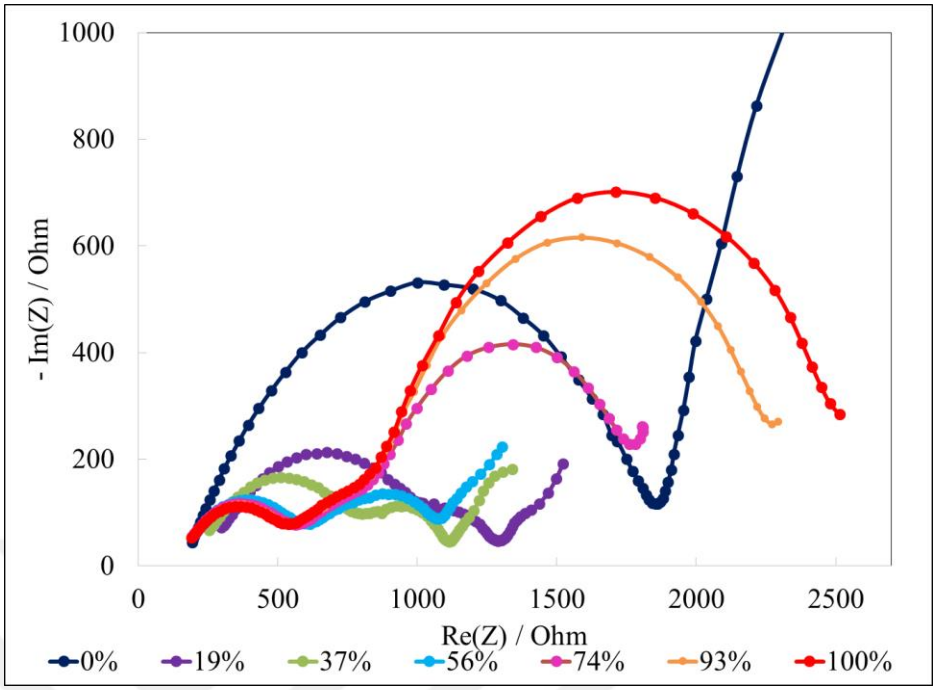

Figure B.5. The EIS spectrums of the cell with a C/S=2 for several discharge points for the second cell.

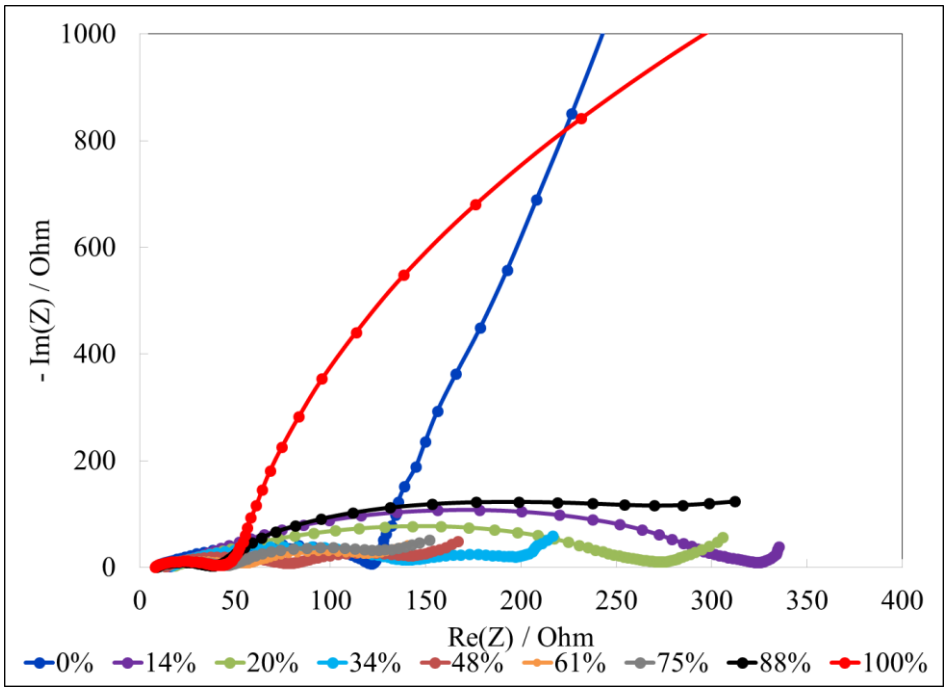

Figure B.6. The EIS spectrums of the cell with a C/S=2 for several discharge points for the third cell.

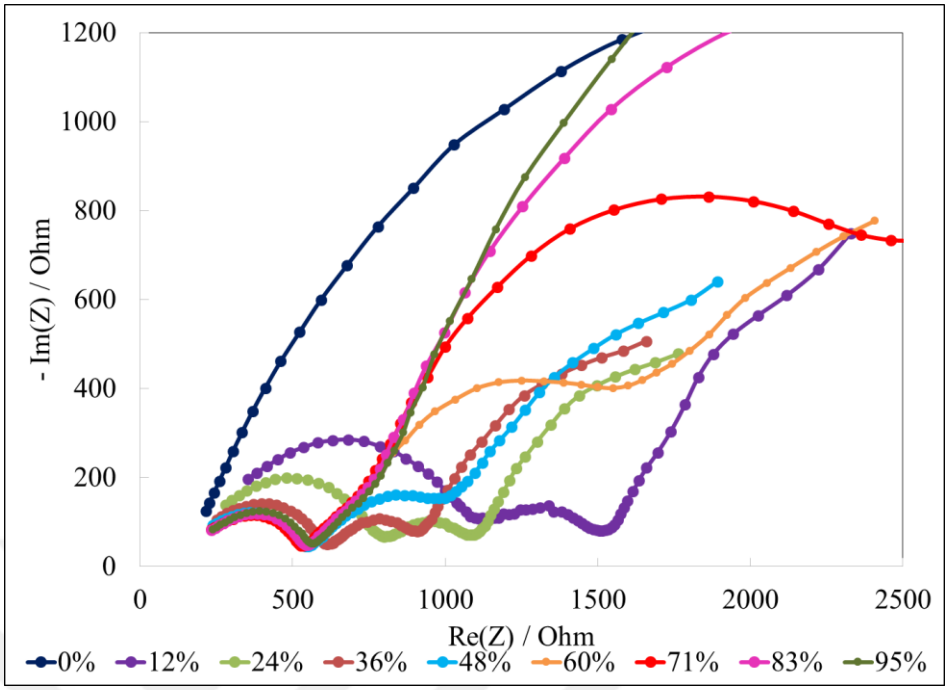

Figure B.7. The EIS spectrums of the cell with a C/S=3.5 for several discharge points for the second cell.

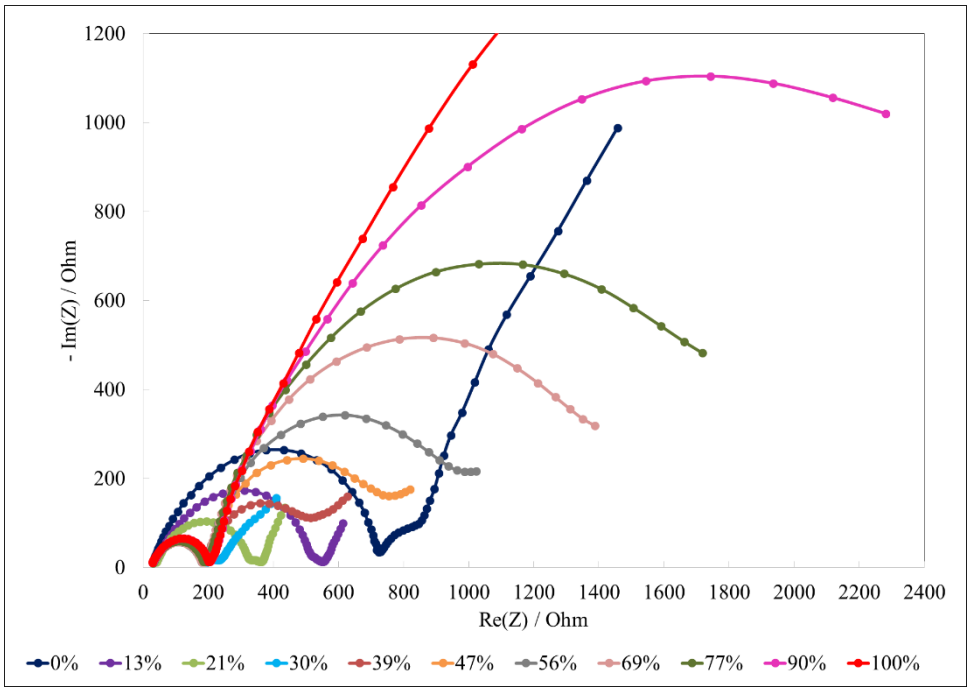

Figure B.8. The EIS spectrums of the cell with a C/S=3.5 for several discharge points for the third cell.